

METAMATERIALS INSPIRED ANTENNA  
MINIATURIZATION FOR MIMO SYSTEM  
APPLICATIONS

BY

**MUHAMMAD UMAR KHAN**

A Dissertation Presented to the  
DEANSHIP OF GRADUATE STUDIES

**KING FAHD UNIVERSITY OF PETROLEUM & MINERALS**

DHAHRAN, SAUDI ARABIA

In Partial Fulfillment of the  
Requirements for the Degree of

**DOCTOR OF PHILOSOPHY**

In

**ELECTRICAL ENGINEERING**

JANUARY 2015

KING FAHD UNIVERSITY OF PETROLEUM & MINERALS  
DHAHRAN 31261, SAUDI ARABIA

DEANSHIP OF GRADUATE STUDIES

This thesis, written by **MUHAMMAD UMAR KHAN** under the direction of his thesis adviser and approved by his thesis committee, has been presented to and accepted by the Dean of Graduate Studies, in partial fulfillment of the requirements for the degree of **DOCTOR OF PHILOSOPHY IN ELECTRICAL ENGINEERING**.

Dissertation Committee



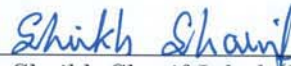
Dr. Mohammad S. Sharawi (Adviser)



Prof. Mohammad A. Al-Sunaidi (Member)



Prof. Raj Mitra (Member)



Dr. Sheikh Sharif Iqbal (Member)



Dr. Ali Muqaibel (Member)



Dr. Ali Ahmad Al-Shaikhi  
Department Chairman

Prof. Salam A. Zummo  
Dean of Graduate Studies



22/1/15  
Date

©Muhammad Umar Khan  
2015

*To my parents, for their never-ending love and support*

# ACKNOWLEDGMENTS

*During my PhD studies, I have met and interacted with several people who helped me in many ways. I would like to sincerely thank each and everyone of them. First and foremost, I would like to wholeheartedly thank my advisor, Dr. Mohammed S. Sharawi. He remained a constant source of inspiration throughout my tenure as a graduate student. His encouragement helped me to meet the deadlines. He always made sure that I was never short of anything that is required in my research work. His AMSD Lab was the reason, I was able to test so many ideas in a short time. He taught me the value of time. I will always cherish the time I spent as his student. I am grateful to all the committee members for their valuable feedback and suggestions. I am also indebted to Dr. Wajih A. Abu Al-Saud for his continuous support throughout my research work. Without his help and guidance, this thesis would not have been possible. To all the current and former members of AMSD Lab, especially to Ahmad Numan, Rifaqat, Omar Rauf, Sagar and Ali for your friendship and valuable discussions. Best of luck to all of you, especially those who are still working on their thesis. I wish you all the best. To all my friends at the university who made my stay pleasant. To Hussain Ali, Adil Khan, Mohsin Butt and Waqas for always taking*

*out time for me. Special Thanks to Shehry, for his help and support during my studies. I am grateful to the department of electrical engineering, deanship of graduate studies and the university for their support and funding. Finally, and perhaps most importantly I would like to thank my family for their unwavering support. Thank you so much. This thesis is for you.*

# TABLE OF CONTENTS

<b>ACKNOWLEDGMENTS</b>	<b>iii</b>
<b>LIST OF TABLES</b>	<b>ix</b>
<b>LIST OF FIGURES</b>	<b>xi</b>
<b>ABSTRACT (ENGLISH)</b>	<b>xvii</b>
<b>ABSTRACT (ARABIC)</b>	<b>xix</b>
<b>CHAPTER 1 INTRODUCTION</b>	<b>1</b>
1.1 Background . . . . .	1
1.2 Motivation . . . . .	4
1.3 Work Contribution . . . . .	6
1.4 Dissertation Overview . . . . .	7
<b>CHAPTER 2 ELECTRICALLY SMALL ANTENNAS AND MINIATURIZATION OF MPA</b>	<b>9</b>
2.1 Electrically Small Antennas (ESA) . . . . .	11
2.2 Microstrip Patch Antenna . . . . .	14
2.3 MPA Miniaturization Techniques . . . . .	19
2.3.1 Material Loading . . . . .	19
2.3.2 Shorting and Folding . . . . .	22
2.3.3 Reshaping or Introducing Slots . . . . .	24
2.3.4 Modifications of the Ground Plane . . . . .	25

2.3.5	Use of Metamaterials . . . . .	29
2.4	Summary and Features of Miniaturization Methods . . . . .	36
<b>CHAPTER 3 PROPOSED METHOD FOR THE MINIATURIZA-</b>		
<b>TION OF MPA</b>		<b>38</b>
3.1	CSRR Loaded MPA . . . . .	39
3.1.1	Complementary Split-Ring Resonator (CSRR) . . . . .	39
3.1.2	Antenna Design . . . . .	40
3.1.3	Results & Parametric Analysis . . . . .	41
3.1.4	Circuit Model . . . . .	50
3.1.5	Design Procedure . . . . .	53
3.2	Design Examples . . . . .	55
3.2.1	Miniaturized MPA for the 750 MHz Band . . . . .	55
3.2.2	Miniaturized MPA for the 5 GHz Band . . . . .	56
3.3	Design Analysis using the Characteristic Mode Theory . . . . .	58
3.3.1	Overview of Theory . . . . .	58
3.3.2	Analysis of the Proposed Design . . . . .	65
3.4	Comparison & Conclusions . . . . .	70
<b>CHAPTER 4 MIMO ANTENNA SYSTEMS</b>		<b>73</b>
4.1	MIMO Systems . . . . .	73
4.2	MIMO Antenna System . . . . .	77
4.3	Performance Metrics for MIMO Antenna System . . . . .	78
4.3.1	Resonance and Isolation . . . . .	78
4.3.2	Total Active Reflection Coefficient (TARC) . . . . .	79
4.3.3	Antenna Efficiency . . . . .	80
4.3.4	Correlation Coefficient . . . . .	82
4.3.5	Radiation Pattern . . . . .	84
4.3.6	Mean Effective Gain (MEG) . . . . .	84
4.3.7	Channel Capacity . . . . .	85
4.4	MIMO Antenna System Designs . . . . .	87



4.4.1	Monopole Based MIMO Antenna System . . . . .	88
4.4.2	Dipole Based MIMO Antenna System . . . . .	93
4.4.3	PIFA Based MIMO Antenna System . . . . .	93
4.4.4	MPA Based MIMO Antenna System . . . . .	95
4.4.5	Other MIMO Antenna System . . . . .	96
4.5	Conclusions . . . . .	100
 <b>CHAPTER 5 MINIATURIZED MPA BASED MIMO ANTENNA</b>		
	<b>SYSTEM</b>	<b>103</b>
5.1	4-Element MIMO Antenna System for ISM band Operation . . .	104
5.1.1	MIMO Antenna Design . . . . .	104
5.1.2	Simulation & Measurement Results . . . . .	105
5.1.3	Antenna Behavior Over a Conducting Plane . . . . .	116
5.1.4	Channel Capacity Estimation . . . . .	119
5.2	4-Element and 8-Element MIMO Antenna Systems Operating in the 5 GHz Band . . . . .	126
5.2.1	MIMO Antenna Design . . . . .	127
5.2.2	Simulation & Measurement Results . . . . .	129
5.2.3	Channel Capacity Estimation . . . . .	142
5.3	2-Element Multi-band MIMO Antenna System . . . . .	144
5.3.1	MIMO Antenna Design . . . . .	145
5.3.2	Simulation & Measurement Results . . . . .	146
5.4	Isolation Enhancement in the MIMO Antenna System . . . . .	151
5.4.1	Isolation Improvement for the ISM Band MIMO Antenna system . . . . .	154
5.4.2	SRR Based Isolation Improvement for Other Bands . . . . .	159
5.5	Comparison & Conclusions . . . . .	162
 <b>CHAPTER 6 CONCLUSIONS &amp; FUTURE WORK</b>		<b>164</b>
6.1	Conclusions . . . . .	164
6.2	Future Work . . . . .	166

REFERENCES	168
VITAE	191
LIST OF PUBLICATIONS	192

# LIST OF TABLES

1.1	Commonly Used Wireless Standards with their Applications . . .	2
1.2	Market Forecast of Wireless Mobile Devices [1] . . . . .	3
2.1	Literature on MPA Miniaturization Grouped According to the Technique Used . . . . .	35
2.2	A Summary of MPA Miniaturization Techniques and their Char- acteristics . . . . .	37
3.1	Design Parameters of the MPA Used in the Parametric Study . .	42
3.2	Simulation Results for the 750 MHz Band MPA . . . . .	56
3.3	Simulation Results for the 5 GHz Band MPA . . . . .	57
3.4	A Comparison of the Proposed Antenna with other Miniaturized MPAs in Literature . . . . .	72
5.1	MEG of the Antenna Elements of the ISM Band MIMO Antenna System . . . . .	115
5.2	Antenna Efficiency, Resonant Frequency and Front to Back Ratio in the Presence of a Conducting Plane . . . . .	117
5.3	MEG of the 4-Element MIMO Antenna Systems . . . . .	142
5.4	MEG for the 8-Element MIMO Antenna Systems . . . . .	143
5.5	MEG, Radiation Efficiency and Correlation Coefficient of the Multi-band MIMO Antenna System . . . . .	150
5.6	Gain and Efficiency of the MIMO Antenna System with and with- out the SRR Based Isolation Structure . . . . .	158

5.7	A Summary & Comparison of the Proposed MIMO Antenna Systems with Other MIMO Antenna Systems in Literature . . . . .	163
-----	---	-----

# LIST OF FIGURES

2.1	A ESA enclosed in a Chu-Sphere. . . . .	13
2.2	A microstrip line feed excited rectangular patch antenna, (a) Top view, (b) Side view. . . . .	15
2.3	A circular patch antenna with solid probe feed, (a) Top view, (b) Side view. . . . .	17
2.4	An MPA with dielectric bars underneath the patch [12]. . . . .	20
2.5	A quarter-wavelength MPA fabricated by using shorting posts [8].	23
2.6	A $\lambda/8$ shorted/folded MPA [19]. . . . .	24
2.7	Multi-layer engineered conductor for use with miniaturized MPA compared to a conventional conductor used in a MPA [31]. . . . .	25
2.8	A miniaturized MPA on an irregular ground structure [50]. . . . .	29
2.9	Geometry of the annular ring patch on an MTM substrate [53]. . . . .	32
2.10	Geometry of the rectangular patch on a MTM substrate [54]. . . . .	34
3.1	Geometry of the split-ring resonator . . . . .	40
3.2	Dispersion diagram of the CSRR etched on the back of a microstrip transmission line [59]. . . . .	41
3.3	Geometry of the proposed miniaturized MPA with CSRR loading, (a) Top side, (b) Bottom side . . . . .	42
3.4	Fabricated CSRR loaded miniaturized MPA . . . . .	43
3.5	Measured and simulated reflection coefficient of the designed MPA	44
3.6	The 2D gain pattern of the miniaturized MPA . . . . .	44

3.7	Variation of the antenna's resonant frequency with change in the CSRR radius . . . . .	45
3.8	Variation of the antenna's resonant frequency with change in the CSRR ring width . . . . .	46
3.9	Variation of the antenna's resonant frequency with change in the spacing between CSRR rings . . . . .	47
3.10	Effect of double-ring CSRR and single-ring CSRR loading on the resonant frequency of the MPA. . . . .	48
3.11	Current density on the CSRR-loaded MPA at the operating frequency, (a) Top side, (b) Bottom side . . . . .	49
3.12	The transmission-line model of the MPA [8]. . . . .	51
3.13	Reactance of a loop antenna [10]. . . . .	52
3.14	The equivalent circuit model of the CSRR-loaded MPA . . . . .	54
3.15	A flow chart representation of the design methodology to make the CSRR-loaded MPA . . . . .	54
3.16	Geometry and dimensions of MPA resonating at 750 MHz. (a) Top side, (b) Bottom side . . . . .	56
3.17	Geometry and dimensions of MPA resonating at 5 GHz. (a) Top side, (b) Bottom side . . . . .	57
3.18	Eigenvalues of the first mode for the MPA structure . . . . .	66
3.19	Eigenvalues of the first mode for the CSRR-loaded MPA structure . . . . .	67
3.20	Modal Significance of the first mode for the CSRR-loaded MPA structure . . . . .	68
3.21	Characteristic current corresponding to the first mode on the CSRR-loaded MPA structure (a) Top side, (b) Bottom side . . . . .	69
4.1	Upper limits of the channel capacity of SISO and MIMO systems. . . . .	76
4.2	Geometry of standard printed antennas, (a) Printed Dipole, (b) Printed Monopole, (c) Patch Antenna, (d) Side view of PIFA . . . . .	88

4.3	Fabricated two element monopole based MIMO antenna system with microstrip line structure for high isolation [113]. . . . .	91
4.4	Fabricated 4-element PIFA based MIMO antenna [99]. . . . .	95
4.5	Geometry of the SRR based patch antenna [55]. . . . .	97
4.6	Classification of literature related to the MIMO antenna systems according to the type of their antenna element. . . . .	101
4.7	Classification of literature related to the MIMO antenna systems according to their band of operation. . . . .	102
5.1	Geometry of the 4-element ISM band MIMO antenna system (a) Top view, (b) Bottom view. . . . .	105
5.2	Fabricated 4-element ISM Band MIMO antenna system, (a) Top layer, (b) Bottom layer. . . . .	107
5.3	Reflection coefficients of the 4-element ISM Band MIMO antenna system (ISM Band) . . . . .	107
5.4	Measured isolation between the elements of the ISM Band MIMO antenna system . . . . .	108
5.5	Current distribution on the ISM Band MIMO antenna system at 2.48 GHz, (a) Patch 1 is active (top layer), (b) Patch 3 is active (top layer), (c) Patch 1 active (bottom layer) and (d) Patch 3 active (bottom layer). . . . .	109
5.6	TARC curves of the ISM band MIMO antenna system with different phase combinations between the 4-elements, (a) elements 1 and 4 are in phase, (b) elements 1 and 2 are in phase, (c) elements 1 and 3 are in phase, (d) all elements are out of phase. . . . .	111
5.7	Correlation coefficient curves of the ISM band MIMO antenna system.	112
5.8	Measured gain patterns of the ISM band MIMO antenna system. (a) x-z plane at 2480 MHz, (b)y-z plane at 2480 MHz. Circles is co-pol element 1, solid is co-pol element 2, dots is cross-pol element 1, dashes is cross-pol element 2. . . . .	113

5.9	Measured gain patterns of the ISM Band MIMO antenna system. (a) x-z plane at 2480 MHz, (b)y-z plane at 2480 MHz. Circles is co-pol element 3, solid is co-pol element 4, dots is cross-pol element 3, dashes is cross-pol element 4. . . . .	114
5.10	3D radiation patterns of the ISM band MIMO antenna at 2480 MHz. (a) Element 1 (b) Element 2 (c) Element 3 (d) Ele- ment 4 . . . . .	115
5.11	Effect of LCD ground plane below the antenna on the reflection coefficient. . . . .	118
5.12	Radiation pattern of antenna element 1 in the presence of a con- ducting plane at 5 mm . . . . .	119
5.13	Current distribution on the conducting plane when the separation distance is (a) 1 mm , (b) 5 mm . . . . .	120
5.14	Measurement setup at the receiver end . . . . .	122
5.15	Layout of measurement scenario (a) LOS measurement , (b) NLOS measurement . . . . .	123
5.16	Average channel capacity in LOS indoor environment . . . . .	124
5.17	Average channel capacity in NLOS indoor environment . . . . .	125
5.18	CDF of the channel capacity of the MIMO antenna system in In- door environment . . . . .	125
5.19	Comparison of the average channel capacity of the printed MIMO antenna system in LOS and NLOS scenario . . . . .	126
5.20	Geometry of the 4-element 5 GHz band MIMO antenna system, (a) Top view, (b) Bottom view. . . . .	128
5.21	Geometry of the 8-element 5 GHz band MIMO antenna system, (a) Top view, (b) Bottom view. . . . .	129
5.22	Reflection coefficient of the 4-element 5 GHz band MIMO antenna system . . . . .	131
5.23	Measured reflection coefficient of the 8-element 5 GHz band MIMO antenna system . . . . .	131



5.24	Isolation between the antenna elements of the 4-element 5 GHz band MIMO antenna system . . . . .	132
5.25	Isolation between the antenna elements of the 8-element 5 GHz band MIMO antenna system . . . . .	133
5.26	Current distribution on the 4-element MIMO antenna system at 5.08 GHz when element 1 is active, (a) Top side, (b) Bottom side	134
5.27	Current distribution on the 4-element MIMO antenna system at 5.08 GHz when element 4 is active, (a) Top side, (b) Bottom side	135
5.28	Current distribution on the 8-element MIMO antenna system at 5.04 GHz when element 1 is active, (a) Top side, (b) Bottom side	136
5.29	Current distribution on the 8-element MIMO antenna system at 5.04 GHz when element 3 is active, (a) Top side, (b) Bottom side	136
5.30	TARC curves for the 4-element 5 GHz band MIMO antenna system	138
5.31	TARC curves for the 8-element 5 GHz band MIMO antenna system	139
5.32	Correlation coefficient curves of the 4-element 5 GHz band MIMO antenna system . . . . .	139
5.33	Correlation coefficient curves of the 8-element 5 GHz band MIMO antenna system . . . . .	140
5.34	Normalized Gain patterns of the 4-element MIMO antenna system measured at 5.08 GHz. (a) x-z plane (b) y-z plane [Black = Element 1, Pink = Element 2, Blue = Element 3, Red = Element 4] . . .	141
5.35	Normalized Gain patterns of the Element 1 to 4 of 8-element MIMO antenna system measured at 5.04 GHz. (a) x-z plane (b) y-z plane [Black = Element 1, Pink = Element 2, Blue = Element 3, Red = Element 4] . . . . .	141
5.36	Normalized Gain patterns of the Element 5 to 8 of 8-element MIMO antenna system measured at 5.04 GHz. (a) x-z plane (b) y-z plane [Black = Element 5, Pink = Element 6, Blue = Element 7, Red = Element 8] . . . . .	142
5.37	Average channel capacity of the 5 GHz band MIMO Antenna Systems	143

5.38 CDF of the channel capacity of the 5 GHz band MIMO antenna systems . . . . .	144
5.39 Geometry of the 2-element LTE band MIMO Antenna System (a) Top side , (b) Bottom side . . . . .	145
5.40 Fabricated 2-element LTE band MIMO Antenna System (a) Top side , (b) Bottom side . . . . .	146
5.41 S-parameters of the 2-element LTE band MIMO antenna system .	148
5.42 Current distribution on the 2-element LTE band MIMO antenna system when element 1 is active, (a) at 750 MHz, (b) at 1170 MHz, (c) at 1700 MHz, (d) at 2350 MHz . . . . .	149
5.43 TARC curves of the 2-element LTE band MIMO antenna system .	149
5.44 Measured gain pattern of the proposed MIMO antenna system (a) 750 MHz x-z plane, (b) 750 MHz y-z plane, (c) 1170 MHz x-z plane, (d) 1170 MHz y-z plane, (e) 1700 MHz x-z plane, (f) 1700 MHz y-z plane, (g) 2350 MHz x-z plane, (h) 2350 MHz y-z plane . . . . .	152
5.45 Geometry of the 4-element ISM band MIMO antenna system with SRR based isolation, (a) Top side, (b) Bottom side . . . . .	155
5.46 Measured S-parameters of the 4-element ISM band MIMO antenna system with SRR based isolation . . . . .	155
5.47 Surface current density on the 4-element MIMO antenna system when antenna element 1 is active,(a) Top side (without isolation structure), (b) Bottom side (without isolation structure), (c) Top side (with SRR based isolation structure),(d) Bottom side (with SRR based isolation structure) . . . . .	157
5.48 Radiation patterns with and without the SRR based isolation structure, (a) Antenna element 1, (b) Antenna element 4 . . . . .	160
5.49 Simulated S-parameters of the 4-element MIMO antenna system operating in the 5 GHz band with SRR based isolation . . . . .	161

# THESIS ABSTRACT

**NAME:** Muhammad Umar Khan

**TITLE OF STUDY:** Metamaterial Inspired Antenna Miniaturization for MIMO System Applications

**MAJOR FIELD:** Electrical Engineering

**DATE OF DEGREE:** January 2015

*Fourth generation (4G) wireless communication standards have adopted multiple-input-multiple-output (MIMO) systems to cater for high data rate requirements. For a successful implementation of these standards, the antenna of MIMO systems is an important design consideration. The MIMO systems require that their antenna with multiple elements should have high port isolation and low correlation between its elements. The wireless devices, where these systems are implemented require that their antenna must be low-profile and fit within the enclosing of the device. Together, these restrictions make the design of antennas for the MIMO systems a challenging task. Antenna is still one of the largest parts of any communication device. A standard antenna dimension correspond to half-wavelength of its operating frequency. Decreasing the size of antenna beyond this limit severely*

*degrades its radiation characteristics. For MIMO systems, accommodating multiple antenna elements in a limited space is therefore a serious issue which requires novel antenna miniaturization techniques. These techniques should try to reach the best possible practical limit of small antennas while maintaining reasonable radiation characteristics. In this work, antennas for MIMO systems are designed for various standards between 0.7 GHz to 6 GHz. All the designed antennas are planar, low-profile and uses modified microstrip patch antennas (MPAs) as the elements. A metamaterial (MTM) inspired technique is proposed which uses the complementary split-ring resonator (CSRR) for MPA miniaturization. We first thoroughly investigate the miniaturization technique and then develop design procedures based on it. An 80% miniaturization in the patch area is achieved using the proposed method in the 700 MHz band and 65% miniaturization is achieved in the 5GHz band. The miniaturized MPA thus developed are used to design 2-element MIMO antenna systems in the lower LTE band, 4-element MIMO antenna systems in the ISM band and 8-element MIMO antenna systems in the WiFi band. All the designs are highly compact and conform to the dimensions of a standard wireless device. An MTM-inspired isolation enhancement technique is also used with the proposed antennas. The technique is simple to implement and give a minimum increase of 5 dB in the isolation between antenna elements.*

## مُلخَص الرسالة

الاسم الكامل: محمد عمر خان

عنوان الدراسة: طريقة تصغير للهوائيات المطبوعة باستخدام مواد جديدة و تطبيقاتها في أنظمة متعددة المدخلات و المخرجات

التخصص: الهندسة الكهربائية

تاريخ الدرجة العلمية: يناير 2015

لقد تبنت معايير تقنية الجيل الرابع للاتصالات (4G) الأنظمة ذات المدخل والمخرج المتعددة (MIMO) لتوفير معدل نقل بيانات عالي السرعة. إن الهوائي يكون جزء مهم وحساس من هذه الأنظمة لكي تعمل بنجاح وفاعلية. بالإضافة إلى حاجة هذه الأنظمة إلى عزل عالي الكفاءة بين العناصر المكونة للهوائي لكي تمنع التداخل بينهم. يجب على هذه الهوائيات أن لا تحتل حيزاً كبيراً وأن تؤدي غرضها بأقل كلفة ممكنة ويجب عليها أيضاً أن يتناسب تصميمها وحجمها لوضعها داخل الأجهزة اللاسلكية. هذه المعطيات تجعل من تصميم الهوائيات للأنظمة ذات المدخل والمخرج المتعددة أمراً صعباً، حيث يُعتبر الهوائي من أكبر الأجزاء في أجهزة الاتصالات. إن الحجم الإعتيادي للهوائي يكون نصف الطول الموجي المطابق للتردد الذي يعمل عليه النظام، وتصغير حجم الهوائي إلى أقل من هذا الحد سوف يؤثر سلباً وبشكل كبير على خصائصه وعمله. إن محاولة وضع عدة عناصر للهوائي في أنظمة المدخل والمخرج المتعددة في مساحة صغيرة هو عمل صعب جداً، وهذا الوضع ساعد على تطوير تقنيات تصغير الهوائيات من دون التأثير على خصائصها. هذه التقنيات سوف تصغر من حجم الهوائيات إلى أقصى حد ممكن مع إبقاء جودة عمل الهوائي ضمن الحد المقبول.

في هذا العمل، تم تصميم هوائيات لأنظمة المدخل والمخرج المتعددة للعمل على عدة مقاييس وترددات بين 700 ميقاهرتز إلى 6 قيقاهرتز. جميع الهوائيات تم تصميمها على سطح مستوي ولا تحتل حيزاً كبيراً وذات كفاءة مقبولة. وتم استخدام الهوائيات ذات القطع السطحية المعدلة (MPAs) كعناصر لهوائي النظام. وأيضاً تم وضع طريقة مستوحاة من المواد الخارقة (MTM) تستخدم مرنان مصنوع من قطه حلقيه مكتملة (CSRR) لتصغير الهوائيات. تم في البداية دراسة واستكشاف الطريقة ثم تطبيقها على الهوائيات. تم تصغير الهوائي بنجاح بنسبة 80% للعمل على التردد 700 ميقاهرتز وبنسبة 65% على التردد 5 قيقاهرتز. تم في هذا البحث استخدام الهوائيات المصغرة لصنع هوائي ذو عنصرين لأنظمة المدخل والمخرج المتعددة (MIMO) للعمل على النطاق المنخفض لتقنية ال(LTE)، وتم استخدامهم أيضاً لصنع هوائي ذو 4 عناصر لأنظمة (MIMO) للعمل

على نطاق (ISM) وأيضاً لصنع هوائي ذو 8 عناصر لأنظمة ال(MIMO) للعمل على نطاق الشبكة اللاسلكية (WiFi). جميع التصاميم ذات أحجام صغيرة ويمكن استخدامها في الأجهزة الذكية صغيرة الحجم. وتم في هذا البحث أيضاً استخدام طريقة أخرى مستوحاة أيضاً من المواد الخارقة (MTM) لزيادة العزل بين عناصر الهوائيات. الطريقة سهلة التطبيق وتوفّر عزل بمقدار 5 ديسيبل بين العناصر المكوّنة للهوائي.

# CHAPTER 1

## INTRODUCTION

### 1.1 Background

The use of wireless devices is widespread. From personal use to industrial, medical and military applications, they are everywhere and encompass different applications. For spectrum sharing among various wireless applications and to define set of protocols for wireless communication, various standards are specified. These standards evolve according to the current and future needs and help in the design of communication system architecture, communication devices, and their seamless integration. Some of the widely used wireless standards along with their bands of operation and applications are shown in Table 1.1. The radio broadcast standards are simple and mainly define the channel and bandwidth. The bluetooth standard is defined for short range communications and uses the licence free band at 2.45 GHz. ZigBee is another wireless standard which utilizes the 915 MHz and 2.45 GHz unlicensed bands. It is defined to make personal area networks for small,

Table 1.1: Commonly Used Wireless Standards with their Applications

Wireless Standards	Frequency Band(s)	Application
Radio Broadcast	148.5 kHz - 283.5 kHz, 530 kHz - 1710 kHz, 3 MHz - 30 MHz, 88 MHz - 108 MHz	Long wave AM radio, Medium wave AM radio Short wave AM radio FM radio
WiFi (802.11)	2.45 GHz, 5 GHz band	Wireless networks
Bluetooth	2.45 GHz ISM band	Short range communication
ZigBee	915 MHz, 2.45 GHz ISM bands	Remote control, sensor application
CDMA	Several bands between 400 MHz - 2.7 GHz	Cellular communication
WiMaX (802.16)	Several bands between 2 GHz - 11 GHz	Cellular communication
GSM	890 MHz - 960 MHz , 1710 MHz-1880 MHz	Cellular communication
LTE	Several bands between 700 MHz - 3 GHz	

low power devices and mostly used in remote control devices, wireless sensors and automation applications.

Among many applications of wireless communication, the most dramatic growth has been witnessed by the cellular mobile communications in the past two decades. It has profoundly changed the way we communicate using voice, video or data services. Today, more than 6.8 billion mobile phones are in use around the globe and mobile communication services are available almost in every country. According to Gartner, an IT research and market survey company, around 1806 million smart phones were sold in the year 2013 [1]. The demand for the smart phones will increase steadily and in the year 2017, there will be a requirement of more than 2 billion smart phones in the market. Table 1.2 shows the demand of different devices in the previous and the coming years.



Table 1.2: Market Forecast of Wireless Mobile Devices [1]

	<b>2012</b>	<b>2013</b>	<b>2014</b>	<b>2017</b>
	(in millions)			
<b>Laptops</b>	341	315	302	271
<b>Tablets</b>	116	197	265	468
<b>Mobile Phones</b>	1746	1875	1949	2129
<b>Total</b>	2212	2410	2554	2964

Due to the huge market of cellular mobile communications, this area has drawn a lot of attention among researchers. That is why the cellular communications has witnessed very swift technological advancements. These advancements have taken place in every field related to cellular communications. These include the evolution of new standards which outline the architecture of cellular communication as well as the design of mobile terminal equipment.

Current and future mobile phones and tablets will work on the 4th generation (4G) standard (*also called the long term evolution (LTE) for mobile communications*) while almost all such devices also provide WiFi services to connect with wireless local area networks (WLAN). The new 4G standards as well as WiFi standards (802.11) are designed to cater for high data rate requirements. In 4G standards, several bands are designated which starts from 700 MHz and goes up to 3 GHz [2]. WiFi on the other hand operates in 2.4 GHz and 5 GHz bands [3]. In both of these standards, multiple-input-multiple-output (MIMO) systems are adopted to provide greater spectral efficiency and enhance the reliability of the communication. In the lower bands of the LTE, up to  $2 \times 2$  channel MIMO systems are recommended while in the higher 5 GHz WiFi bands, up to  $8 \times 8$  channel MIMO

systems are proposed. These standards therefore, require challenging design considerations when designing the communication block as well as radio-frequency (RF) front-end of the mobile phones and tablets.

## 1.2 Motivation

An important part of any wireless communication device is its antenna. Although it was a very simple structure *e.g. extended wire* in most of the initial wireless communication devices and did not receive much attention during the design process, its design has become much more complex and now receives special consideration. The performance of the communication device greatly depends on the design of its antenna. Thus, with the advent of the new WiFi and 4G standards, several research groups have pursued to present novel antenna designs for these standards. The special focus is on the design of antennas for mobile terminal devices, owing to its huge market. The main design consideration for such antennas comes from the guidelines within the standards as well as from the shape and mechanical structure of the mobile terminal device. The new standards require that the antenna of the device consist of multiple antenna elements called the ‘MIMO antenna system’. The MIMO antenna system(s) must cover the LTE bands and WiFi band(s) with good radiation and performance characteristics. The mobile terminal design requires the antenna to be low-profile with small form factor (*i.e. completely enclosed in the device and occupying minimal space*). Together, these requirements make the design of MIMO antenna system very challenging espe-

cially in the lower LTE bands.

These challenges have motivated the antenna designers to come up with novel antenna miniaturization methods, to increase isolation between closely placed antenna elements and to design low profile MIMO antennas with good performance characteristics. The real hurdle lies in the fact that a conventional antenna has a minimum dimension of a half-wavelength corresponding to its resonant frequency. This length is 210 mm at the lower LTE band which is much greater than the size of a normal mobile terminal device. While other parts of a communication device have seen a considerable reduction in their size thanks to the use of the micro-fabrication technology, reducing the size of the antenna is still a difficult and challenging task. Thus, without appropriate miniaturization, design of MIMO antenna system for mobile terminal devices is impossible.

Any decrease in the size of antenna beyond this limit greatly degrades the performance of the antenna. Theoretically, a small antenna has limits on the bandwidth and efficiency that it can achieve [4]. Many researchers are constantly struggling to develop designs and methods for miniaturized antennas that achieve the best possible performance close to the theoretically defined limits. Such efforts are more focused towards the miniaturization of planar printed antennas since they are rugged and best integrated with other electronics in the mobile communication device.

### 1.3 Work Contribution

This research work is also aimed at developing a methodology for the design of printed low-profile miniaturized antennas for use as elements of a MIMO antenna system in the 700 MHz to 5 GHz range. A microstrip patch antenna (MPA) is investigated for miniaturization and for subsequent use as the basic element of low-profile and planar MIMO antenna systems. The goal is to develop a miniaturization technique which: (i) effectively reduces the size of MPA while keeping the design planar; (ii) is applicable for the design of MPA in several bands; and (iii) has minimum effect on the performance of the antenna.

Using the miniaturized MPA elements, MIMO antenna systems are designed for various bands which conform to the dimensions of standard mobile devices. The antennas are characterized by measuring their performance characteristics separately as well as at the system level by using a software defined radio (SDR) platform. The **main contributions** of this dissertation work are as follows;

- The development of a metamaterial (MTM) inspired technique for MPA miniaturization which can be applied to design the antenna for various bands. The method provides more than 80% miniaturization in the patch area in the 700 MHz band. A design methodology based on the proposed technique as well as its comparison with other known techniques is presented.
- The proposed design is analyzed using the theory of characteristic modes. The modes supported by the design, radiation characteristic corresponding to the mode as well as excitation of the modes are analyzed using the

application of the theory.

- Design and performance evaluation of 2-element, 4-element and 8-element MIMO antenna systems based on the proposed miniaturized MPA elements for 700 MHz LTE band, 2.4 GHz Wifi/LTE band, and 5 GHz Wifi band, respectively.
- System level characterization of the proposed MIMO antenna systems in a real wireless indoor environment.
- An MTM-inspired isolation enhancement technique for the proposed MIMO antenna systems.

## 1.4 Dissertation Overview

The dissertation is divided into six chapters. In chapter 2, an overview on the theoretical limits on small antenna is given. Various techniques found in literature for MPA miniaturization are discussed and analyzed in the same chapter.

In chapter 3, a novel technique is proposed for MPA miniaturization. The technique is thoroughly analyzed and discussed. The analysis is based on parametric simulations as well as characteristic mode analysis (CMA) based theoretical technique. A design methodology is developed based on the proposed technique for the design of small MPA. The proposed miniaturization technique is also compared with other techniques found in literature.

Chapter 4 presents the performance evaluation metrics to assess the perfor-

mance of a MIMO antenna system. A literature survey on the current state and trends in the design of MIMO antenna systems is also given in the same chapter.

Chapter 5 presents the proposed designs of the various MIMO antenna systems in this work. The designs are made in the lower LTE band, the ISM band and the new 5 GHz WiFi band. A complete evaluation of these designs based on MIMO performance metrics is given. A novel isolation enhancement technique for the proposed MIMO antenna systems are also given.

Chapter 6 summarizes the research work, give conclusions and future work.

## CHAPTER 2

# ELECTRICALLY SMALL ANTENNAS AND MINIATURIZATION OF MPA

Although initial antennas were mostly wire-type, and wire antennas are still widely used in many applications, considerable attention has been given to printed antennas during the past few decades. Printed antennas are the foremost choice for use with mobile devices application. This is mainly due to their low-profile, ease of fabrication and compatibility with integrated circuit technology. A printed antenna is normally fabricated by using printed circuit technology. Printed antennas were first presented during the 50's of the last century, but they didn't gain much importance until the early 80's. Many designs of printed antennas have appeared in the literature since the 80's. Several of these designs were thoroughly analyzed analytically as well as numerically and their theory was developed for

better understanding of their performance characteristics. The most commonly used printed antennas are microstrip patch antennas (MPAs), printed monopoles and dipoles, slot antennas, loop antennas, and printed inverted F-shaped antennas (PIFA).

MPA is a well known planar printed antenna, whose theory of operation is well developed. Due to its better understanding, and therefore ease of its design, it has received considerable attention in literature. There are hundreds of research articles on MPA and it is the topic of more than a dozen books [5]. Like any other resonant antenna, a standard MPA also has dimensions equal to half-wavelength corresponding to its operating frequency. Due to the low-profile requirements and compact size of most of the current wireless devices, the conventional MPA fails to be a contender for their antenna due to its size especially in the lower bands. It becomes further useless to be considered as an element of MIMO antenna system in the LTE and WiFi bands for these devices. Any attempt to use the MPA for such devices therefore require it to be miniaturized beyond its conventional dimensions.

It was noted long time ago that while other electronics were getting smaller and smaller, the field of antennas and propagation was immune to digitization and miniaturization [4]. Nevertheless, many attempts were made to understand the limits on the size of antenna theoretically. This topic has been of interest for more than a half century and even today, it receives considerable attention. Various attempts have been made to analyze effect of antenna size on its bandwidth and



gain and to find a relation between size, bandwidth and gain of antenna. It is well established now that the size of antenna puts a fundamental limit on the bandwidth and gain it achieves. Although, most of the work presented in literature under the topic of electrically small antennas (ESA) is theoretical in nature and does not clearly mention the methods to miniaturize a particular kind of antenna, yet it gives a good insight into ESA and helps in better analysis of ESA designs.

With the help of novel materials and/or the intelligent design of antenna structure, many designs have been presented in literature which have resulted in the miniaturization of antennas of various kinds. Like all other antennas, MPA has also received such attention and several research articles have appeared in literature which presents various methods to reduce the size of the MPA.

This chapter starts with an overview of the theoretical work on the fundamental limits of ESAs. The theory gives the fundamentals of ESA and the limits of such antennas. Since the focus of this work is on the miniaturization of MPA, it then discusses the basics of MPA followed by a summary of research work that has appeared in literature related to the miniaturization of the MPA.

## **2.1 Electrically Small Antennas (ESA)**

It is well known that for a resonant antenna, to operate with good radiation characteristics, a minimum dimension of half-wavelength is required. Any attempt to decrease the size beyond the half-wavelength results in degradation of the performance of the antenna. However, there was always a need to have small antennas.

Therefore, many studies were undertaken to know the limits of antenna size and to understand how the size reduction would affect the radiation performance of an antenna.

The pioneer efforts on this topic can be traced in the work of Wheeler that was carried out in 1947 [6]. He was the first one to note that the size of antenna imposed a fundamental limit on its bandwidth. Thus, reducing the size of antenna resulted in a decrease in its bandwidth. Although he made rough approximations which were true for a very small antenna, his analysis laid the foundation for other work to follow on the same topic. Today, the limits of a small antenna are well known. The ESA is defined as an antenna, whose maximum dimension is less than  $\lambda/2\pi$ . Another commonly used definition of ESA is :

$$ka < 0.5 \tag{2.1}$$

where  $k$  is the wave number and  $a$  is the radius of a sphere enclosing the antenna as shown in Fig. 2.1. The sphere enclosing the antenna is called "*Chu – Sphere*". This term has been widely used in most of the analysis of the ESA. Another commonly accepted definition of ESA is that the antenna satisfies the condition  $ka < 1$  [4].

The main performance measures of an ESA are its size, Q-factor (*or bandwidth*), gain and efficiency. Since the size of an antenna limits its bandwidth, most of the theoretical work was focused on finding the theoretical lower limit of ESA's Q that it could achieve. The bandwidth of antenna is inversely related to

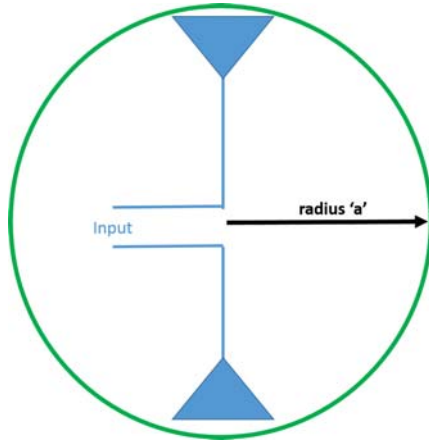


Figure 2.1: A ESA enclosed in a Chu-Sphere.

its  $Q$ -factor. Another important parameter of small antenna is its radiation efficiency. As the size of the antenna decreases, its radiation resistance also decreases and loss resistance starts to dominate. This results in decrease in the radiation efficiency of ESA. These losses are mainly due to frequency-dependent conduction and dielectric losses in the antenna. In some recent work [7], it is shown that by careful design of ESA, a high efficiency is possible at the loss of directivity of antenna. However, as shown in the subsequent section of this chapter while reviewing the miniaturized MPA designs, it is found that most of the practical ESA designs reported in literature had low radiation efficiency. Gain is another parameter of interest in ESA. Since the size of antenna hits on its efficiency or/and directivity, the gain of ESA is always low. Some of the work has, therefore, tried to find the theoretical limit of maximum gain to  $Q$  ratio that an ESA can achieve. In his initial work, Wheeler used a lumped circuit element representation of ESA. He introduced a term *radiation power factor* (RPF) and analyzed the ESA for RPF. The RPF was inverse of the  $Q$ . Since, all of the later work derived the  $Q$  for

ESA, the results of Wheeler's work were also translated into  $Q$ . Thus according to Wheeler's work, the theoretical minimum  $Q$  that an ESA could achieve was given by;

$$Q_{min} = \frac{1}{(ka)^3} \quad (2.2)$$

His work also showed an important point that the antennas which best utilized the volume of sphere enclosing them had the minimum possible  $Q$ .

Many other works used different approaches to find ESA's  $Q$  and reached almost to the same answers as that derived by Wheeler. All these theoretical work gave a good insight into the analysis of ESA and also hinted that in order to design the best possible ESA, the design must use the maximum volume of Chu sphere. The design of small antennas therefore is a an art of compromise between size, bandwidth and gain.

## 2.2 Microstrip Patch Antenna

MPAs are fabricated by placing a conductor on a substrate backed by a ground plane. While they can be designed in various shapes, circular and rectangular patches (see Fig. 2.2 & Fig. 2.3) are the ones that are widely used, since their design procedure is simple and well developed [8]. MPAs have several advantages; (i) they have been extensively studied and their theory is well understood, making them easy to design; (ii) their planar geometry makes them easy to fabricate and integrate with other electronic devices; (iii) they can be fabricated on a variety of cheap available substrates, making them a cost-effective choice for many ap-

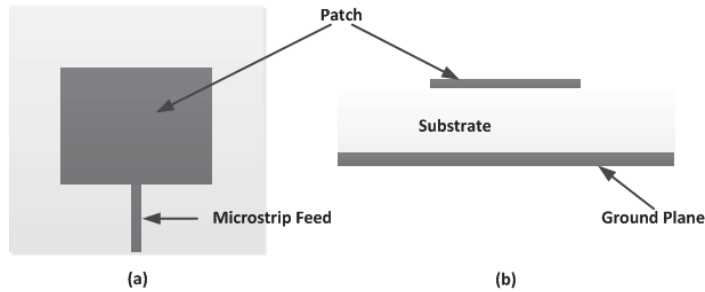


Figure 2.2: A microstrip line feed excited rectangular patch antenna, (a) Top view, (b) Side view.

plications; and (iv) they are rugged and low profile, which make them ideal for use in a number of practical applications such as in GPS receivers, Tablets, Personal digital assistants (PDAs), and so on. In addition to circular and rectangular shapes, MPAs with other geometries also exist, for instance triangular and annular ring-slot shapes [8].

MPAs are typically analyzed by using the cavity model [9]. An MPA can be considered as a cavity filled with a dielectric with non-PEC side walls. Thus the radiation from this cavity takes place due to leakage from these side walls. To find the radiation characteristics and resonant frequency of the MPA, the fields inside the cavity are solved first. The top and bottom parts of the cavity are considered as perfect electric conductors (PECs) while the sides are assumed to be perfect magnetic conductors (PMCs). The field distribution inside the cavity is found by applying appropriate boundary conditions on the cavity walls. The solution is then used to find the resonant frequency of the patch for different modes, as well to determine as the radiating fields. The input impedance and the quality factor ( $Q$ ) of the antenna are also obtained from the same model. The resonant frequency of a rectangular MPA is a function of the material properties of the

substrate, its thickness and the dimensions of the patch. The resonant frequency ( $f_r$ ), obtained from the cavity model, is given by [10]:

$$(f_r)_{mnp} = \frac{1}{2\pi\sqrt{\mu\epsilon}} \sqrt{\left(\frac{m\pi}{h}\right)^2 + \left(\frac{n\pi}{L}\right)^2 + \left(\frac{p\pi}{W}\right)^2} \quad (2.3)$$

where  $h$  is the height of the substrate,  $L$  is the length of the patch,  $W$  is the width of the patch,  $\mu$  is the permeability of the substrate and  $\epsilon$  is the permittivity of the substrate. The integers  $m$ ,  $n$ , and  $p$  correspond to the modes of operation. In a standard MPA,  $h \ll L$  and  $h \ll W$ . If the condition  $h < W < L$  is met, the lowest resonance corresponding to the dominant mode occurs when  $m$ ,  $n$  and  $p$  are 0, 1 and 0, respectively. The resonant frequency of the dominant mode is given by:

$$(f_r)_{010} = \frac{1}{2L\sqrt{\mu\epsilon}} \quad (2.4)$$

Apart from the rectangular MPA, the theory of circular MPAs (see Fig. 2.3) is also well developed and it is also widely used [10]. The circular MPA can also be analyzed by using the cavity model [9]. In this case, the cavity is circular with its top and bottom surfaces are assumed to be PEC discs while the boundary around the circular periphery of the cavity is assumed to be PMC. By solving for field distribution in the cavity, various parameters of the antenna are found. The resonant frequency of the dominant mode of a circular patch of radius  $d$  is given by:

$$f_r = \frac{1.842 \times c}{2\pi d \sqrt{\epsilon_r}} \quad (2.5)$$

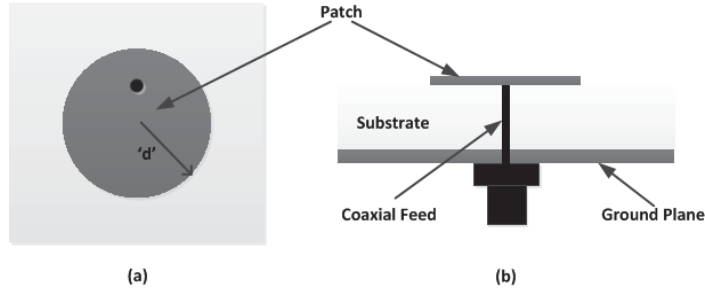


Figure 2.3: A circular patch antenna with solid probe feed, (a) Top view, (b) Side view.

where  $c$  is the speed of light and  $\epsilon_r$  is the permittivity of the patch substrate.

Transmission line theory is also used to model the MPA. It offers a simpler model and provides more intuitive understanding. However, it yields less accurate results as compared to those derived from the cavity model. In this model, a rectangular MPA is represented by two radiating slots separated by a low impedance transmission line of length  $L$  [10]. By finding the equivalent admittance of each slot, different antenna parameters including the resonant frequency and resonant input resistance is calculated.

Full-wave models are also used to determine the design parameters and the performance characteristics of the MPA. These models often use computer-intensive numerical techniques such as the Finite-Difference Time-Domain (FDTD), the Finite Element Method (FEM), or the Method of Moments (MoM), to solve for the fields in complex geometries; however, they provide little physical insight. Nonetheless, with the availability of commercial full-wave solvers such as HFSS, FEKO, WiPL-D, IEEA, etc., and powerful computing platforms on which to run these solvers, full-wave methods are now almost exclusively used to design the MPAs.

An MPA can be excited in several different ways. Most common methods include the coaxial-line feed excitation and the microstrip transmission-line feed [10]. In the transmission-line feed method, a conducting strip is attached to the edge of the patch. This is a simple way to excite the MPA and antenna-feed system can be easily fabricated. Fig. 2.2 shows a rectangular MPA excited by a microstrip line feed. In the coaxial-line feed method, a coaxial cable whose inner conductor is connected to the patch while the outer conductor is attached to the ground plane is used. It provides a simple way to match the antenna input impedance and it is also easy to fabricate. Fig. 2.3 shows a circular MPA excited by a coaxial-line feed method.

Although both of these methods are easy to implement, their use limits the operating bandwidth of the MPA. There are alternate approaches for feeding the MPAs, such as using the proximity-coupled and aperture-coupled feeding methods. However, they lead to complex designs and are used very rarely, although they can provide wider operating bandwidths.

MPAs suffer from the problem of high  $Q$ ; and, hence their bandwidth is limited. Several techniques for enhancing the bandwidth of MPAs do exist and they can be found in [5] and [9]. As mentioned earlier, desirable attributes such as ease of its integration with other components, good radiation characteristics and low cost, make the MPA one of the foremost choices in thousands of practical applications.



## 2.3 MPA Miniaturization Techniques

In principle, there are two ways to minimize the MPA. The first method is to change the material properties of the MPA substrate such that the effective wavelength in the substrate region is decreased. The second method is to change the geometry of the antenna in such a way so as to increase the electrical size (current path). Various methods for MPA miniaturization have been reported in the literature that are based on these two major techniques. They are grouped into five categories in this work and are described in detail in the following sub-sections.

### 2.3.1 Material Loading

The simplest way to decrease the size of an MPA is to use a substrate with a high permittivity ( $\epsilon_r$ ). The length and width of the patch are inversely proportional to the square root of ( $\epsilon_r$ ). However, such a miniaturization method results in an increased level of surface wave excitation within the substrate and results in lower bandwidth as well as decrease in radiation efficiency. The truncation of the ground plane not only results in poor polarization purity but also changes the radiation characteristics of the MPA.

Various studies have investigated different materials as well as configurations to effectively use the above approach to miniaturize an MPA. In [11], MPAs with relatively thick substrates ( $0.02\lambda_o$  to  $0.03\lambda_o$ ) and with relative permittivities of 10 and 13 were analyzed experimentally. The input impedances and radiation characteristics of these antennas were found to be different from those of a con-

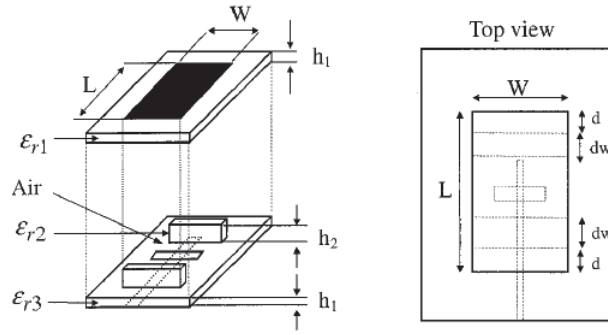


Figure 2.4: An MPA with dielectric bars underneath the patch [12].

ventional patch. The input impedances were less than the one predicted by the theoretical models for MPAs with thin substrates. A four-element array was fabricated by using this thick substrate in which distortion of the radiation pattern was observed in the E-plane.

While designing a miniaturized MPA for Korean Cellular band, the authors of [12] employed a partially filled high-permittivity substrate. They used a low permittivity substrate and placed rectangular-shaped dielectric bars of high permittivity underneath the radiating edges of the patch, as shown in Fig. 2.4. This resulted in a 50% decrease in the antenna size while it achieved a fractional bandwidth of 10% and a gain of 6 dB.

Many groups have investigated the use of ceramic substrates for MPA miniaturization. In [13], several MPA designs were investigated by using various types of ceramic substrates. A square MPA was fabricated on a low temperature co-fired ceramic (LTCC) substrate of  $\epsilon_r = 100$ . A reduction of the area of the patch by a factor of 8 was achieved as compared to that of a conventional patch printed on the FR4 substrate. However, the substrate was chosen to be relatively thick

( $0.031\lambda_o$ ) to mitigate the problem of low bandwidth. The antenna had a fractional bandwidth of 7.2% and a gain of 2.8 dBi at 1.88 GHz. Another MPA was fabricated by using textured ceramic substrate, which a mixture of LTCC and Stycast, and which resulted in an effective permittivity of 23.5. The MPA printed on this substrate was 2.5 times smaller than the conventional MPA fabricated on an FR4 substrate. The measured gain of the antenna was 3 dBi and it had a fractional bandwidth of 9.1% centered around 1.7 GHz. The bandwidth of the MPA was also found to improve, albeit at the expense of its gain, by using a bow-tie shape. Thus, through various design choices, significant miniaturization was achieved using ceramic substrates while maintaining good antenna gain as well as bandwidth.

In [14], MPAs on different ceramic substrates were investigated experimentally. The substrates used were barium-titanate with  $\epsilon_r = 37$  and neodymium-titanate with  $\epsilon_r = 85$ . The truncation of the ground plane was also analyzed. The MPAs designed on these ceramic substrates were found to have very limited bandwidths. For a resonant frequency of around 1.5 GHz, the antenna was found to have a bandwidth of only 2.4 MHz. Also, the ground plane reduction resulted in nearly omni-directional radiation patterns.

MPA miniaturization using magnetodielectric substrate has been analyzed in detail in [15]. A magnetodielectric substrate design was presented in [16]. The MPA fabricated on the proposed substrate was found to be 65% smaller, as compared to a conventional patch resonating at 2.45 GHz. The MPA had a fractional

bandwidth of 0.5% and radiation efficiency was 45%.

Many other works have also appeared in literature which followed approaches that are similar to the ones mentioned previously. A modified ceramic substrates was used in [17] while [18] used a perforated substrate to miniaturize an MPA. In summary, ceramics substrates and modified substrates can provide a significant reduction in the patch size. However, the major disadvantages of this method of size reduction are the cost of such substrates as well as reduction of their bandwidth.

### 2.3.2 Shorting and Folding

Folding an MPA and the use of shorting posts has been used to reduce the size of MPAs, and to render it electrically small [8]. For a half-wavelength rectangular MPA, the E-field distribution under the patch has a sinusoidal pattern with a maximum E-field at the radiating edges and zero in the middle. If an electric wall is placed at the middle of the patch, and the other half is removed, it would still resonate at the same frequency. Such a patch is called a quarter-wavelength MPA. The theoretical analysis shows that a quarter-wavelength patch has the same Q as that of its half-wavelength counterpart [8]. However, because the quarter-wavelength patch only has a single radiating edge of quarter wavelength patch, its radiation efficiency is lower than that of a half wavelength MPA.

In the practical implementation of a quarter-wavelength MPA, placing a continuous conducting sheet at the edge between the patch and the ground plane is

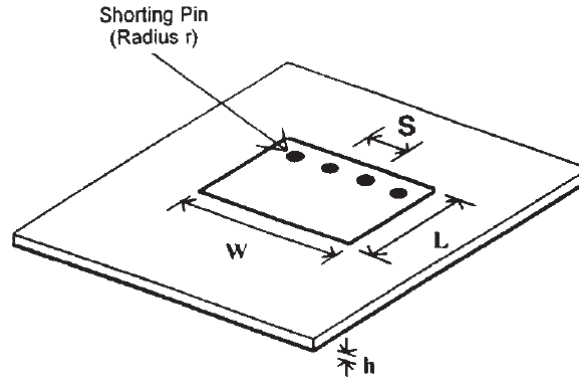


Figure 2.5: A quarter-wavelength MPA fabricated by using shorting posts [8].

difficult. An easier approach to fabricating a quarter-wavelength MPA is to add an array of shorting pins near the edge of the patch, as shown in Fig. 2.5.

A number of reports have appeared in literature that present the design or analysis of miniaturized MPAs using the shorting or folding techniques [19–27]. In [19], a shorted patch was folded to make it a  $\lambda/8$  MPA. The radiation efficiency of the antenna was found to be 90% while it had a bandwidth of 4%. The schematic diagram of the shorted-folded patch is shown in Fig. 2.6. In [27], the results of a parametric study of using a single, double or multiple shorting posts with a circular MPA have been presented. Various parameters were analyzed. It was found that the MPA size could be reduced by more than a factor of 3, as compared to a standard patch via the use of optimal placement of the shorting posts. A theoretical analysis of an MPA with a shorting post has been provided in [24].

MPA can therefore be miniaturized by using folding and shorting. However, this method complicates the geometry of the MPA at times and also makes it non-planar, which adds to the complexity of the structure and its conformity. However, when properly applied, this method has little effect on the efficiency of

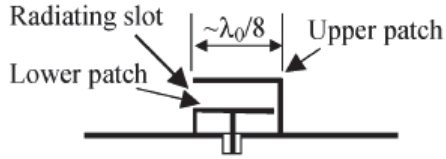


Figure 2.6: A  $\lambda/8$  shorted/folded MPA [19].

the antenna.

### 2.3.3 Reshaping or Introducing Slots

An MPA can also be miniaturized by making changes in the shape of the patch or by adding slots in the MPA. Miniaturized patches can be shaped and optimized to obtain a large electrical length in limited space by using the Genetic Algorithm (GA) [28], running on high performance computing platforms. Fractal geometries are also used to obtain miniaturized MPAs with good efficiency [29], [30]. Fractals are space filling contours in which electrically large features can be effectively packed in a relatively small space, with a reduction in bandwidth, however.

A miniaturized MPA suffers from higher ohmic losses, which lead to a lower radiation efficiency. To mitigate this problem, an engineered conductor has been presented in [31], which consists of layers of conductors separated by laminations. The total thickness of the conductor was equal to that of the conductor in a conventional MPA. The engineered conductor, separated by laminations, is shown in Fig. 2.7. It helps to increase the gain and efficiency of the small antenna. Such a conductor has also been used with different miniaturized MPAs. It has been shown that the gain and efficiency of antenna improves as the number of

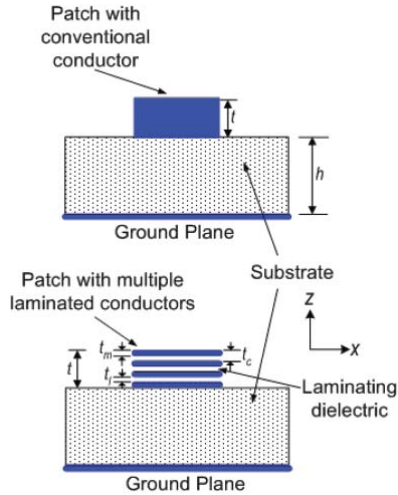


Figure 2.7: Multi-layer engineered conductor for use with miniaturized MPA compared to a conventional conductor used in a MPA [31].

conducting layers is increased. The use of a 5-layer conductor improves the efficiency of a miniaturized antenna by 30% as compared to a conventional single layer conductor.

Several reports [32–41] have appeared in the literature in which the size of the MPA has been reduced by introducing various types of slots in the MPA. A miniaturization of 40% to 75% has been achieved by inserting different types of slots in the MPA. Although this method is widely used in different designs and provide several degrees of miniaturization, this method lacks a general design methodology. Most of the presented designs based on this method had low radiation efficiency and provided wider operating bandwidths when using slots.

### 2.3.4 Modifications of the Ground Plane

MPAs can also be miniaturized by modifying their ground planes. In the general models for MPAs, an infinite ground plane is assumed. However, in any practical

MPA design, the ground plane is finite. For greater miniaturization, the size of the ground plane is further reduced such that at times it is only slightly larger than the patch dimensions. The MPAs with truncated ground planes have been analyzed analytically in various reports [42–44]. It was found that such antennas had poor polarization purity and reducing ground plane size also affected the input impedance. Also, due to edge diffraction, there was significant back lobe radiation which decreases the front-to-back ratio.

Along with reducing the ground plane, many other modifications in the ground plane are possible to miniaturize an MPA. These modification include the insertion of various types of slots in the ground plane. These slots, when properly designed, help to increase the current path within the patch area. This helps to lower the resonant frequency of the MPA and, therefore, leads to size reduction. Many designs have appeared in the literature which use slots in the ground plane to miniaturize the MPA [45–49].

In [45], a single slot of 1 mm width was etched out underneath an MPA to reduce its size. A parametric study was carried out by changing the length and position of the slot underneath the patch. The MPA initially resonated at 2.87 GHz without the slot. Using the optimal placement and length of the slot, the resonant frequency was decreased to 1.38 GHz, which represents a 52% decrease. The size reduction in terms of area of the MPA was 90%. In [46], three slots were etched underneath the patch and its shape was modified which resulted in 50% decrease in terms of the size of the MPA. Similar use of slots in [47],



[48] and [49] resulted in 56% to 83% miniaturization in the size of patch. It is important to note that while all of these reports focused on the miniaturization of MPA, they did not clearly analyze other parameters that are affected by such miniaturization. Therefore, in most of these reports, the effect of miniaturization on antenna efficiency, bandwidth, radiation properties, or cross-polarization levels was not clearly mentioned. Furthermore, at times this information was missing altogether. Also, these reports provided little physical insight into the underlying principles of the miniaturization method. They also did not elaborate on the generic application of the provided method. Specifically, they did not mention any design guidelines based on the slot in ground plane method for various frequency bands.

Another method which made use of an irregular ground structure was presented in [50] for antenna miniaturization. A two-layer substrate was used to fabricate the MPA. The lower substrate had an array of vertically placed small metallic cylinders, and their lower end was touching the ground plane. An array of these metallic structures was placed underneath the four diagonal corners of the patch, which was separated from these metallic structures by using another substrate, as shown in Fig. 2.8. The proposed structure introduced capacitive as well as inductive loadings, and this, in turn, resulted in miniaturization of the antenna. Using this arrangement, a 75.6% reduction in the size of MPA was achieved. The size reduction was accompanied by a bandwidth reduction of the MPA. The antenna resonated at 5.32 GHz in the absence of the irregular ground

structure with a bandwidth of 8.3%. The resonant frequency of the antenna was decreased to 2.635 GHz by using the proposed scheme; however, the bandwidth was reduced to 1.9%. The same technique for size reduction was also successfully demonstrated for a circularly polarized MPA.

Many miniaturized MPA designs utilize defected ground structures (DGS). DGSs have a variety of shapes, including simple ones such as spiral, V-shape, U-shape and H-shape, as well as complex ones such as dumbbell-shaped and splitting resonators (SRR). DGSs have been used with printed antennas for improving their radiation characteristics, as well as for improving the isolation between antenna elements in MIMO/array antenna designs, and for impedance matching of microstrip feed designs [51].

In [52], a DGS of certain shape was proposed for miniaturizing an MPA. The DGS consisted of four connected E-shape slots that were etched out from underneath the MPA. This resulted in a 68% antenna miniaturization in terms of the size of the MPA. The proposed DGS was analyzed and compared with other cross-shaped and dumbbell-shaped DGS-based miniaturized patch antennas. It was shown that the proposed DGS provided greater miniaturization than did the other two DGS-based designs. The use of DGS structures usually provides lower efficiency and yields narrower operating bandwidths. In addition, re-tuning of the antenna is usually needed to compensate for the shift in the resonant frequency due to the alterations of the ground currents especially if the DGS is close to resonant structures.

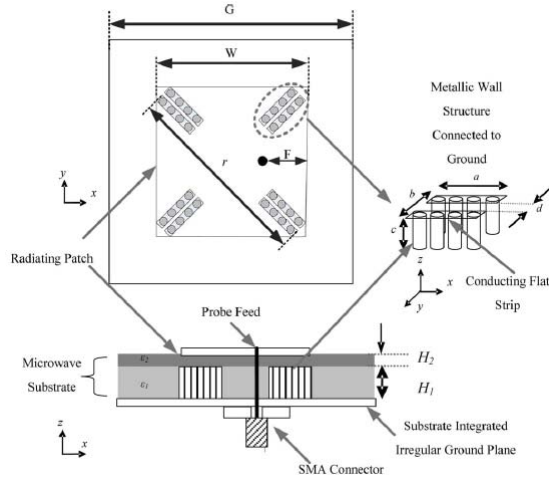


Figure 2.8: A miniaturized MPA on an irregular ground structure [50].

### 2.3.5 Use of Metamaterials

Metamaterials (MTM) are artificially engineered materials designed to provide material properties not readily available commercially. MTMs can be designed to realize materials with near zero values of permittivity; negative permittivity or permeability; or simultaneous negative permittivity and permeability. A material with only negative permittivity is called epsilon negative (ENG) while one with only negative permeability is referred to as a  $\mu$ -negative (MNG) material. A material with both negative permittivity and permeability is called double-negative (DNG). During the past decade, a number of structures have been realized which when arranged periodically, exhibited MTM properties over a certain frequency range. These structures have been of interest to many areas of research and have been widely studied and improved. They have also been used in many RF, microwave and photonics devices to achieve interesting properties.

The concept of MTM as well as MTM structures have also been used to design

various types of antennas with enhanced performance, such as high gain as well as improved efficiency. Additionally, they have been used for the miniaturization of antennas. Two terms are used in literature for antennas utilizing MTM. Ones that make use of ENG, MNG or DNG substrate are called *MTM-based antennas*. Others, that only utilize the MTM unit cell such as the split-ring resonator (SRR), complementary split-ring resonator (CSRR), omega structures, etc., are referred to as *MTM-inspired antennas*. The former exist mostly as hypothetical antennas which are studied theoretically using the ENG, MNG or DNG media. A true realization of MTM-based antenna is not possible. The latter are not truly MTM antennas since they do not make use of ENG, MNG or DNG properties of a MTM. However, since they make use of MTM unit cells, and since they are analyzed using the theories of MTM unit cells, they are referred to as MTM-inspired antennas.

The effect of an MTM substrate on the size of the MPA can be analyzed from the expression of its resonant frequency which can be derived by using the cavity model. From Eq. (2.3), it can be seen that there is an inverse square root relationship between the resonant frequency of the MPA and the permittivity and permeability of its substrate. Consequently, an MPA placed on a homogeneous ENG or MNG substrate will not resonate. Furthermore, no special feature can be realized by using a homogeneous DNG substrate.

In [53] and [54], MPAs on MTM substrates have been theoretically investigated. The equation for the resonant frequency for an annular ring patch on an MTM substrate has been derived in [53]. The geometry of the antenna is shown

in Fig. 2.9. The substrate of the patch was a combination of DNG medium (*called the backward wave (BW) medium in [53]*), and the normal medium with  $\epsilon$  and  $\mu$  values that are both positive (*also called double positive medium (DPS) in the literature*). The DNG formed the inner circle, which was surrounded by the DPS medium. From the derived expression of the dominant resonant mode, it was found that patch miniaturization was possible by carefully selecting the ratios of area filled by the DNG and DPS media and their properties.

In [54], the MPA on MTM substrate have been further analyzed analytically, and numerical results have been presented to validate the analytical ones. A rectangular patch on an inhomogeneous substrate have been analyzed by using the cavity model. The patch was transversally loaded with inhomogeneous substrate as shown in Fig. 2.10. The substrate was composed of two homogeneous substrates of permittivities  $\epsilon_1$  and  $\epsilon_2$ , and permeabilities  $\mu_1$  and  $\mu_2$ , respectively. The ratio of the volumes of the two material media underneath the patch was defined by a term  $\eta$  called the filling ratio.

The antenna is analyzed by using the cavity model. By applying the boundary conditions and solving for the resonant frequency, the solution for the dominant mode is derived from the solution of the following transcendental equation [54]:

$$\frac{k_1}{\omega\mu_1}\tan[k_1\eta W] = -\frac{\omega\mu_2}{k_2}\tan[k_2(1-\eta)W] \quad (2.6)$$

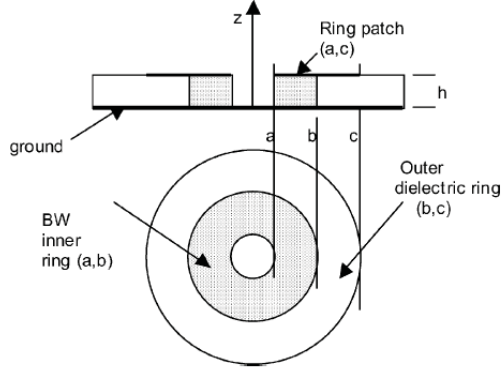


Figure 2.9: Geometry of the annular ring patch on an MTM substrate [53].

Assuming that the patch is small, a solution to Eq. (2.6) is given by:

$$\frac{\eta}{1 - \eta} = -\frac{\epsilon_2}{\epsilon_1} \quad (2.7)$$

The above equation has been analyzed under the assumption that the materials are non-dispersive. It has been shown that by changing the filling ratio and appropriately setting the values of the permittivities of substrates, a size-reduction is possible. Using the above solution, a MPA of  $W = 50$  mm has been analyzed in which the filling ratio was  $\eta = 50\%$ . It has been found that an arbitrarily low resonant frequency when  $\epsilon_1$  was chosen to be  $2\epsilon_o$  and  $\epsilon_2$  was chosen to be  $-2\epsilon_o$ . It was thus demonstrated in [54] that antenna miniaturization was possible by using the combination of DPS and ENG medium. However, further analysis of the antenna by using far field patterns showed that the antenna efficiency was relatively low.

A similar procedure has been followed to determine the resonant frequency of a circular patch [53]. A circular patch of radius  $a$  was analyzed on a substrate

comprising of two different homogeneous media. The core substrate had a permittivity and permeability of  $\epsilon_1$  and  $\mu_1$ , respectively, and had a radius of  $\eta a$ . The outer substrate covered the core substrate and extended up to the edges of the patch. It had a permittivity and permeability of  $\epsilon_2$  and  $\mu_2$ , respectively. The cavity model was used to solve for the resonant frequency of the dominant mode, and a transcendental equation was derived in terms of Bessel functions. Under small antenna assumptions, the solution to the equation was:

$$\frac{1 - \eta^2}{1 + \eta^2} = -\frac{\mu_2}{\mu_1} \quad (2.8)$$

From the analysis of the above equation, it was found that it was possible to design a small antenna by choosing the core as an MNG medium and using DPS for the outer medium. The computed far field radiation patterns showed that such an antenna had better radiation characteristics than a rectangular patch on an ENG / DPS medium.

There are no naturally occurring homogenous ENG or MNG media, and realizing a practical miniaturized MPA based on the above design is not possible unless the above mentioned media are synthesized artificially. Artificially created MNG or ENG structures are frequency dependent and highly dispersive. Furthermore, the size of the unit cells making the MNG or ENG medium sometimes makes it impossible to realize a practical antenna. Nevertheless, many MTM-inspired MPA designs have been presented in the literature among which, many are for MPA miniaturization.

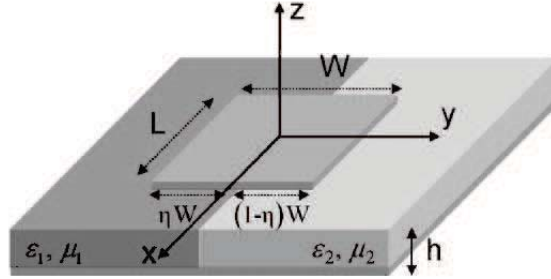


Figure 2.10: Geometry of the rectangular patch on a MTM substrate [54].

A magnetic-permeability-enhanced MTM substrate for MPA miniaturization has been presented in [55]. The substrate consisted of periodically arranged SRRs placed vertically between the patch and the ground plane. This resulted in significant miniaturization of the patch antenna. The area of the MPA was reduced by a factor of 10 as compared to a conventional MPA printed on an FR4 substrate. However, since the design called for a vertical arrangement of the SRRs, the substrate was much thicker than the normal substrate.

In [56], an MTM-inspired technique was used for MPA miniaturization. A CSRR was inserted in the substrate horizontally between the circular patch and the ground plane, which resulted in a decrease in antenna size as well as its bandwidth. This decrease was 75% at 2.45 GHz, as compared to that of a conventional MPA fabricated on an FR4 substrate. However, this was also accompanied by a decrease in the bandwidth and the radiation efficiency of the antenna. The antenna had a fractional bandwidth of only 0.4% and an efficiency of 28.1%.

An MNG medium created by three helices was placed between a circular patch and the ground plane to reduce the size of the patch [57]. This resulted in 60% miniaturization in the patch area. The antenna resonated at 735 MHz with a



Table 2.1: Literature on MPA Miniaturization Grouped According to the Technique Used

<b>Tech.</b>	Material Loading	Folding & Shorting	Reshaping or Introducing Slots	Modification of the Ground Plane	Use of MTM
<b>Ref.</b>	[12]–[18].	[19]–[27].	[28]–[41].	[42]–[50], [52].	[53]–[58].

fractional bandwidth of 0.5% and a maximum gain of -7.9 dBi. In [58], an 80% reduction in the size of patch was achieved by loading it with MTM transmission-line.

In summary, various MTM-inspired techniques have been implemented for MPA miniaturization. While they have been successful in reducing the size, this has been at a substantial cost in terms of complex material use, very narrow operating bandwidths and low radiation efficiency. In addition, in MTM miniaturization methods, care should be taken with the models used to analyze such structures as such models usually ignore the polarization of the field that might cause different behavior as compared to the normal incidence/non-polarized models used in most analysis to derive the effective medium properties. Thus caution has to be taken and full understanding of the physics is required of the MTMs.

## 2.4 Summary and Features of Miniaturization

### Methods

Table 2.1 groups together various references that have appeared in literature according to the miniaturization techniques used. As seen from the table, it is evident that almost all techniques have received almost the same amount of attention in the literature. The slightly less references for the MTM-inspired techniques is mainly due to relatively new use of this technique. Table 2.2 summarizes these techniques according to their features, and lists their major advantages and disadvantages. As seen in this table, almost all the mentioned techniques lead to significant miniaturization. However, some techniques such as folding or MTM-inspired can make the antenna structure more complex and non-planar. Also, most techniques reported so far provide little insight into a general design procedure, and they do not mention how the technique can be applied to design antennas in other bands. Hence, more attention is required in this direction. It is also important to mention that many of the patch miniaturization figures reported in literature only mention the decrease in patch size (or radiating structure size) and do not take into account the size of the ground plane. Since the size of the ground plane greatly affects the performance of an MPA, it cannot be neglected when defining the size of the antenna which has been miniaturized. In addition, none of the designs reported in literature breach the fundamental limits of ESA, and thus the tradeoff between size, efficiency and the bandwidth needs to be carefully managed based on the application at hand.

Table 2.2: A Summary of MPA Miniaturization Techniques and their Characteristics

Miniaturization Technique	Features	Advantages	Disadvantages
Material Loading	<ul style="list-style-type: none"> <li>- High dielectric substrates</li> <li>- Ceramic substrates</li> <li>- Magnetodielectric substrates</li> </ul>	<ul style="list-style-type: none"> <li>- High degree of miniaturization</li> <li>- Easy design procedure</li> </ul>	<ul style="list-style-type: none"> <li>- Expensive materials</li> <li>- Limited bandwidth</li> </ul>
Shorting and Folding	<ul style="list-style-type: none"> <li>- Shorting Pins</li> <li>- Shorting Wall</li> <li>- Folding</li> </ul>	<ul style="list-style-type: none"> <li>- Up to 4 times miniaturization</li> <li>- Cost effective solution</li> </ul>	<ul style="list-style-type: none"> <li>- No standard design procedure</li> <li>- Makes antenna geometry complex</li> <li>- Non-planar due to folding</li> </ul>
Reshaping a Patch or Introducing Slots	<ul style="list-style-type: none"> <li>- Fractal Antenna</li> <li>- Engineered Conductors</li> <li>- Slots in the patch</li> </ul>	<ul style="list-style-type: none"> <li>- Can provide wider bandwidth</li> <li>- Up to 8 times miniaturization</li> </ul>	<ul style="list-style-type: none"> <li>- Make antenna geometry complex</li> <li>- Affects the radiation characteristics</li> <li>- No standard design procedure</li> </ul>
Modifications in Ground Plane	<ul style="list-style-type: none"> <li>- Slots in GND</li> <li>- Use of DGS</li> </ul>	<ul style="list-style-type: none"> <li>- Up to 8 times miniaturization</li> <li>- Antenna geometry remains planar and simple</li> </ul>	<ul style="list-style-type: none"> <li>- Low efficiency</li> <li>- Increases the back lobe level</li> <li>- No standard design procedure</li> </ul>
Use of Metamaterials	<ul style="list-style-type: none"> <li>- Use of ENG, MNG or DNG substrates</li> <li>- Use of metamaterial inspired techniques</li> </ul>	<ul style="list-style-type: none"> <li>- High degree of miniaturization</li> </ul>	<ul style="list-style-type: none"> <li>- Limited bandwidth</li> <li>- Low efficiency</li> <li>- Complex antenna geometry</li> <li>- No standard design procedure</li> </ul>

## CHAPTER 3

# PROPOSED METHOD FOR THE MINIATURIZATION OF MPA

In this chapter, a MTM-inspired miniaturization technique is proposed for MPA miniaturization. The technique is based on the use of the complementary split-ring resonator (CSRR) structure with a patch antenna. This technique provides significant degree of miniaturization. The technique is analyzed through parametric studies and a design methodology is developed to make miniaturized MPA using the technique. Different characteristics of the proposed MPA are evaluated. Several miniaturized MPAs are designed in different bands using the proposed technique in order to verify its utility. To get a better insight into the operation of the antenna, an equivalent circuit model is developed. The antenna is further analyzed using the theory of characteristic modes.

## 3.1 CSRR Loaded MPA

### 3.1.1 Complementary Split-Ring Resonator (CSRR)

A CSRR is a negative image of the SRR. It is made by removing the conductor in the shape of an SRR from a conducting sheet, which is usually a ground plane. The CSRR is a resonant structure. It has been used widely in the study of metamaterials and by periodic arrangement of the CSRR, effective negative  $\epsilon$  can be obtained around its resonant frequency. The resonant frequency of a CSRR is the same as that of an SRR of the same dimension, and it is modeled as an LC circuit. The lumped element model for an SRR and a CSRR was derived in [59], which also gave the quasi-analytical equations for finding the resonant frequency of the SRR and the CSRR. In [60], an empirical model for the resonant frequency of the SRR was given, which was easy to implement. Fig. 3.1 shows double ring rectangular and circular SRRs. Different shapes of SRR exist in literature but the double slit circular and rectangular SRR are the most studied and commonly used SRRs. They are made up of two concentric loops with a slit in each loop. The width of each loop ( $w$ ), the spacing between the loops ( $s$ ) and the size of the loop ( $L$ ) govern the resonance properties of the SRR or the CSRR. Other common types of the CSRR include the single-ring CSRR, double-slit CSRR, and the spiral resonator.

In [59], the dispersion diagram of the double-ring CSRR was computed for its array etched out on a ground plane of a microstrip transmission-line. The dielectric substrate was RO3010 with a height of 1.27 mm and dielectric constant

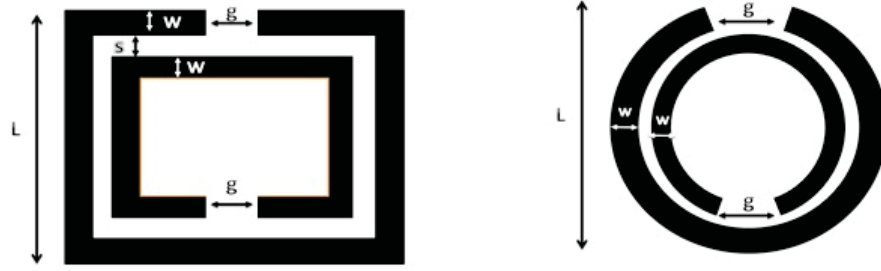


Figure 3.1: Geometry of the split-ring resonator

of 10.2. The outer radius of the CSRR was 3 mm, while the thickness of the ring and the spacing between the rings was 0.3 mm. For these dimensions, the CSRR had a resonant frequency of 2.8 GHz. The dispersion diagram obtained for the CSRR is shown in Fig. 3.2. The CSRR created a stop-band for the transmission-line around the frequency of its resonance. This was attributed to the effective negative permittivity due to the CSRR around this frequency.

### 3.1.2 Antenna Design

The geometry of the proposed antenna is shown in Fig. 3.3. It was made up of a standard rectangular patch on any standard substrate. On the bottom side, a double-ring CSRR was etched out underneath the MPA. The arrangement resulted in decrease in the resonant frequency (*or reduction in the size of antenna*) of the MPA without adding any lumped components or disturbing the volumetric dimensions of the MPA. In the next sections, it is shown that this decrease was up to 85% in the area of the patch designed for the 700 MHz band and up to 65%

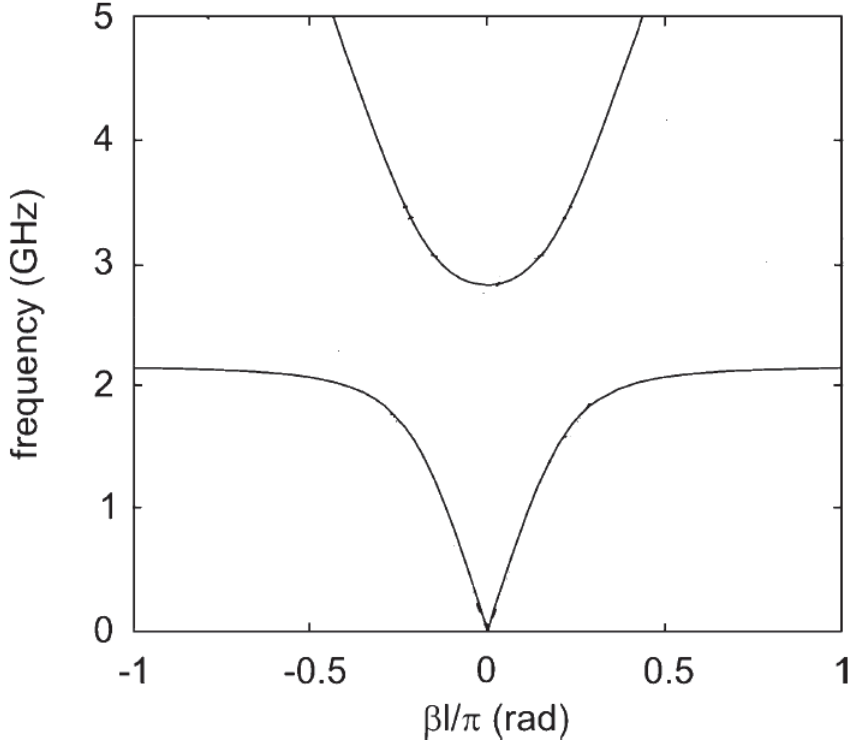


Figure 3.2: Dispersion diagram of the CSRR etched on the back of a microstrip transmission line [59].

in the area of the patch designed for 5 GHz band. The antenna was fed using a microstrip transmission line. The feed was not exactly at the center of the patch and therefore, the design was asymmetric. It was designed this way in order to excite the proper modes. The feed was inset into the patch for the impedance matching.

### 3.1.3 Results & Parametric Analysis

The proposed design was analyzed rigorously through parametric simulation studies and all parameters were analyzed. An initial design was made in HFSS<sup>TM</sup>. The geometrical parameters used for the MPA in Fig. 3.3 are given in Table 3.1. These design parameters were chosen in such a way that it was easy to fabri-

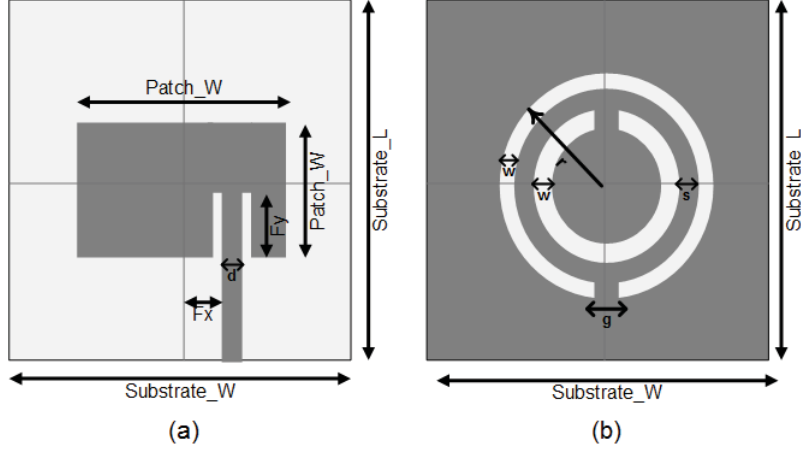


Figure 3.3: Geometry of the proposed miniaturized MPA with CSRR loading, (a) Top side, (b) Bottom side

Table 3.1: Design Parameters of the MPA Used in the Parametric Study

Parameter	Value
Substrate Length ( $SubstrateL$ )	50 mm
Substrate Width ( $SubstrateL$ )	50 mm
Substrate Height ( $t$ )	0.8 mm
Dielectric Constant ( $\epsilon_r$ )	4.4
Patch Length ( $PatchL$ )	14 mm
Patch Width ( $PatchW$ )	18 mm
Microstrip Feed Width ( $d$ )	1.52 mm

cate the antenna in the lab. The substrate chosen was FR4, which is cheap and readily available. The thickness of the substrate was according to one of the standard available boards. The thickness of microstrip transmission-line corresponds to  $50\Omega$ . With all these parameters, the antenna had a resonant frequency at 5.04 GHz.

A double-ring CSRR was etched out underneath the patch in a similar way as shown in Fig. 3.3. The outer radius of the CSRR  $r$  was 6 mm, the width of the rings  $w$  was 0.5 mm, the spacing between the two rings  $s$  was 0.5 mm. The split in each ring was of 0.5 mm. The design was simulated and the results



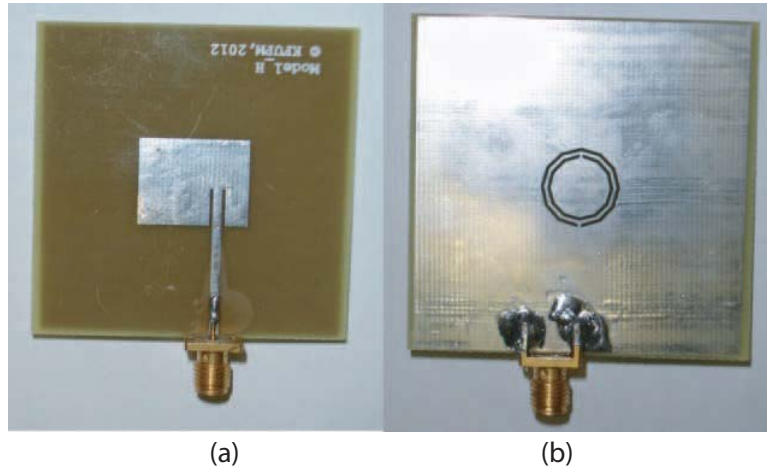


Figure 3.4: Fabricated CSRR loaded miniaturized MPA

showed that antenna had a resonance at 2.46 GHz. Thus, a 51% decrease in the resonance frequency was achieved by the CSRR loading. A standard patch without the CSRR loading on a similar substrate would require a patch dimensions of  $29 \times 37 \text{ mm}^2$ . Thus, the size reduction in terms of patch size due to the CSRR loading was 76.5%. This, however, was accompanied by a decrease in antenna radiation efficiency which was 30%. With such a high level of miniaturization, this value is expected.

The antenna was fabricated (see Fig. 3.4). The measurement results of the antenna showed a close agreement with the simulation results. Fig. 3.5 shows the reflection coefficient of the measured as well as simulated results. The antenna had an impedance bandwidth of 40 MHz. The 2D radiation gain pattern of the antenna is shown in Fig 3.6. As evident from the figure, due to significant miniaturization as well as with the use the CSRR, the antenna had a significant back lobe. The front-to-back (F/B) lobe ratio was 2.8 dB while the maximum gain of antenna at the operating frequency was 0.5 dBi.

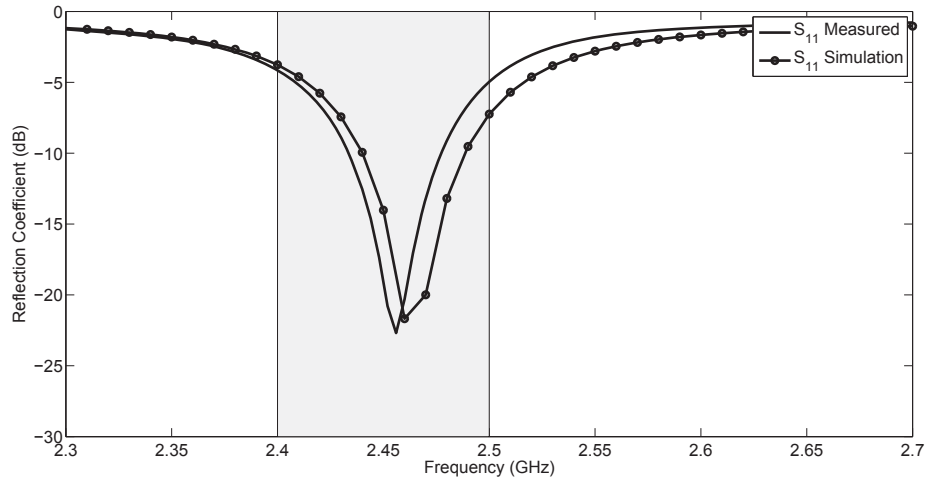


Figure 3.5: Measured and simulated reflection coefficient of the designed MPA

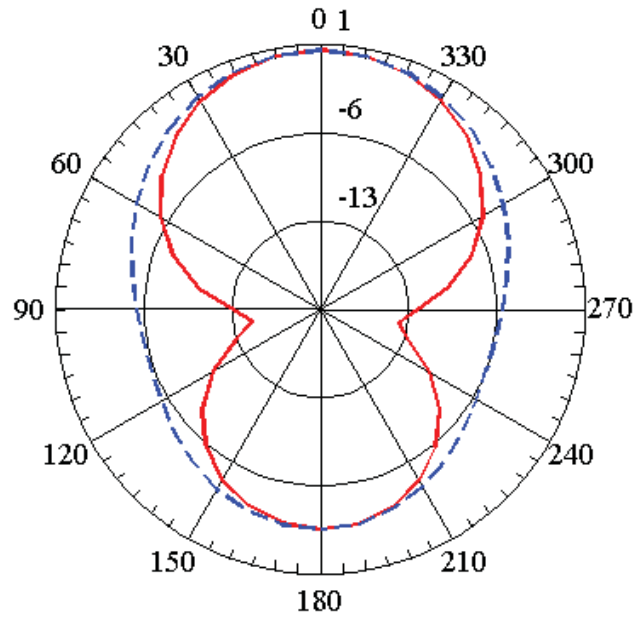


Figure 3.6: The 2D gain pattern of the miniaturized MPA

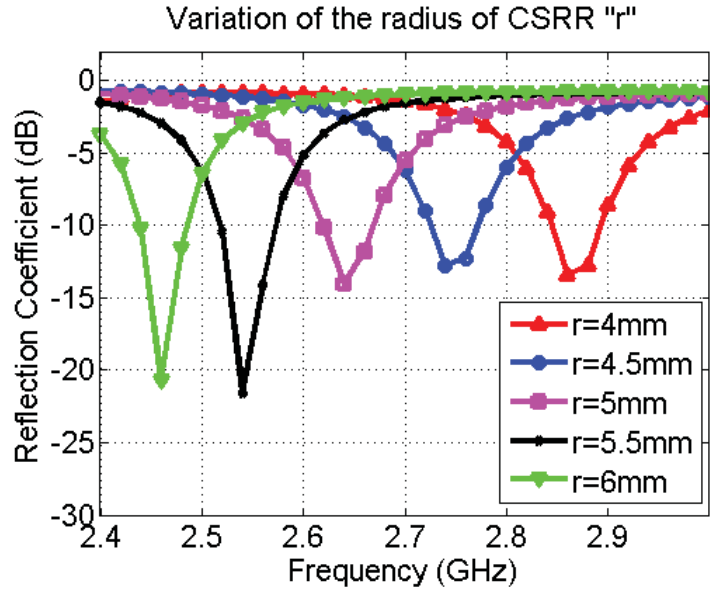


Figure 3.7: Variation of the antenna's resonant frequency with change in the CSRR radius

Once the miniaturization was established using the CSRR loading technique, a parametric study was carried out to find the effect of the CSRR dimensions on the degree of miniaturization. To start with, initially all design parameters were kept the same while the outer radius  $r$  of the CSRR was varied from 4 mm to 6 mm in a step of 0.5 mm. The reflection coefficients obtained corresponding to the change in CSRR outer radius are shown in Fig. 3.7. It was found that as the radius of the CSRR was increased, the resonant frequency of the antenna decreased. Thus, resonant frequency of antenna decreased from 2.87 GHz to 2.46 GHz when the radius of the CSRR was increased from 4 mm to 6 mm. For the design under consideration, a 0.5 mm increase in the CSRR radius resulted in 100 MHz decrease in the resonant frequency.

The effects of other parameters of the CSRR were also analyzed. It was found that the slits in the ring had very little effect on the change in resonant frequency

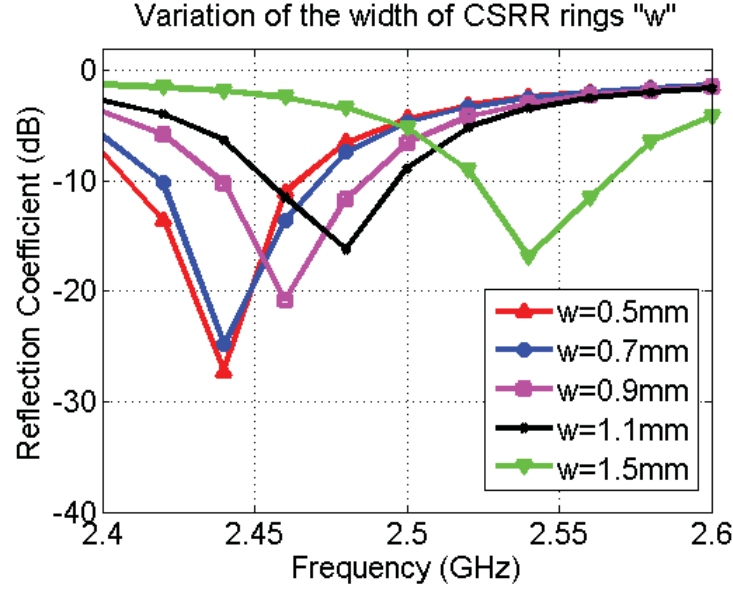


Figure 3.8: Variation of the antenna's resonant frequency with change in the CSRR ring width

of the antenna. Therefore, it was kept at 0.5 mm. The effect of the width of the CSRR's ring as well as the spacing between each ring was analyzed individually. When the width  $w$  of the rings was increased while keeping other parameters constant, it was found that the resonant frequency of the antenna also increased. Fig. 3.8 shows the reflection coefficient of the antenna with increase in  $w$  while keeping  $r=6$  mm and  $s=0.5$  mm. The width was increased from 0.5 mm to 1.5 mm in the steps of 0.2 mm. It was found that with a change of 1 mm, the shift in the resonance was less than 100 MHz.

The spacing between the rings  $s$  was varied from 0.3 mm to 1.5 mm in steps of 0.2 mm. Fig. 3.9 shows the reflection coefficient of the antenna with changing  $s$  while keeping  $r=6$  mm and  $w=0.5$  mm.. As seen from the results, it was found that increase in the spacing between the rings increased the resonant frequency of the antenna. However, like the effect of  $w$ , this change was also minor as compared to

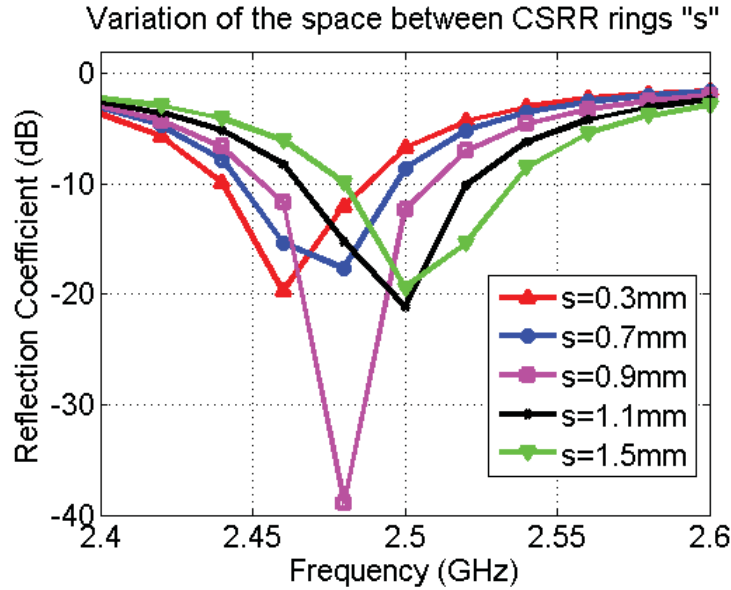


Figure 3.9: Variation of the antenna’s resonant frequency with change in the spacing between CSRR rings

the effect of the CSRR’s radius  $r$  on the resonant frequency of the antenna. Thus, in order to tune the antenna to a desired resonant frequency, the main parameter was found to be  $r$ , which could be varied to bring the resonant frequency of the antenna near the desired value while  $w$  and  $s$  could be used for fine tuning.

The sensitivity of the design parameters on the antenna’s resonant frequency can also be deduced from this parametric study. Apart from the conventional MPA parameters effect, (*e.g. increase in dielectric constant lowers the resonant frequency*) any change in the CSRR dimensions during fabrication process would also effect the results. Thus, if after fabrication, the radius of the CSRR  $r$  is less than the one used in simulation, the resonant frequency will be higher than the one obtained in simulations. The amount of shift depends the difference between the values defined in simulation and the one obtained after fabrication.

Apart from the conventional double-ring CSRR, the loading of a single-ring

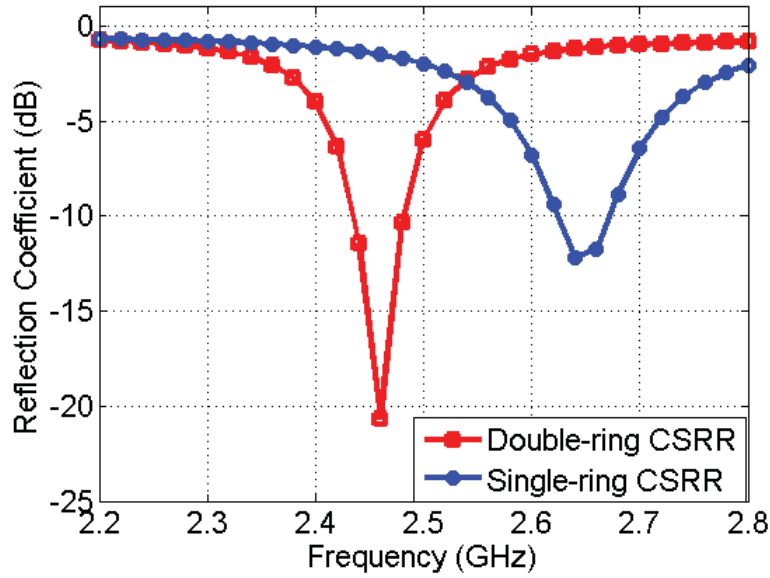


Figure 3.10: Effect of double-ring CSRR and single-ring CSRR loading on the resonant frequency of the MPA.

CSRR was also analyzed. It was found that the single-ring CSRR also provided miniaturization. For the same design, when the inner ring was removed to make it single-ring CSRR, the resonant frequency of the antenna was 2.64 GHz. It was 180 MHz higher than the one obtained by using the double-ring CSRR. Fig. 3.10 shows the reflection coefficient of the antenna when the two different CSRR's were used.

The reduction in the resonant frequency due to the CSRR loading was also analyzed from the surface current density on the MPA. Fig. 3.11 shows the current density on the top and bottom of the miniaturized MPA loaded with the CSRR. Under normal conditions, the current path was along the patch length. This length was 14 mm which corresponded to the 5 GHz frequency for the given dielectric. With the introduction of the CSRR, it can be clearly seen from Fig. 3.11 that the

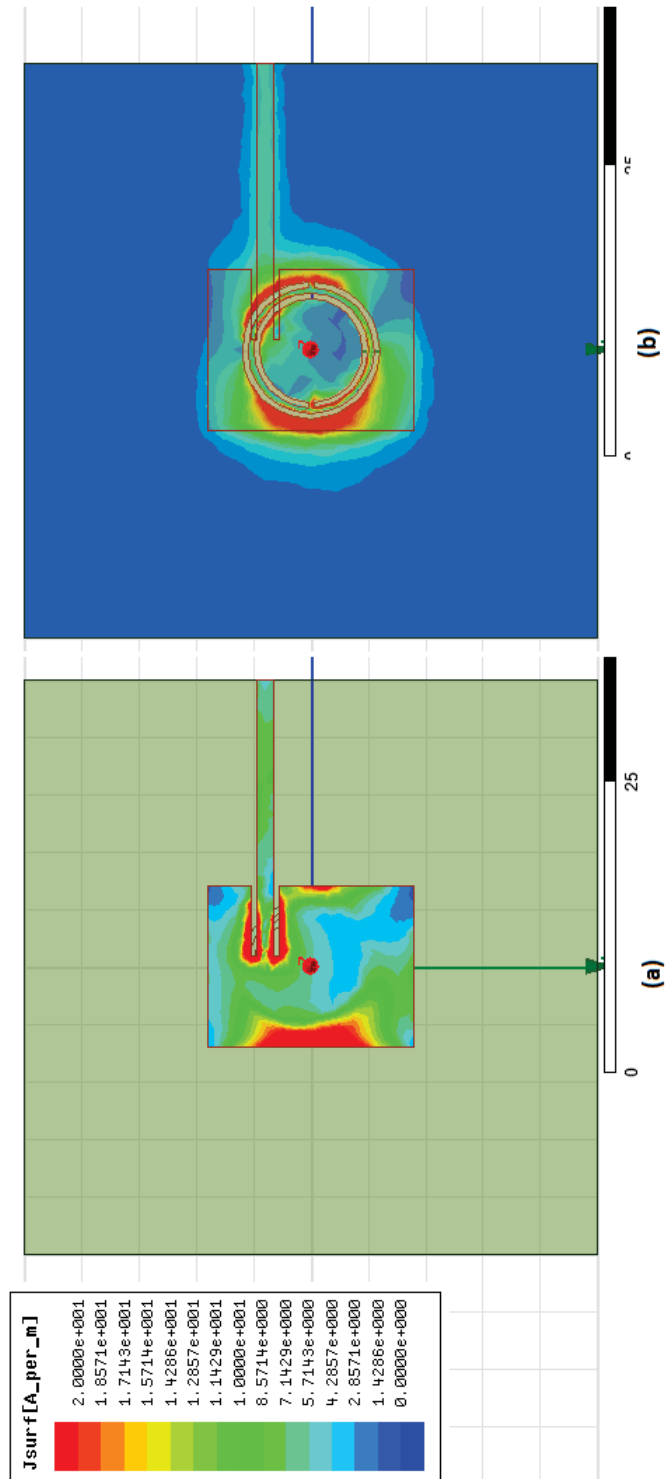


Figure 3.11: Current density on the CSRR-loaded MPA at the operating frequency, (a) Top side, (b) Bottom side

current path has changed and it is now curved along the periphery of the CSRR. Thus, the introduction of the CSRR increased the effective current path in the resonant structure which resulted in the decrease in the frequency. Also seen in the Fig. 3.11, there is an increased current density on the ground plane of the patch around the CSRR as compared to a standard MPA. This also contributed towards radiation and that is why, the antenna had a low F/B ratio as compared to the MPA.

### 3.1.4 Circuit Model

A circuit model of the proposed miniaturized MPA was derived using the transmission-line theory [8]. For simplicity, a single-ring CSRR loaded patch antenna was modeled. To start with, it is known that using transmission-line theory, a simple patch antenna is modeled as two radiating slots which are connected in parallel to each other through a transmission-line. At the resonant frequency, the transmission line is of half wavelength. The circuit model of the patch is shown in Fig 3.12.

In the circuit model, the load admittance of each slot is  $Y_s = G_s + jB_s$ .  $G_s$  represents the conductance which is associated with the power radiated by the slot while  $B_s$  is the susceptance which is associated with the reactive power stored near the slot. The transmission line was divided into  $L_1$  and  $L_2$  where the feed point is located at the point after length  $L_1$ . The total length of the transmission line was  $\lambda/2$ .



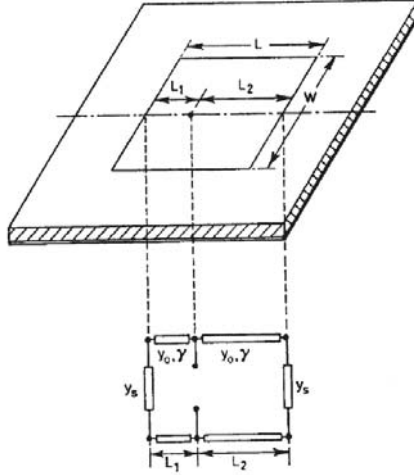


Figure 3.12: The transmission-line model of the MPA [8].

A single-ring CSRR can be modeled with the help of Babinet's Principle [10]. According to Babinet's principle, the impedance  $Z_c$  of a structure which is unknown can be found with the help of another structure whose impedance  $Z_s$  is known and it is the complementary of the first structure. The two are related to each other by

$$Z_c Z_s = \frac{\eta^2}{4} \quad (3.1)$$

where  $\eta$  is the intrinsic impedance of the medium containing the complementary structure and the original structure. Using this principle, the impedance of the single-ring CSRR can be found from its complementary shape which represents a loop antenna. The impedance characteristics of a loop antenna are well known. In [10], the reactance of circular loop antenna is plotted versus the circumference of the loop antenna as shown in Fig 3.13.

In the case of the CSRR-loaded antenna, the circumference of the CSRR corresponding to the resonant frequency of the miniaturized MPA was in between the

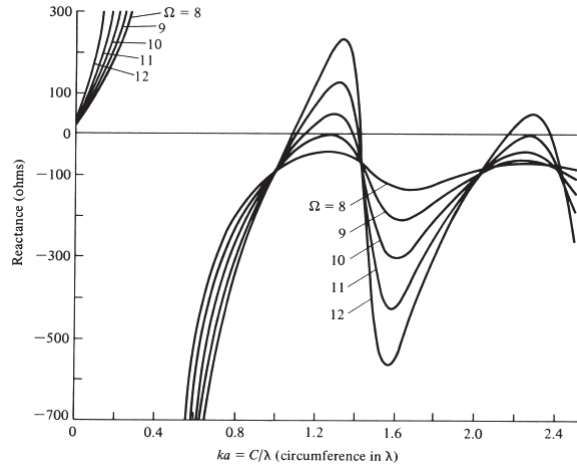


Figure 3.13: Reactance of a loop antenna [10].

half-wavelength and full wavelength. Based on the circumference times the wave number, the reactance of the loop can be found from the graph shown in Fig 3.13. For such a case, it can be seen that the reactance of the equivalent loop antenna is always capacitive. Using Eq.( 3.1), it can be found that for this case, the effect of the CSRR loading was inductive which resulted in the decrease in the MPA resonance.

The final equivalent circuit of the CSRR-loaded patch antenna is shown in Fig. 3.14.

The equivalent circuit model was made in the CST microwave studio where the inductive loading effect of the CSRR was verified and a decrease in the resonant frequency of the circuit was observed as the inductance was increased.

### 3.1.5 Design Procedure

Based on the parametric studies and analysis of the antenna, a design methodology was developed to design miniaturized MPA for any frequency band using the CSRR loading technique. The design guideline is given as follows :

1. Come up with approximate patch dimensions using the transmission-line / Cavity model for a resonant frequency which is twice of the required resonant frequency.
2. Model the patch antenna in a simulation software.
3. Etch out a CSRR underneath the center of the patch such that the outer radius of the CSRR is covering the edges of the patch.
4. Run the simulation and find the resonant frequency of the antenna.
5. If the resonant frequency is lower than the desirable frequency, tune the antenna to the desired frequency by decrease the radius  $r$  of the CSRR or by varying  $s$  and/or  $w$  of the CSRR.
6. While tuning the CSRR, if the resonant frequency is lost, shift the feedline along the patch until the resonance is recovered.
7. During all this process, make sure that the main radiator remains the patch.  
This can be observed from the surface current density figures.

Fig. 3.15 gives the flow chart of the design process.

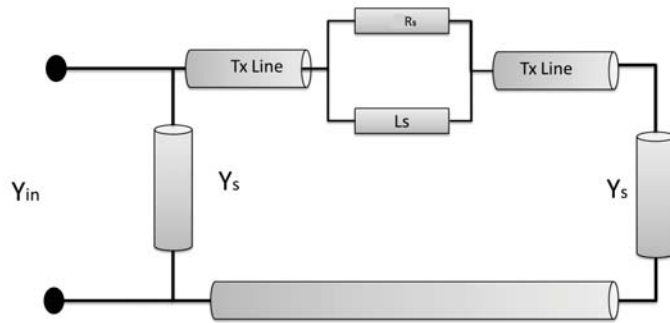


Figure 3.14: The equivalent circuit model of the CSRR-loaded MPA

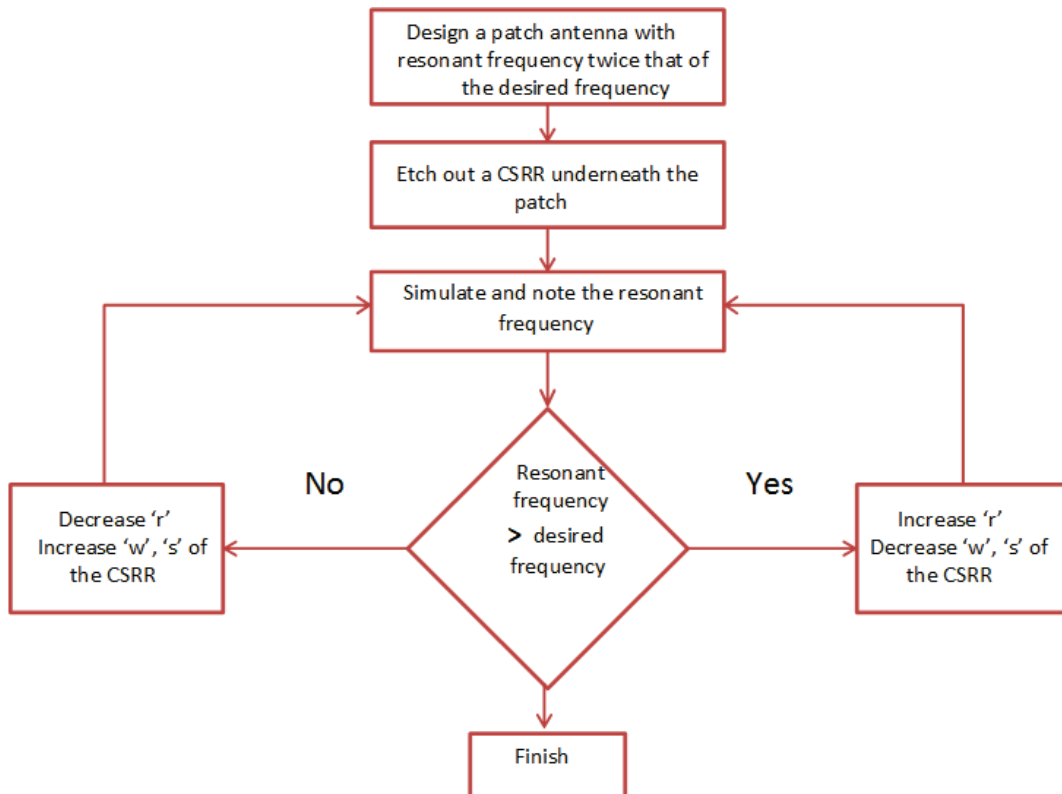


Figure 3.15: A flow chart representation of the design methodology to make the CSRR-loaded MPA

## 3.2 Design Examples

Using the outlined design methodology developed for CSRR loaded miniaturized MPAs, two different miniaturized antennas were designed. The first one was designed to operate at 750 MHz while the second one was designed for the 5 GHz band. The design and analysis of these antennas are given in the following sections.

### 3.2.1 Miniaturized MPA for the 750 MHz Band

A patch of dimensions  $44 \times 35 \text{ mm}^2$  was modeled on a substrate of dimensions  $60 \times 60 \times 0.8 \text{ mm}^3$ . The dielectric constant of the substrate (FR4) was 4.4. The MPA was excited using a microstrip line whose width was 1.52 mm. This width was chosen to keep the characteristic impedance of the transmission line as  $50\Omega$ . The transmission line was inset into the patch in order to match the MPA with  $50\Omega$ . The MPA had a resonant frequency of 2 GHz. In order to bring the frequency down, the proposed technique was used. A CSRR was etched out underneath the patch in its ground plane. The parameters of the CSRR were varied till the desired resonance was achieved.

The antenna resonated at the desired frequency when the radius of the CSRR  $r$  was 19 mm, the width of the rings  $w$  was 1.5 mm and the spacing between the rings was 1 mm. The geometry along with the dimensions of the antenna are shown in Fig. 3.16. A 62.5% reduction in the resonant frequency of the antenna was achieved while the reduction in the area of the patch was 85%.

The antenna was analyzed from the simulation results. The antenna had an

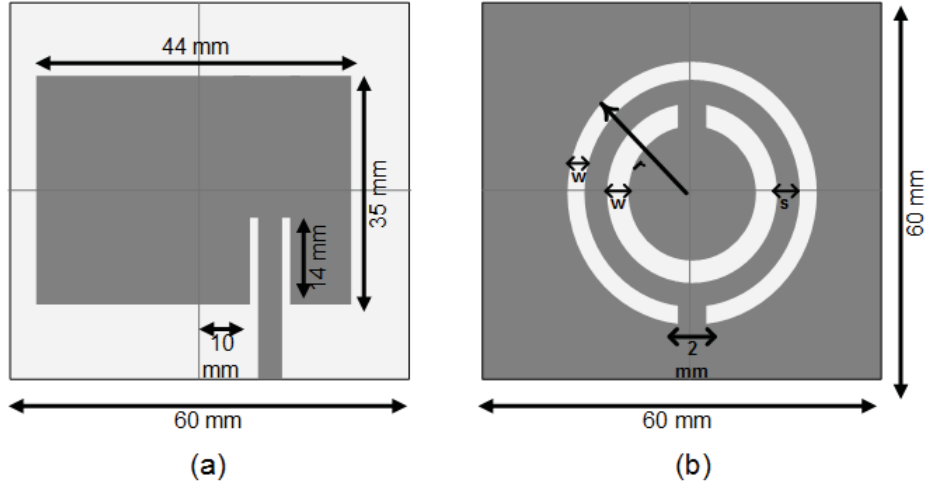


Figure 3.16: Geometry and dimensions of MPA resonating at 750 MHz. (a) Top side, (b) Bottom side

Table 3.2: Simulation Results for the 750 MHz Band MPA

Parameter	Value
Impedance Bandwidth	15 MHz
Maximum Gain	1 dBi
Radiation Efficiency	28%
F/B Ratio	2.5 dB
Reduction in Frequency	62.5 %
Reduction in Patch Area	85%

impedance bandwidth of 15 MHz while its radiation efficiency was 28%. It had a maximum operating gain of 3 dBi. The results obtained from the simulations are summarized in Table 3.2.

### 3.2.2 Miniaturized MPA for the 5 GHz Band

A similar approach was followed to design the miniaturized MPA for 5 GHz. A patch of size  $8 \times 11 \text{ mm}^2$  was designed on a  $50 \times 50 \text{ mm}^2$  FR4 substrate. The thickness and dielectric constant of the substrate were 0.8 mm and 4.4, respectively. The patch was excited with an inset feed microstrip transmission line with a char-

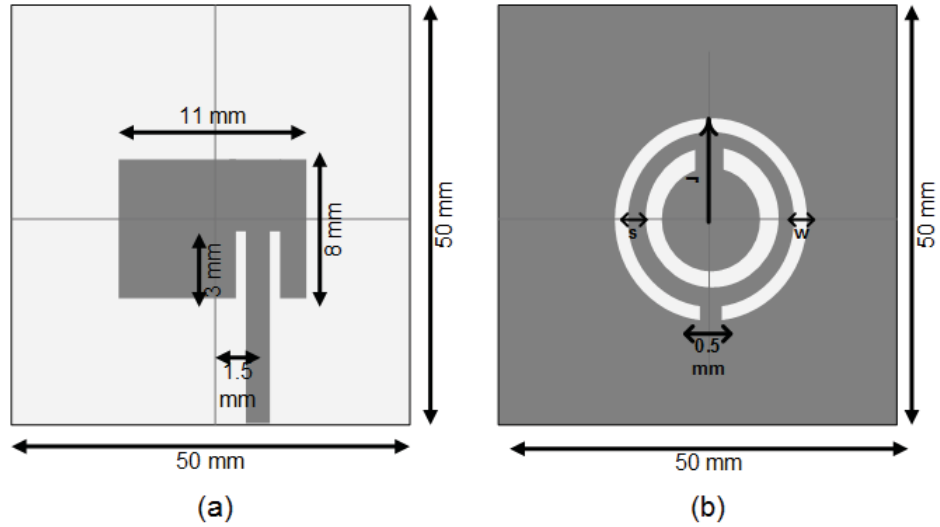


Figure 3.17: Geometry and dimensions of MPA resonating at 5 GHz. (a) Top side, (b) Bottom side

Table 3.3: Simulation Results for the 5 GHz Band MPA

Parameter	Value
Impedance Bandwidth	65 MHz
Maximum Gain	0.5 dBi
Radiation Efficiency	30%
F/B Ratio	4.2 dB
Reduction in Frequency	20 %
Reduction in Patch Area	65%

acteristic impedance of  $50\Omega$ . The antenna had a resonant frequency of 6.52 GHz.

The CSRR was etched out and design steps were followed to tune the antenna at 5 GHz. The antenna was tuned to the desired frequency when  $r$  was 2.5 mm,  $w$  was 0.25 mm and  $s$  was 0.5 mm. The geometry of the antenna is shown in Fig. 3.17

The antenna parameters were evaluated from the simulations. The antenna had a radiation efficiency of 30% and a maximum operating gain of 0.5 dBi. The impedance bandwidth of the antenna was more than 60 MHz. Various parameters of the antenna that were evaluated are summarized in Table 3.3.

## 3.3 Design Analysis using the Characteristic Mode Theory

To get a better insight of the proposed design, and to analyze the current modes of the geometry and its radiation characteristics, the theory of characteristic modes was used. The theory is a powerful tool which has very recently been applied to the design and analysis of antennas [61]. In this section, an overview of the theory is presented followed by the analysis of the proposed design based on the same theory. The analysis is performed using the characteristic mode feature of the FEKO<sup>TM</sup> simulation software.

### 3.3.1 Overview of Theory

In the past, complex antenna structures were difficult to analyze since the only known techniques to find their radiation characteristics were analytical. To analyze a structure, it was simplified and several assumptions were made to solve it. In doing so, maximum effort was placed in finding a computationally simple solution. These methods provided good insight into the operating principle of an antenna but they were limited to very basic and simple designs. With time, several numerical techniques were used for the analysis of the antenna with complex geometries. These techniques included the MoM, FDTD method, FEM etc. To get a correct solution of the problem using the numerical techniques, a large number of computations were required. In the recent years, with the ever increasing computational power of digital machines, numerical techniques have been exclusively



used for the design of complex antenna structures using well developed softwares. These softwares provide a high degree of accuracy. While they give very detailed description of various antenna parameters and its behavior, they seldom provide a meaningful insight into the physics of it.

To address this issue, the theory of characteristic modes was used recently for analyzing radiating structure [61]. Although, the theory was formulated several decades ago [62–64], its use remained dormant mainly due to lack of high performance machines at that time.

This technique is based on the MoM. In this technique, the generalized impedance matrix of the structure is computed in the same way as solved in the MoM. However, it does not calculate the total current on the radiating body by a known excitation which is the procedure in MoM based solvers. Rather, it formulates an eigenvalue equation from the generalized impedance matrix whose solution provides the various modes of currents which are supported by the radiating body. In this way, this technique do not require any known excitation and it is valid for any conducting body. These modal currents are used to find the radiation patterns corresponding to each mode. This helps in the systematic design of the antenna to get the required radiation characteristics by later exciting the correct mode.

The formulation of the theory of characteristic modes start with the calculation of generalized impedance matrix. Consider a conducting body  $S$  in an impressed field  $E^i$  procured by some external source. The tangential component of the filed

will induce a surface current  $J$  on the surface of the conducting body. The relation between  $E^i$  and  $J$  can be written using a linear operator  $L$  and it is given by [63],

$$L(J) - E^i = 0 \quad (3.2)$$

Using the MoM, the surface current  $J$  can be expanded as a sum of basis functions given by

$$J = \sum_n \alpha_n J_n \quad (3.3)$$

where  $J_n$  are the basis function. Substituting Eq.(3.3) in Eq.(3.2), we get

$$\sum_n \alpha_n L(J_n) = E^i \quad (3.4)$$

Now, a set of testing function  $W_n$  is defined and by taking the inner product of Eq.(3.4) with  $W_n$  to get

$$\sum_n \alpha_n \langle L(J_n), W_m \rangle = \langle W_m, E^i \rangle \quad (3.5)$$

Eq.(3.5) in matrix form can be written as

$$[Z_{mn}][I_n] = [V_m] \quad (3.6)$$

where

$$[I_n] = \begin{bmatrix} \alpha_1 \\ \alpha_2 \\ \dots \\ \dots \\ \alpha_n \end{bmatrix} \quad (3.7)$$

$$[V_m] = \begin{bmatrix} \langle W_1, E^i \rangle \\ \langle W_2, E^i \rangle \\ \dots \\ \dots \\ \langle W_m, E^i \rangle \end{bmatrix} \quad (3.8)$$

and

$$[Z_{mn}] = \begin{bmatrix} \langle W_1, L(J_1) \rangle & \langle W_1, L(J_2) \rangle & \dots & \dots & \langle W_1, L(J_n) \rangle \\ \langle W_2, L(J_1) \rangle & \langle W_2, L(J_2) \rangle & \dots & \dots & \langle W_2, L(J_n) \rangle \\ \dots & \dots & \dots & \dots & \dots \\ \dots & \dots & \dots & \dots & \dots \\ \langle W_m, L(J_1) \rangle & \langle W_m, L(J_2) \rangle & \dots & \dots & \langle W_m, L(J_n) \rangle \end{bmatrix} \quad (3.9)$$

The matrix  $[Z_{mn}]$  is called the generalized impedance matrix,  $[I_n]$  is called the generalized currents and  $[V_m]$  is called the generalized voltages. In a general antenna problem, the known excitation defines the generalized voltage matrix while the generalized impedance matrix is computed from the structure of the antenna and the solution frequency. Knowing these, the generalized currents are

computed which are then substituted in Eq.(3.3) to find the total current on the antenna's surface. The far-field radiation patterns, and input impedance are then calculated using the known surface current.

The characteristic mode theory make use of the fact that conducting body is characterized by the generalized impedance matrix. Even, in the absence of any excitation, the current modes  $J_n$  that can be supported by a conducting body can be computed by using this matrix. The impedance matrix is symmetric [63], thus its can be written as sum of real and imaginary parts given by

$$[R] = \frac{1}{2} [Z + Z^*] \quad (3.10)$$

$$[X] = \frac{1}{2j} [Z - Z^*] \quad (3.11)$$

In such case,  $Z = R + jX$  where R and X are both real and symmetric. With the basis function  $J_n$ , the matrix makes an eigenvalue equation given by

$$[X][J_n] = \lambda_n [R][J_n] \quad (3.12)$$

Using the Galerkin's method, the testing function  $W_n$  will be equal to the basis function  $J_n$ . For such condition, the entries of the  $Z$  matrix depends on the number of segments into which the conducting body S is divided. It is given by

$$[Z_{ij}] = j\omega \iint_s (J_i \cdot A_j + \sigma_i \phi_j) dS \quad (3.13)$$

where  $A_i$  is the vector potential due to the surface current  $J_i$  and  $\phi_j$  is the scalar potential due to charge  $\sigma_j$ . They are given as

$$A = \mu \iint_s J \frac{e^{-jkR}}{4\pi R} dS \quad (3.14)$$

,

$$\phi = \frac{1}{\epsilon} \iint_s \sigma \frac{e^{-jkR}}{4\pi R} dS \quad (3.15)$$

and

$$\sigma = -\frac{1}{j\omega} \iint_s \nabla \cdot J \quad (3.16)$$

The matrix is calculated for a particular frequency. After finding the matrix, the eigenvalue equation is solved to find the  $\lambda_n$  which are also called the "eigenvalues" and corresponding eigenfunctions  $J_n$  which are also called the "characteristic current". These  $\lambda_n$  and the corresponding  $J_n$  are important as they give a lot of information about the radiating structure. The value of  $\lambda_n$  tells whether the particular mode will resonate at that frequency or not. If its value is close to zero, the particular mode will radiate well when excited. However, as its value gets away from zero in either positive or negative directions, the mode does not radiate at that frequency. Additionally, the sign of  $\lambda_n$  determines whether the mode contributes to the stored electric or magnetic energy. If it is positive, it contributes to the stored magnetic energy and for negative value, it contributes to the stored electric energy.

There are many other representations of  $\lambda_n$  used in the literature for better

interpretation of results. It helps in finding the bandwidth of a particular mode as well as the modal quality factor. An important way of analyzing the radiating structure corresponding to its mode is to convert the  $\lambda_n$  into modal significance (MS). It is given by

$$MS = \left| \frac{1}{1 + j\lambda_n} \right| \quad (3.17)$$

The MS varies from 0 to 1 where 1 signifies that the mode is efficiently radiating. It also helps in finding the radiating bandwidth of a mode for the range where its value is greater than 0.707. Using the inverse of the calculated fractional modal bandwidth, modal quality factor can also be computed.

Another representation of  $\lambda_n$  used in literature is called the characteristic angle. It is given by

$$CharacteristicAngle = 180 - \tan^{-1}(\lambda_n) \quad (3.18)$$

The mode is a good radiator when its characteristic angle is in between  $135^\circ$  and  $225^\circ$  with  $180^\circ$  being the center resonant frequency. Thus, it is also used to find the radiation bandwidth and quality factor of the mode.

Another important term used in this theory is the "characteristic fields"  $E_n$ . These are the fields produced by the  $J_n$ . Like  $J_n$ , characteristic fields also make an orthogonal set in the far-field. They can be computed by first calculating the vector potential  $A_n$  (given in Eq.(3.14)) corresponding to the characteristic current  $J_n$ . The characteristic field  $E_n$  is then computed as

$$E_n = -j\omega A_n - j \frac{1}{\omega\mu\epsilon} \nabla(\nabla \cdot A_n) \quad (3.19)$$

The total surface current on a conducting body is the weighted sum of all the characteristic currents. Same goes for the far-field patterns. The weighting factor depends on how much each mode is excited and its depends on the excitation. For electrically large structures, the total field is due to the excitation of several modes. However, for electrically small structures, only few modes are excited.

### 3.3.2 Analysis of the Proposed Design

To analyze the design, the structure was modeled in FEKO<sup>TM</sup> which is a MoM based solver. The generalized impedance matrix was calculated by the solver by first meshing the structure into discrete points and then find the eigenvalues and characteristic currents. The solver chose appropriate basis function by itself to find the impedance matrix and subsequent solution to eigenvalue equation. A higher mesh was required to compute the characteristic modes. The use of a dielectric in the geometry further complicates it, and it was only recently, that the software was updated to handle such problems <sup>1</sup>. However, for such problems, the simulator solves for a very small frequency range and for a limited number of modes. Since the problem at hand was an electrically small antenna, only first mode was required to be analyzed.

Initially, a standard MPA was modeled. The substrate used was FR4 with a dielectric constant of 4 and thickness of 1.5 mm. The patch size was 29.5×38 mm<sup>2</sup>. The antenna had a resonant frequency of 2.35 GHz when properly excited. For the

<sup>1</sup>Most of the work in literature including the most recent ones have only used wire-like or planar geometries.

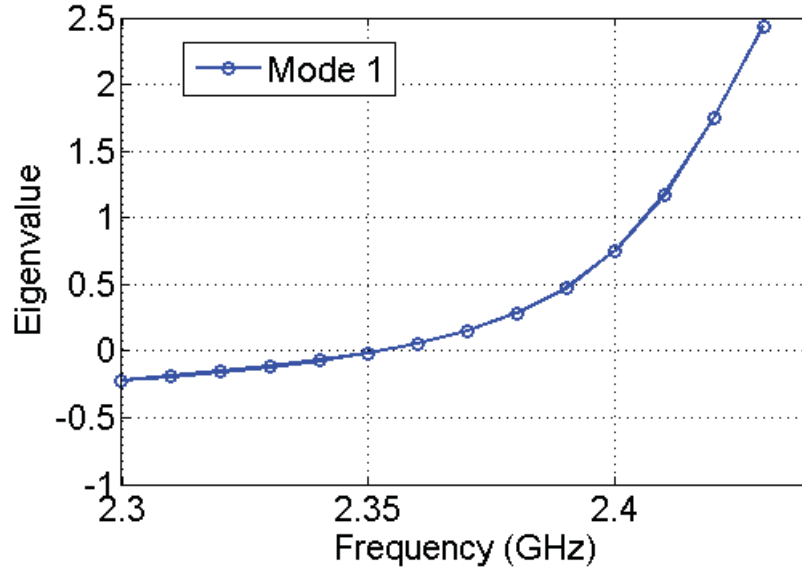


Figure 3.18: Eigenvalues of the first mode for the MPA structure

characteristic mode analysis, no excitation was defined and no feed structure was modeled. Due to the limitation on calculations, only the first mode was analyzed in a limited frequency range of 2.3 GHz to 2.44 GHz with 21 points. Since the lowest resonant frequency of the structure was to be analyzed, the first mode was enough.

The computed impedance matrix corresponding to the structure had  $2616 \times 2616$  entries for each frequency point. The eigenvalues of the first mode of the patch structure versus the frequency were obtained as shown in Fig. 3.18. The eigenvalue was zero at around 2.35 GHz which shows that when the first mode of the structure is properly excited, it will resonate at 2.35 GHz. This is also the lowest possible resonance of the structure since all higher modes attain a value zero at higher frequencies.

To analyze the affect of CSRR using the Characteristic modes theory, a single-



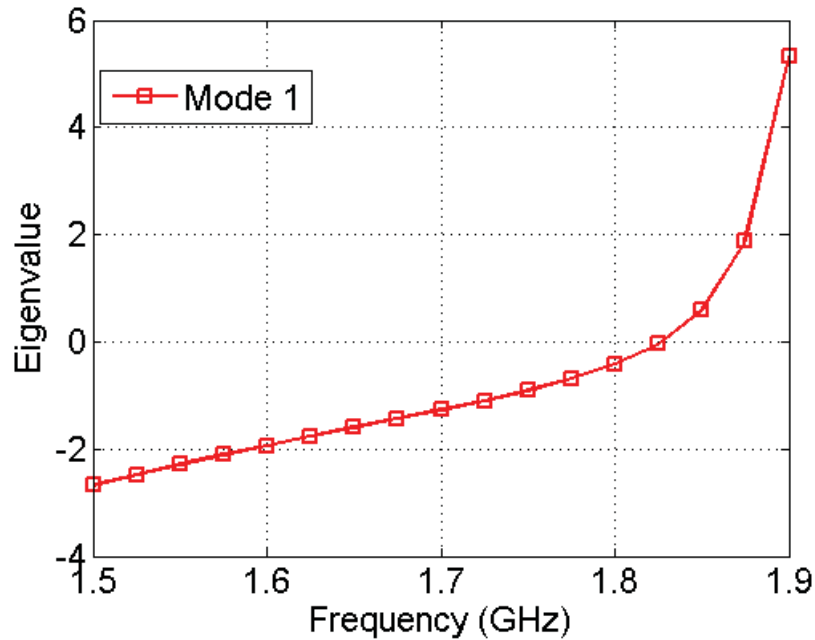


Figure 3.19: Eigenvalues of the first mode for the CSRR-loaded MPA structure ring CSRR was etched out in the same MPA structure. The outer radius of the CSRR was 12 mm while its thickness was 1 mm. Again, the structure was analyzed without any excitation. The simulation was run for a frequency range of 1.5 GHz to 1.9 GHz with 21 discrete equally spaced points. The eigenvalues of the first mode obtained versus the frequency is shown in Fig. 3.19. As evident from the curve, the eigenvalue corresponding to the lowest order mode crossed the zero line at 1.825 GHz clearly showing that the CSRR loading lowered the resonant frequency of the structure. The higher order modes had a much higher magnitude and therefore did not contribute to the resonance of the structure in this frequency range.

For better analysis and computation of the radiating bandwidth and quality factor of the first mode, the MS was computed from the eigenvalue. The MS for

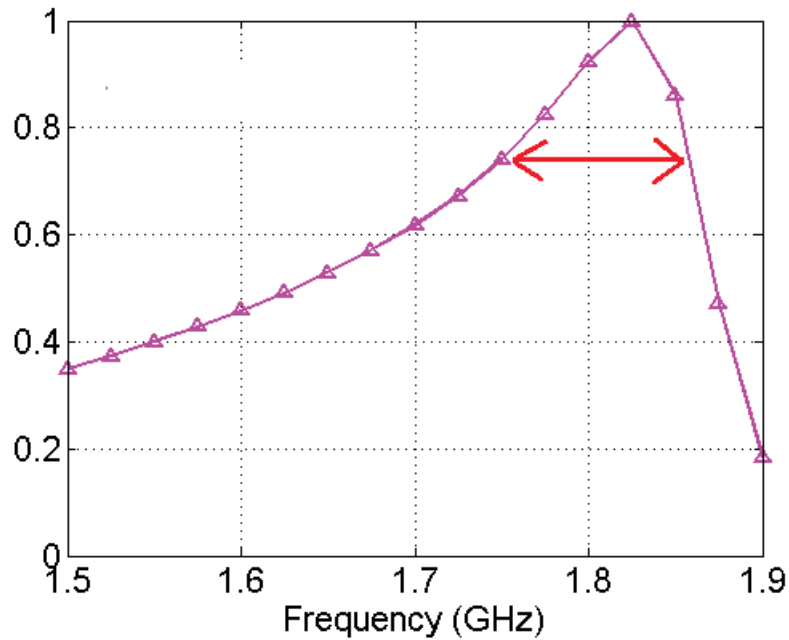
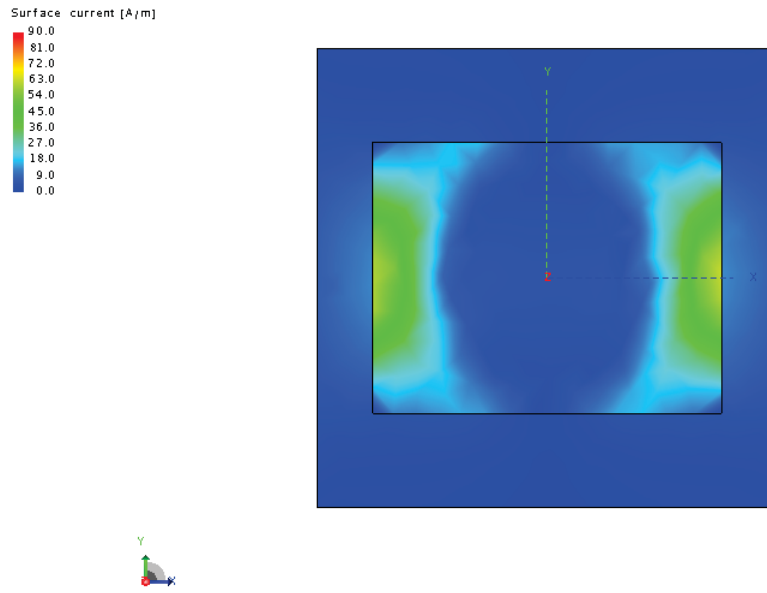


Figure 3.20: Modal Significance of the first mode for the CSRR-loaded MPA structure

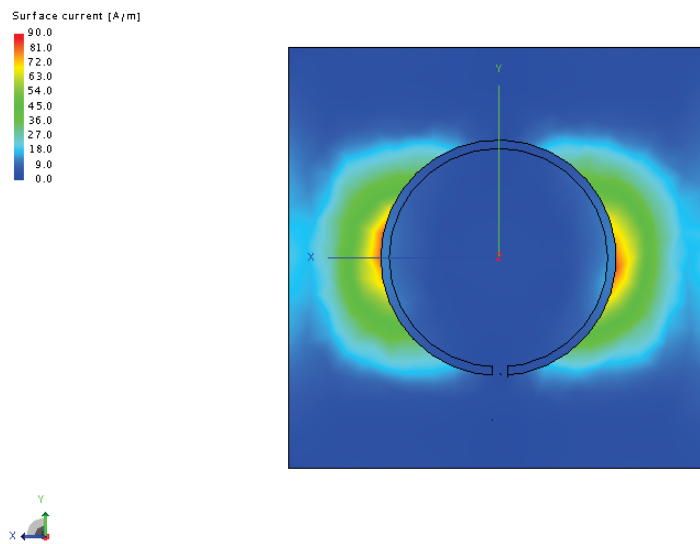
the first mode versus frequency is shown in Fig. 3.20. The MS was 1 at 1.825 GHz, which corresponded to the resonant frequency of the structure. From the curve, the radiating bandwidth of the first mode was 110 MHz and the modal quality factor was 16.5. These values in reality can be achieved if the mode is properly excited.

Fig. 3.21 shows the current on the top and bottom side of the CSRR-loaded structure which corresponds to the first mode. The current had a curve shape along the periphery of the CSRR while a high current density was along the edges of the MPA which corresponded to the non-radiating edges of the normal MPA. This explains why the shift in the microstrip feedline was required along the width of the patch to excite the proper mode.

The analysis using the theory of characteristic mode clearly indicated that the



(a)



(b)

Figure 3.21: Characteristic current corresponding to the first mode on the CSRR-loaded MPA structure (a) Top side, (b) Bottom side

CSRR-loading on the patch resulted in lowering the resonant frequency of the structure. From the characteristic currents on the structure, the increase in the current path was evident which resulted in the lower resonant frequency of the structure. The analysis also gave an idea of location for better excitation of the mode to get the required resonance.

### **3.4 Comparison & Conclusions**

The proposed design of miniaturized MPA is compared with other small MPA designs found in literature. Table 3.4 summarizes different features of some of the well cited references from literature along with the proposed antenna features. Most of the reported designs have limited bandwidth. This is in line with the theoretical limits of ESA. The bandwidth is much more limited in the designs which are miniaturized using the MTM-inspired techniques. Most of the designs are also not planar and employ complex structures by bending, folding and shorting the MPA. Some designs which are based on the material loading have simple design methodology but they use the expensive dielectric substrates which are not readily available. Others do not provide the proper design methodology for using the technique to design MPA in different band.

Since the proposed technique is a MTM-inspired one, a close comparison of this technique with other MTM-inspired techniques reveal its usefulness. The bandwidth provided by this technique is much better than the other reported MTM-inspired miniaturized MPA designs. It provides a bandwidth of 2% while

the other MTM-inspired techniques have reported a bandwidth of 0.5% for the miniaturized MPA designs. The miniaturization achieved by the technique is also better than other MTM-inspired techniques. The antenna has comparable radiation efficiency and gain. The proposed technique therefore, results in a simple and planar MPA structure which can be designed for several bands using a simple design methodology and offers several advantages over many of the reported designs.

Table 3.4: A Comparison of the Proposed Antenna with other Miniaturized MPAs in Literature

Ref.	Band	BW	Size	Size Reduction	$\eta$ or G	Miniaturization Technique	Antenna Structure	Comments
[12]	900 MHz (Single Band)	10%	$148 \times 103 \times 31 \text{ mm}^3$	50%	G = 6 dBi	Material Loading	Non-planar	Specifically designed for Korean Band
[17]	1.24 GHz (Single Band)	1%	$15 \times 15 \times 3.3 \text{ mm}^3$	90%	Not reported	Material Loading	Non-planar	Use of textured dielectric not readily available
[19]	2.45 GHz (Single Band)	4%	$15 \times 15 \times 6 \text{ mm}^3$	75%	$\eta = 90\%$	Shorting & Folding	Non-planar	Can be designed for other bands
[26]	2.45 GHz (Wide-band)	40%	$54 \times 24 \times 8 \text{ mm}^3$	50%	G = 2 dBi	Shorting & Folding	Non-planar	No design guideline for other bands
[39]	935 MHz (Single Band)	0.3%	$15 \times 30 \times 3.2 \text{ mm}^3$	75%	Not reported	Slots in Patch	Planar	No design guideline for other bands
[29]	2.45 GHz (Wide-band)	34%	$30 \times 30 \times 10 \text{ mm}^3$	50%	$\eta = 70\%$	Reshaping Patch	Non-planar	Giuseppe Peano fractal geometry
[45]	1.5 GHz (Single Band)	7%	$20 \times 30 \times 1.5 \text{ mm}^3$	90%	Not reported	Modification of GP	Planar	No design guideline for other bands
[50]	2.635 GHz (Single Band)	1.9%	$20 \times 30 \times 1.5 \text{ mm}^3$	77%	$\eta = 67.5\%$	Modification of GP	Planar	Complex SIW structure in GP, No design guideline for other bands
[56]	2.45 GHz (Single Band)	0.4%	-	75%	$\eta = 28.1\%$	MTM-inspired	Non-planar	Circular patch with MTM structure in between patch and GP
[57]	700 MHz (Single Band)	0.5%	-	60%	G = -7.9 dBi	MTM-inspired	Non-planar	Circular patch with MTM structure in between patch and GP
This Work	2.45 GHz (Single Band)	2%	$14 \times 18 \times 0.8 \text{ mm}^3$	76.5%	$\eta = 30\%$	MTM-inspired	Planar	Easy guidelines for the design, can be made for other bands e.g. 700 MHz band, 5 GHz band

## CHAPTER 4

# MIMO ANTENNA SYSTEMS

Since the goal of this work is to design MIMO antenna systems, it is important to first go over the basics of MIMO systems, importance of MIMO antenna in these systems, evaluation parameters for a MIMO antenna system and review of different MIMO antenna designs found in literature. This chapter covers all of these issues. It starts with a description of MIMO system and explains how it offers better communications over a SISO system. The importance of antenna used in a MIMO system is highlighted and the performance evaluation metrics of MIMO antenna system are described. The chapter also summarizes the main work found in literature on the design of MIMO antenna systems to date.

### 4.1 MIMO Systems

Digital communications using MIMO systems has emerged as an important technology breakthrough in recent years. The MIMO system makes use of the diversity in a multipath environment and provides an improved performance in terms of

reliability of the communication or higher data rates as compared to a single-input-single-output (SISO) system. Such a multipath scenario normally exists in an urban environment where the communication is mainly non-line-of-sight (NLOS). In the 4G-LTE wireless standards, MIMO systems have been adopted to achieve such high data rates.

The research covering MIMO systems gained momentum after 2000 when it was first proposed by Bell labs [65]. Since then, a lot of literature has been published in various journals covering various aspects of the topic. Some of the important work covering the topic can be found in [66–69].

The use of MIMO systems results in an improved performance due to the diversity gain, array gain, multiplexing gain and interference reduction [69]. However, due to conflicting demands of these operating methods, it is not possible for the MIMO system to fully exploit all these gains simultaneously.

Diversity is a powerful feature of a MIMO system. For an  $N \times N$  MIMO system, if the same signal is transmitted over all the channels, and all the channels fade independently, then the probability of receiving the signal at the receiver is much higher than a SISO system. The gain obtained in this way is called diversity gain. The diversity gain of a MIMO system highly depends on the number of uncorrelated channels.

The array gain of MIMO antenna system can be utilized when the channel state information is known to receiver and transmitter. By assigning different weights to different channels, an increase in the average SNR is achieved.



Cellular systems use frequency reuse in cells which causes co-channel interference. A MIMO system is capable of reducing such interference. The MIMO system can differentiate between the spatial signature of the desired signal and co-channel signal thus reducing such interferences.

Multiplexing gain is another powerful feature of a MIMO system. In this scheme, the transmitter sends independent data signals on each channel. In this way, the channel capacity of a MIMO system increases linearly with the increase in the number of uncorrelated channels.

The upper limit of the channel capacity of a SISO system can be computed by Shannon's equation. MIMO antenna systems can achieve a capacity beyond this limit by utilizing multiplexing gain. The channel capacity of an  $N \times N$  MIMO antenna system when the power is equally divided among the  $N$  channels is given by [66];

$$C = N \times \log_2 \left( 1 + \frac{SNR}{N} \right) \quad (4.1)$$

where SNR is the signal-to-noise ratio.

Fig. 4.1 shows the upper limit on the capacities of SISO,  $2 \times 2$  MIMO system,  $4 \times 4$  MIMO system and  $8 \times 8$  MIMO system in an ideal environment. As seen from Fig. 4.1, the capacity of an  $8 \times 8$  MIMO system is 5 times higher than a SISO system at an SNR of 20 dB. This capacity however gets limited due to the correlation in antenna patterns and propagation channel effects [66]. Therefore, an important consideration in the MIMO system is the design of its antenna. For a MIMO system to be implemented in a compact wireless device, there is a

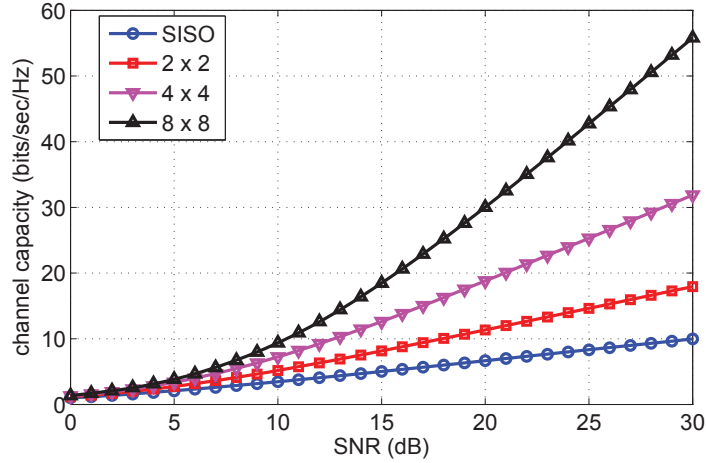


Figure 4.1: Upper limits of the channel capacity of SISO and MIMO systems.

limited space for its antenna. For closely placed multiple antenna elements in such arrangement results in high coupling between antenna elements and induces a high correlation among channels. This can severely reduce the actual capacity limits of the MIMO system. To achieve a better capacity, good isolation and low spatial correlation are required between the elements of the MIMO antenna system. The capacity of single user  $N \times N$  MIMO system in a real multipath environment is given by [66];

$$C = \log_2 \left( \left| I + \frac{SNR}{N} H H^* \right| \right) \quad (4.2)$$

where ' $\mathbf{I}$ ' is the identity matrix of dimension  $N \times N$  and ' $\mathbf{H}$ ' is called the channel coefficient matrix. The entries of the channel matrix contains the gain and phase information of the propagation paths between the transmitter and receiver elements. The channel matrix can be computed from theoretical models of different propagation environments or through measurements.

## 4.2 MIMO Antenna System

The front end of the MIMO systems is the MIMO antenna. It is an important part of the MIMO systems and its design and performance directly affects the performance of the overall system. Therefore, the design of novel MIMO antennas has received considerable attention in the recent years. The desirable features of a MIMO antenna system are low profile design with small antenna elements. To maximize the diversity gain of a MIMO system, the elements of the MIMO antenna must also have high isolation between them [70], and all antenna elements should have the same average received signal strength [71]. The requirement of implementing a MIMO system in compact devices asks its antenna designer to look into two main issues which are as follow;

- (i) Find miniaturization techniques for low-profile antenna elements so that multiple elements can be accommodated in limited space.
- (ii) Find techniques to enhance isolation between closely places antenna elements.

Some of the initial papers on the topic of MIMO antenna system appeared in 2005 such as [70], [72]. These papers included some basic designs using monopole antennas where the performance of the MIMO antenna was discussed and the evaluation of the parameters of the MIMO antenna were described. Many designs were proposed in the years to follow. In all of the work, it was noted that novel small antenna elements were required and novel methods were pursued to increase the isolation between antenna elements.

## 4.3 Performance Metrics for MIMO Antenna System

The improvement that the MIMO system offers over its SISO counterpart in communication systems is highly dependent on the performance of its MIMO antenna. Therefore, it is vital to evaluate the performance of a MIMO antenna system. Conventional antenna performance metrics are no longer sufficient to describe and predict the performance of a MIMO antenna system in a real wireless environment.

The performance evaluation of a MIMO antenna system is based on various parameters as opposed to a SISO system whose performance measures are mainly its s-parameters and far-field radiation characteristics. These parameters (performance metrics) characterize a MIMO antenna system for its frequency response, mean effective gain in a particular environment and the degree of its diversity gain. The parameters needed to evaluate a MIMO antenna system include the s-parameters, the total active reflection coefficient (TARC) [73], the mean effective gain (MEG) [74], the correlation coefficient [75] and the channel capacity [76]. The detail description of each is given in following sections.

### 4.3.1 Resonance and Isolation

The scattering parameters of any antenna system are the first measure of its performance. For a MIMO antenna system, the S-parameters give the resonance and bandwidth of each antenna element and the port isolation between different an-

tenna elements. In a MIMO system, it is desirable that all antenna elements of the MIMO antenna system have same frequency response. For good radiation efficiency of the antenna, a high isolation (low mutual coupling) is required between antenna elements.

### 4.3.2 Total Active Reflection Coefficient (TARC)

Although we get some basic measures of the performance of a MIMO antenna system from its S-parameters, yet they are not the best representation of its frequency response especially its effective bandwidth. Therefore, total active reflection coefficient (TARC) was introduced for broadband characterization of multi-port antenna system. The TARC for a MIMO antenna is defined as the ratio of the square root of the total reflected power to the square root of the total incident power. Mathematically it is expressed as [73];

$$\Gamma = \sqrt{\frac{\sum |b_i|^2}{\sum |a_i|^2}} \quad (4.3)$$

where  $b_i$  and  $a_i$  is the reflected and incident signals, respectively. The incident and reflected signals are related to each other by the S-parameter of the MIMO antenna system. They are given as [73];

$$[b] = [S].[a] \quad (4.4)$$

where  $S$  is the  $N \times N$  scattering parameter matrix of the  $N$ -element MIMO antenna system.

As evident from Eq.(4.3), the TARC has a value between 0 and 1. When the entire incident signal is reflected back, TARC has a value equal to one while it has a value equal to zero when the entire incident signal is radiated and no part of the incident signal is reflected back. Thus zero signifies the best performance and one signifies a total loss. For a MIMO antenna system, a TARC versus frequency plot gives the effective bandwidth of the MIMO antenna. Often, the TARC is computed in decibels. TARC takes into account the coupling between different antenna elements as well as the combination of randomly phased incoming signals. TARC also gives a measure of the antenna efficiency of a lossless MIMO antenna system. TARC is calculated for different combination of excitation signals at the input ports. To calculate TARC from the measured S-parameters of an  $N$ -element MIMO antenna system, Eq.(4.4) is used to calculate the reflected signals. The incident signals are taken with unity amplitude and different phase differences. After calculation of reflected signal, Eq.(4.3) is used to calculate the TARC of the MIMO antenna system.

### **4.3.3 Antenna Efficiency**

In general, most of the miniaturized antennas are not lossless and they have low radiation efficiencies. When using such antennas as the elements of a MIMO antenna system, it is important to know their radiation efficiency as this parame-

ter is directly related to the diversity and multiplexing gain of a MIMO antenna system. The efficiency of an antenna is the sum of its radiation efficiency and matching efficiency. While the s-parameters and TARC gives a good measure of the matching efficiency of a MIMO antenna system, they cannot give information about the dielectric and ohmic losses within the antenna. Although the reflection efficiency may be high, the dielectric and ohmic losses within antenna can considerably decrease the radiation efficiency and performance of an antenna. Therefore, it is important to have knowledge of the radiation efficiency of the antenna which cannot be obtained from the S-parameters and TARC curves. There are different methods to measure the total efficiency as well as the radiation efficiency of the antenna [77]. One such method is the gain-directivity method. In this method, the gain and directivity of an antenna are measured and the ratio of the two gives the antenna efficiency. The method requires anechoic chambers for accurate results where far field radiation patterns of the antenna can be measured. Another method to measure the efficiency of the antenna is the Wheeler cap method [77]. This method is much simpler as it requires measurements taken from network analyzer only. In this method, initially the input reflection coefficient of the test antenna is measured. The antenna is then placed on a ground plane and covered with a conducting cap. The reflection coefficient of the antenna is again measured for this arrangement. The radiation efficiency is then given as [77];

$$\eta = 1 - \frac{1 - |\Gamma_{cap}|^2}{1 - |\Gamma_{in}|^2} \quad (4.5)$$

The basic principle behind this method is that when the antenna is covered by a conducting cap, the radiated signal is reflected back to the antenna. Therefore, a lossless or low loss antenna will have high reflection at the input when covered with a conducting cap. For a very lossy antenna, since the input signal is lost within the antenna, nothing much will be reflected back due to conducting cap.

#### 4.3.4 Correlation Coefficient

The correlation coefficient is a parameter which gives a measure of how much the signals received by the elements of a MIMO antenna system are correlated due to antenna patterns. This parameter is a function of the radiation patterns of the MIMO antenna elements. The diversity performance of a MIMO antenna system degrades with the increase in mutual coupling between the antenna elements of the MIMO antenna system. The envelop correlation ( $\rho_e$ ) between two antenna elements is computed from their far-field radiation characteristics. It is given as [75];

$$\rho_e = \frac{|\iint F_1(\theta, \phi) * F_2(\theta, \phi) d\Omega|^2}{\iint |F_1(\theta, \phi)|^2 d\Omega \iint |F_2(\theta, \phi)|^2 d\Omega} \quad (4.6)$$

where  $F_i(\theta, \phi)$  is the radiation pattern when element 'i' is active and '\*' represents the Hermitian product.

The correlation coefficient is the square root of envelope correlation  $\rho_e$ . The value of the correlation coefficient lies between 0 and 1 where 0 signifies totally uncorrelated antennas and 1 tells that the two antenna elements are the same to the channel i.e. they are like a single antenna. For a good diversity performance



in the new 4G standards, the correlation coefficient between the antenna elements must be below 0.3 and envelop correlation coefficient must be less than 0.5

The calculation of the correlation coefficient is difficult as it involves the radiation patterns of the antenna elements. However, if the MIMO antenna is operating in a uniform multipath environment which is the one where fading envelope is Rayleigh distributed, the incoming field arrives in the horizontal plane only, the incoming fields orthogonal polarizations are uncorrelated, the individual polarizations are spatially uncorrelated, and the time-averaged power density per steradian is constant [78], then the correlation coefficient between two antenna elements can be computed from it S-parameters if the antenna efficiency is also high. It is given as [75];

$$\rho = \frac{|S_{11} * S_{12} + S_{21} * S_{22}|}{\sqrt{(1 - |S_{11}|^2 - |S_{21}|^2)(1 - |S_{12}|^2 - |S_{22}|^2)}} \quad (4.7)$$

Eq.(4.7) is valid for lossless antennas only. Normally, miniaturized antennas used as the elements of the MIMO system have low radiation efficiency. In order to factor in the affect of efficiency of the antenna elements in Eq.(4.7), a modified version of this equation is normally used for antenna elements with low radiation efficiency. It is given by

$$\rho = \frac{|S_{11} * S_{12} + S_{21} * S_{22}|}{\sqrt{(1 - |S_{11}|^2 - |S_{21}|^2)(1 - |S_{12}|^2 - |S_{22}|^2)\eta_i\eta_j}} \quad (4.8)$$

where  $\eta_i$  and  $\eta_j$  are the radiation efficiency of antenna element  $i$  and  $j$ , respectively.

### 4.3.5 Radiation Pattern

The radiation pattern of an antenna gives the spatial dependence of its field strength. They are measured for an antenna and graphically represented by two-dimensional and three-dimensional polar plots. In a MIMO antenna system, it is measured for each antenna element. To calculate the radiation pattern of an element of a MIMO antenna, the element is excited by a source and the rest of the antenna elements are terminated with a  $50\Omega$  load. The field patterns are then obtained either by simulation or by measuring them at an antenna testing facility.

### 4.3.6 Mean Effective Gain (MEG)

The gain of an antenna is an important measure in the calculation of its link budget which determines the coverage area and achievable data rates of the system. In a mobile propagation environment, the directive gain of an antenna cannot be used to get the accurate results. In such environments, the mean effective gain (MEG) of the system is calculated. The MEG of an antenna is defined as the ratio of mean received power to the mean incident power. The MEG of an antenna operating in an urban mobile environment is determined by the mutual relation between the field patterns of the antenna and the statistical distribution of the signal in the environment [74].

For a mobile wireless environment with the assumptions defined in [78], the MEG of an antenna can be computed using its two-dimensional gain patterns. It

is given as,

$$MEG = \frac{1}{2\pi} \int_0^{2\pi} \left[ \frac{\Gamma}{1+\Gamma} G_\theta\left(\frac{\pi}{2}, \phi\right) + \frac{1}{1+\Gamma} G_\phi\left(\frac{\pi}{2}, \phi\right) \right] d\phi \quad (4.9)$$

where  $\Gamma$  is the cross-polarization discrimination (XPD) of the incident field (ratio between the vertical and horizontal power densities),  $G_\theta$  and  $G_\phi$  are the gain pattern components of the antenna elements. Using the above definition, the maximum possible MEG with 100% antenna efficiency is -3 dB [78]. For a MIMO antenna system, the MEG of all elements should be the same to get the best diversity performance. The ratio of the MEG of the antenna elements of the MIMO antenna system should be close to unity and should not exceed 3dB for good performance.

### 4.3.7 Channel Capacity

As mentioned in the previous sections, a MIMO system can be used to increase the channel capacity by utilizing the multiplexing gain. The design of a MIMO antenna has profound affect on the multiplexing gain of the MIMO system. Therefore, the antenna should also be evaluated for the upper limit of channel capacity it can give in a particular environment. For this, either measurements can be carried out in real environments or theoretical models are used which predict the performance of the antenna based on the radiation characteristics of the antenna elements. Recently, reverberation chambers were designed to test the channel capacity and other performance of the MIMO antenna [79]. The reverberation

chamber emulates an isotropic multipath environment of similar type as of urban or indoor environments. Thus it helps in measuring the MIMO system channel capacities without driving around in the urban environment or moving around in with measurement equipment in indoor environment.

Some models are developed for estimating the channel capacity of a MIMO antenna system for isotropic multipath environments [76]. The models use Eq.(4.2) to find the channel capacity and calculates the channel matrix based on the 2D radiation patterns of the antenna. When the same MIMO antenna systems are used at both the transmitter and receiver ends, the channel matrix  $\mathbf{H}$  is given as [76];

$$H = \sqrt{\Psi}G\sqrt{\Psi} \quad (4.10)$$

where  $\mathbf{G}$  is a random matrix with independently identically distributed complex Gaussian entries.  $\Psi$  is the transmit and receive correlation matrix. The entries of  $\Psi$  matrix are calculated using

$$\Psi_{i,j} = \frac{\mu_{ij}}{\sqrt{\mu_{ii}\mu_{jj}}} \quad (4.11)$$

$\mu_{ij}$  is calculated based on the field patterns of antenna element  $i$  and  $j$ . It is given by

$$\mu_{ij} = \int_0^{2\pi} [\Gamma A_{i\theta} A_{j\theta}^* + A_{i\Phi} A_{j\Phi}^*] d\Phi \quad (4.12)$$

where  $A(\theta)$  and  $A(\Phi)$  are the 2D radiation pattern of the antenna elements in the two planes.

Thus, the radiation patterns of the elements of MIMO antenna systems are required in estimating the performance of the antenna in terms of channel capacity when they are used in urban environment.

## 4.4 MIMO Antenna System Designs

While the MIMO system was proposed more than a decade ago, the antenna design for such system did not receive much attention initially. Some of the initial work in the MIMO antenna design included the performance analysis of MIMO antenna systems whose elements were made up of standard wire based monopole antennas [70]. The performance of the MIMO antenna system was measured and compared to the theoretical capacity of the MIMO systems. Although the design was unsuitable for any practical use, it helped in studying the effects of antenna design on MIMO system performance. The main conclusion drawn out of this work was that mutual coupling between antenna elements significantly degrades the performance of the MIMO systems.

Since the main use of MIMO systems is in the portable wireless devices, most of the proposed designs in the literature are related to printed antennas and mostly planar structures. Most of the designs that appeared in the literature were made up by adding multiple modified printed monopoles [70, 80–93], printed dipoles [94–96], slot antennas [97, 98], Printed Inverted F-shape antennas (PIFA) [72, 99–108], MPA [55, 109, 110], or a combination of these antennas [111, 112]. Fig. 4.2 shows the geometries of the standard printed antennas such as dipoles, monopoles, MPA

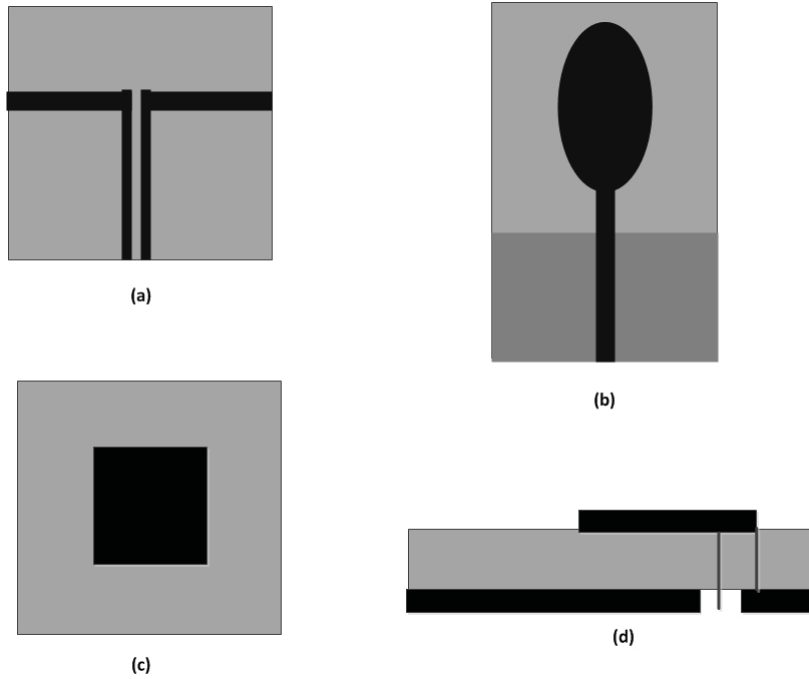


Figure 4.2: Geometry of standard printed antennas, (a) Printed Dipole, (b) Printed Monopole, (c) Patch Antenna, (d) Side view of PIFA

and PIFA.

#### 4.4.1 Monopole Based MIMO Antenna System

Printed monopoles are easy to design and fabricate and exhibit good operating bandwidth. A number of MIMO antenna designs are presented in the literature whose elements are printed monopoles. The size limitations of antennas are often overcome by shaping, bending and meandering the monopoles. However, these types of MIMO antennas suffer from high mutual coupling among its antenna elements. Therefore, a number of designs are solely based on improving the isolation between closely placed monopoles e.g. [90, 113–115].

Among the initial designs of the MIMO antenna systems was a 6-element

MIMO antenna system made up of monopoles [70]. In this work, the MIMO antenna was analyzed and it was concluded that isolation between antenna elements of the MIMO system is an important factor which greatly affects the performance of the MIMO system. High isolation between antenna elements was therefore concluded to be important for the MIMO antenna system design.

In [80], a two element MIMO antenna system was proposed for WiBro applications. The elements of the antenna were folded monopoles. The isolation was improved by adding a ground wall at one end of the antenna. A 4-element MIMO antenna system made up of monopoles was proposed in [81]. The total size of the antenna was  $95 \times 60 \times 0.8$  mm<sup>3</sup> and it was made on an FR4 substrate. The antenna was designed to cover the UMTS band with a center frequency of 2 GHz and a bandwidth of 320 MHz. A simple and compact decoupling network based on transmission lines was proposed in [82]. It improved the isolation between two printed monopoles by more than 10 dB. In [83], a two element MIMO antenna system was proposed whose elements were C-shaped monopoles. The antenna was designed for WLAN operation and was frequency reconfigurable. It could switch between 2.4 GHz and 5 GHz using the RF switches. A neutralization line method was used between the antenna elements to improve the isolation.

A 2-element MIMO antenna system was presented in [84] using folded monopoles as its elements. The antenna operated in the 2.4 GHz ISM band and was designed for mobile hand held devices. An E-shape monopole triband antenna proposed as an element for MIMO antenna system was presented in [85]. The an-

tenna resonated at 2.4 GHz, 5.2 GHz and 5.8 GHz effectively covering the WLAN bands. Different configurations of an array of two elements were analyzed to measure the performance of the antenna. In [87], a monopole based 2-element dual band MIMO antenna system was proposed. The antenna resonated at 2.4 GHz and 5.6 GHz. The isolation between the elements was improved by a transmission line network.

In [86], a MIMO antenna system for 2.4 GHz WLAN and WiMAX application was proposed. The antenna consisted of two elements of meandered line monopoles. A metamaterial based ring resonator structure was designed and placed between the two elements to increase the isolation. In [89], a 2-element MIMO antenna system for use in the portable wireless devices was presented. The antenna resonated at 2.45 GHz and 5.8 GHz. The antenna was made up of two monopoles. A shorting strip and an isolation stub was designed to reduce the mutual coupling between the antenna elements. The volume of the antenna was  $15 \times 50 \times 0.8 \text{ mm}^3$  and it was fabricated on FR4 substrate. In [91], a 2-element MIMO antenna system made up of meandered monopoles was proposed for mobile handset application. The antenna was designed for the LTE operation and covered the 800 MHz band. The design was compact and occupied a volume of  $40 \times 50 \times 0.8 \text{ mm}^3$ . A frequency reconfigurable 2-element MIMO antenna system composed of printed monopoles was presented in [116]. PIN diodes were embedded in the design to switch the band of operation of the antenna. The antenna operated in either the WLAN band or the WiMAX band depending on the state



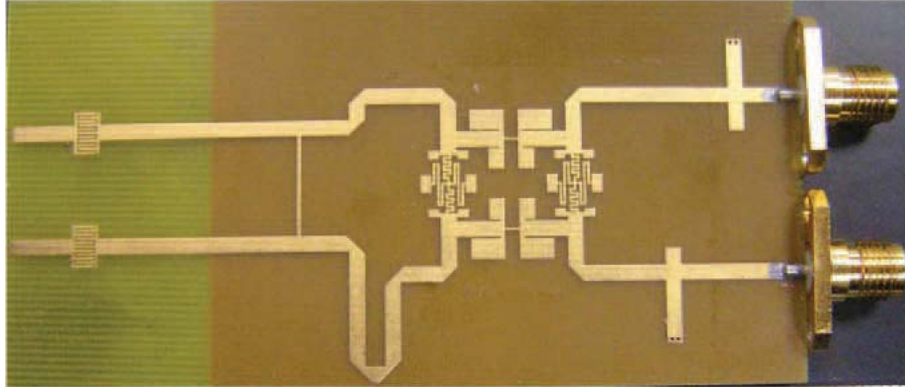


Figure 4.3: Fabricated two element monopole based MIMO antenna system with microstrip line structure for high isolation [113].

of PIN diodes.

Many of the recent papers that appeared in the literature related to printed monopole based MIMO were oriented towards new methods to increase isolation between antenna elements. In [90], a 2-element monopole based MIMO antenna system was presented. The antenna covered a wide band and resonated from 2.4 GHz to 6.25 GHz. Two bend slits in the ground plane were proposed to increase the isolation between the antenna elements. In [113], [114], [115] and [117], different isolation enhancement mechanisms were proposed between two printed monopoles. The band of all these antennas system was 2.4 GHz ISM band. In [113], a synthesized microstrip line structure to decrease mutual coupling between monopoles was presented. Fig 4.3 shows the photo of fabricated antenna. The antenna had a dual band operation in the 2.4 GHz and 5.2 GHz band. Using the proposed decoupling technique, more than 20 dB improvement in isolation was achieved in both the bands.

In [115] a decoupling network using parasitic elements was presented. A neu-

tralization line technique was introduced in [117] to increase isolation between monopoles. A metamaterial based isolation technique was presented in [114]. In this work, split-ring resonator like structures were placed between two monopoles to increase the isolation.

A compact design of 2-element MIMO antenna system was proposed by [93]. The elements were wideband monopoles. The antenna covered the band from 3.1 GHz to 10.6 GHz and was designed for portable ultra wideband applications. In [92], a compact MIMO antenna system was presented. The elements of the antenna were folded monopoles with varactor diodes. The antenna was frequency reconfigurable between 2.3 GHz and 2.6 GHz band. It was also electronically beam steerable.

In summary, a majority of the MIMO antenna designs proposed were made using monopoles as their element. This was mainly due to the easy design and the limited space occupied by monopoles on printed structures. However, these type of antennas suffered from high correlation and coupling between their antenna elements. Therefore, a major part of the sited work consisted of designs where strategies for increasing the port isolation for closely placed printed monopoles was presented. Most of the monopoles based MIMO antenna systems consisted of 2-element with only a few were 4-elements designs. The design presented in literature covered different bands but most of the designs were presented for the 2.45 GHz ISM band.

#### 4.4.2 Dipole Based MIMO Antenna System

A printed dipole is also an easy to fabricate and simple antenna structure. It has an omnidirectional radiation pattern. However, in MIMO application, this antenna type suffers from large size and high mutual coupling. Nevertheless, the dipole has been analyzed for MIMO system application and few MIMO antenna system designs are proposed in literature based on dipole.

In [94], a 4-element MIMO antenna system based on folded-dipoles was proposed for use in laptops. The folding of antenna elements and dielectric loading was used to reduce the antenna size. The antenna operated in the 5.2 GHz WLAN band. A spiral-dipole antenna for MIMO application was proposed in [95]. The antenna was circular polarized and resonated at 5.2 GHz. A 2-element MIMO antenna system was proposed in [96]. Each antenna element was made up of dipole with a magnetic slot. The antenna covered a band from 2.0 GHz to 5.6 GHz. It was designed for mobile phone applications.

#### 4.4.3 PIFA Based MIMO Antenna System

PIFA can be viewed as a folded monopole or a shorted  $\lambda/4$  patch. It is widely used in many wireless mobile phones. They are small in size but require a large ground plane. Isolation among elements in PIFA based MIMO antenna system is also an issue. Several MIMO antenna systems are proposed based on PIFA or modified versions of PIFA.

In [72], a 2-element MIMO antenna system was proposed for mobile handset

applications. The elements of the antenna were modified PIFAs. The antenna operated in the 5.2 GHz band. In [108], a modified PIFA based MIMO antenna system was proposed and analyzed for handheld devices application. The antenna worked in the 2.5 GHz band. A quad-band MIMO antenna system composed of two PIFA was proposed in [105]. The antenna resonated in the 2.4 GHz band, 3.5 GHz band, 5.2 GHz band and 5.8 GHz band covering the WLAN and WiMAX bands. A combination of a C-shaped slot and a T-shaped slit was used to make the PIFA multiband. In [118], a compact 2-element PIFA based MIMO system was presented. The antenna covered the 0.9 GHz GSM band and 2.4 GHz WLAN band. A dual band 2-element MIMO was proposed in [119]. The antenna resonated in the 2.4 GHz and 5.2 GHz WLAN Band. The antenna occupied a space of  $100 \times 50 \text{ mm}^2$ . A parasitic element was placed between the antenna elements to improve isolation. A 4-element MIMO antenna system was presented in [99]. The elements were modified PIFA resonating in the ISM band. The antenna occupied a space of  $120 \times 120 \times 16.4 \text{ mm}^3$ . Fig. 4.4 shows the photo of the fabricated 4-element antenna.

A MIMO antenna system consisting of two compact PIFAs was designed for USB dongle [102]. In [103], an isolation method for two closely placed PIFAs was proposed in the 2.4 GHz WLAN band. A T-shaped ground slot with a chip capacitor was designed to improve isolation. In [100], a 4-element MIMO antenna system was proposed. The elements of the antenna were miniaturized PIFA. The PIFA was miniaturized by meandering the structure. The total area occupied

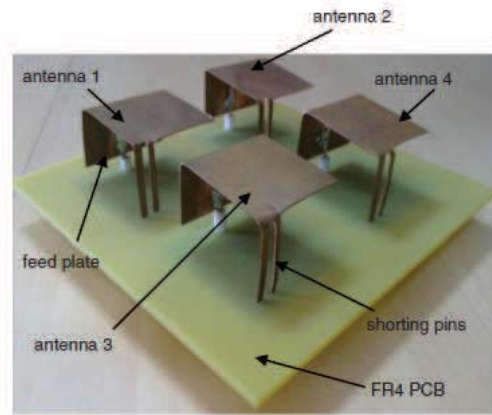


Figure 4.4: Fabricated 4-element PIFA based MIMO antenna [99].

by the antenna system was  $105 \times 55 \text{ mm}^2$ . A tunable 2-element MIMO antenna system composed of compact multiband PIFA is proposed in [101]. The antenna miniaturization and tunability is achieved by inductor and varactor loading. The antenna can be tuned electronically from 720 MHz to 970 MHz.

Due to the compact size and ease of design, PIFA has been widely used as an element of the MIMO antenna system. Its use is comparable to that of printed monopole. The designs reviewed here and others found in literature covered several bands and there were many designs which covered multiple bands simultaneously. Thus, PIFA remained a foremost choice in the MIMO antenna design.

#### 4.4.4 MPA Based MIMO Antenna System

MPAs are very common and widely used. Because of their easy design, low profile, planar structure and easy integration with integrated circuit technology, they have found application in many wireless devices. Despite their several advantages, they are seldom used in the MIMO antenna system design, mainly due to their large

size. However, some papers can be found in literature where MPA has been used as the element of the MIMO antenna system.

In [109], a three element MIMO antenna system based on the triangular patches was proposed. The antenna operated at the 2.65 GHz. The performance of the antenna was evaluated and it was found that the antenna had a high diversity gain. A 4-element MIMO antenna system consisting of proximity coupled patch antennas was proposed in [120]. The antenna was designed for 2.4 GHz WLAN operation. In [55], a miniaturized patch was proposed for use in the MIMO application. The miniaturization of patch was achieved by using a metamaterial substrate. The metamaterial substrate was designed by placing perpendicular SRR in between the patch and the ground plane. Although the substrate became thick, significant miniaturization, low mutual coupling and correlation coefficient was achieved in the MIMO antenna system that was based on this substrate. Fig. 4.5 shows the geometry of the SRR based patch antenna.

In [121], a patch antenna based 2-element MIMO antenna system was presented. The antenna operated in the 5.8 GHz WLAN band. The isolation between the antenna elements was improved by a slot in the ground plane.

#### **4.4.5 Other MIMO Antenna System**

Several MIMO antenna system designs are proposed in literature with novel antenna element designs. In [122], a 24 element and a 36 element MIMO antenna system was analyzed for channel capacity. The elements of the antenna system

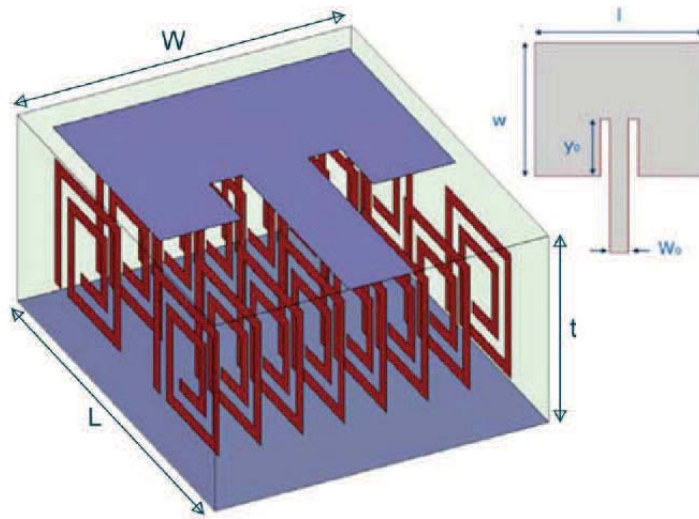


Figure 4.5: Geometry of the SRR based patch antenna [55].

were quarter wavelength slot antennas. The elements were arranged in a cube shape and it was shown how the MIMO antenna system increased the channel capacity and how the coupling between antennas degrades the performance of MIMO systems. In [123], a two element MIMO antenna system made up of loop antennas was proposed. The antenna operated in the ISM band. The antenna was compact and occupied a volume of  $38 \times 28 \times 1.5 \text{ mm}^3$ . In [124], a 4-element MIMO antenna system was proposed. The elements of the MIMO antenna were quarter wavelength slot antenna. The antenna covered a band from 1.6 GHz to 2 GHz. A multi-band MIMO antenna system was proposed in [125]. The antenna was designed for WLAN access point applications and consisted of dual loop antenna. The antenna resonated in the 2.4 GHz, 5.2 GHz and 5.8 GHz bands. The size of each antenna element was  $10 \times 20 \times 40 \text{ mm}^3$ .

A 3-element MIMO antenna system was proposed in [126]. The elements

of the MIMO antenna system were printed Yagi-Uda antenna with integrated balun. The elements were arranged in such a way that they had orthogonal radiation patterns, thus yielding a very low correlation coefficient. The antenna was designed for WLAN operation and covered the 2.4 GHz and 5 GHz band. A 2-element MIMO antenna system was designed in [127] for the 750 MHz LTE band. The elements of the MIMO antenna were ferrite antennas. The total space occupied by the antenna system was  $110 \times 55 \times 1.5 \text{ mm}^3$ . A 2-element cavity backed slot antenna was described in [128]. The antenna operated in the 5.2 GHz band and had a good isolation between antenna elements. The antenna was compact and targeted the mobile phone applications. The antenna was also analyzed for the channel capacity.

A 2-element magneto-dielectric based antenna was proposed in [129]. The antenna operated in the 700 MHz LTE band. Although the efficiency of the antenna elements were 30% but the antenna was highly compact and the total size of the antenna system was  $85 \times 40 \text{ mm}^2$ . A 2-element pattern reconfigurable MIMO antenna system was presented in [130]. The antenna elements consisted of U-slot patch antenna and operated in the 5.2 GHz band. Each edge of the patch was shorted with a PIN diode. The proposed antenna could electrically reconfigure the radiation pattern between conical and boresight patterns based on the switching of the PIN diode. A dual band MIMO antenna was presented in [131]. It consisted of two 4-shaped antennas. The isolation between the antenna was improved by a defected ground structure. The lower band of the antenna



covered 803-823 MHz and in the higher band, it covered 2440-2900 MHz. The antenna was designed for the mobile terminals and occupied a total volume of  $100 \times 50 \times 1.5 \text{ mm}^3$ . A 4-element MIMO antenna system was proposed in [132]. The antenna elements were made up of 4-shaped antennas. The antenna covered the 750 MHz LTE band and 2.4 GHz band. The volume of the antenna was  $58 \times 110 \times 1.56 \text{ mm}^3$ .

Many of the proposed designs consisted of a combination of standard antenna element types. In [133], a 2-element MIMO antenna system was presented with a broadband operation. The antenna covered several bands including the GSM, WLAN, UMTS and some LTE bands. The antenna elements were combination of monopoles and halfwave dipoles. An ultra wideband MIMO antenna system was proposed in [111]. The antenna was designed for USB dongle application and operated from 1.7 GHz to 5.15 GHz. The elements of the MIMO antenna were a combination of slot antenna and monopoles. A MIMO antenna system for WLAN operation in the 2.4 GHz band was proposed in [134]. The antenna elements were a combination of ring patch antenna and PIFA. A MIMO antenna system operating in the 2.55 GHz band was proposed by [135]. The antenna had a non-planar structure in which three elements made up of dipole and half-wave slot antenna were placed perpendicular to each other.

## 4.5 Conclusions

The design of antenna for MIMO system require special consideration which was outlined in this chapter. The metrics used for the MIMO antenna evaluation are different than for a normal single element antenna, and these must be used to properly characterize the performance of a MIMO antenna system.

A comprehensive survey of the MIMO antenna system was presented. Various designs of MIMO antenna systems were presented in literature during the past few years. Most of these designs utilized printed monopole or PIFA as the element of MIMO antenna system. There were others which utilized novel elements but such cases were few in number. Fig. 4.6 shows the classification of MIMO antenna systems according to the antenna element used which clearly depicts the high use of printed monopoles and PIFAs in MIMO antenna system design. MPA has received less attention due to its size. However, with proper miniaturization, this element can be as useful as any other antenna type.

The designs found in literature were made for several bands. The 2.45 GHz ISM band received considerable attention. This was mainly due to the wide use of this band by many applications. Also, some of the designs proposing the generalized concept for isolation enhancement between the antenna elements used this band for easy measurements. Few designs were presented for frequencies lower than 1 GHz. These designs mainly covered the lower LTE bands. Similarly, there were some designs which covered the new 5 GHz WiFi band. Most of the designs consisted of only 2-elements while a few also presented 4-element designs. Due to

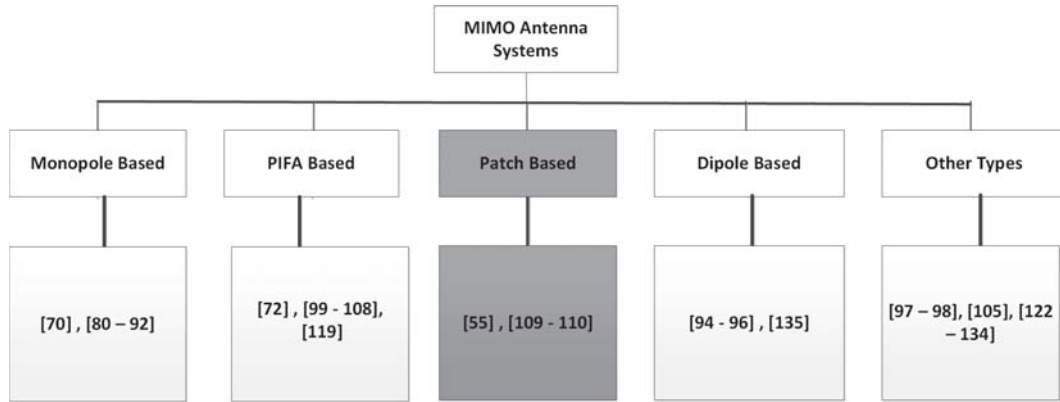


Figure 4.6: Classification of literature related to the MIMO antenna systems according to the type of their antenna element.

limited space and compact size of the wireless device, it remained a challenge for many to accommodate more elements specially in the lower LTE band. Fig. 4.7 summarizes the classification of the MIMO antenna designs according to the band of operation.

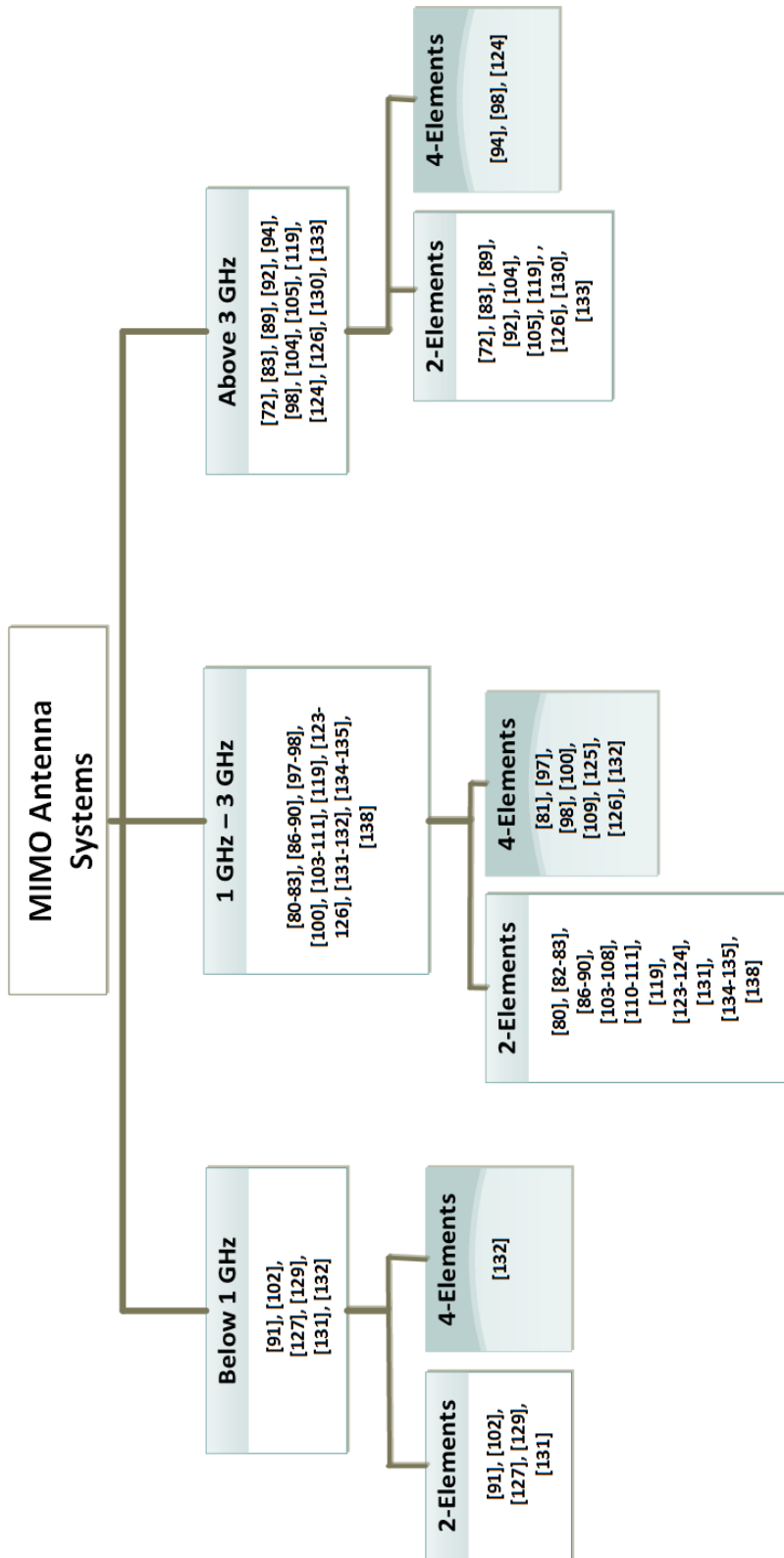


Figure 4.7: Classification of literature related to the MIMO antenna systems according to their band of operation.

## CHAPTER 5

# MINIATURIZED MPA BASED MIMO ANTENNA SYSTEM

As mentioned in the previous chapter, very few MIMO antenna designs have appeared in literature which employ MPAs as the elements of MIMO antenna system. In this chapter, various MIMO antenna systems for practical applications are designed using the proposed miniaturized MPA and it is shown that MPA can be a good choice for MIMO antenna system design when properly miniaturized. The designs are made for the ISM band, the 5 GHz WiFi band and the lower LTE band. Each design is thoroughly analyzed through the MIMO antenna system performance metrics. The proposed MIMO antenna system designs are compared with other well known designs. An MTM-inspired isolation improvement technique is also proposed and analyzed in this chapter.

## 5.1 4-Element MIMO Antenna System for ISM band Operation

The industrial, scientific and medicine (ISM) radio bands are free and largely unregulated bands which were reserved for the use of RF energy for applications other than telecommunications. However, with time, many of these bands have been in regular use for short range communication. Among them, the 2.45 GHz ISM band which has a bandwidth of 100 MHz is widely used for wireless internet (WiFi), remote control applications, and bluetooth devices. This finds applications in mobile phones, laptops, wireless routers etc. Therefore, this band has received considerable attention by antenna designers and various antenna designs have been presented covering this band. These include the MIMO antenna designs covering this band for 4G communications. Apart from the application specific antenna designs in this band, many antenna designers chose this band for their design just for the proof of concept since it is easy to test and characterize an antenna in this band due to easy availability of many devices in this band.

### 5.1.1 MIMO Antenna Design

Due to wide use of the 2.45 GHz ISM band in hand-held devices, a compact 4-element MIMO antenna system was designed for the same band. Initially, a single MPA was designed with the same parameters as discussed in Chapter 3. The miniaturized patch element was made on the FR4 substrate with a dimensions of  $14 \times 18 \text{ mm}^2$  and tuned to 2.45 GHz using the CSRR loading technique.

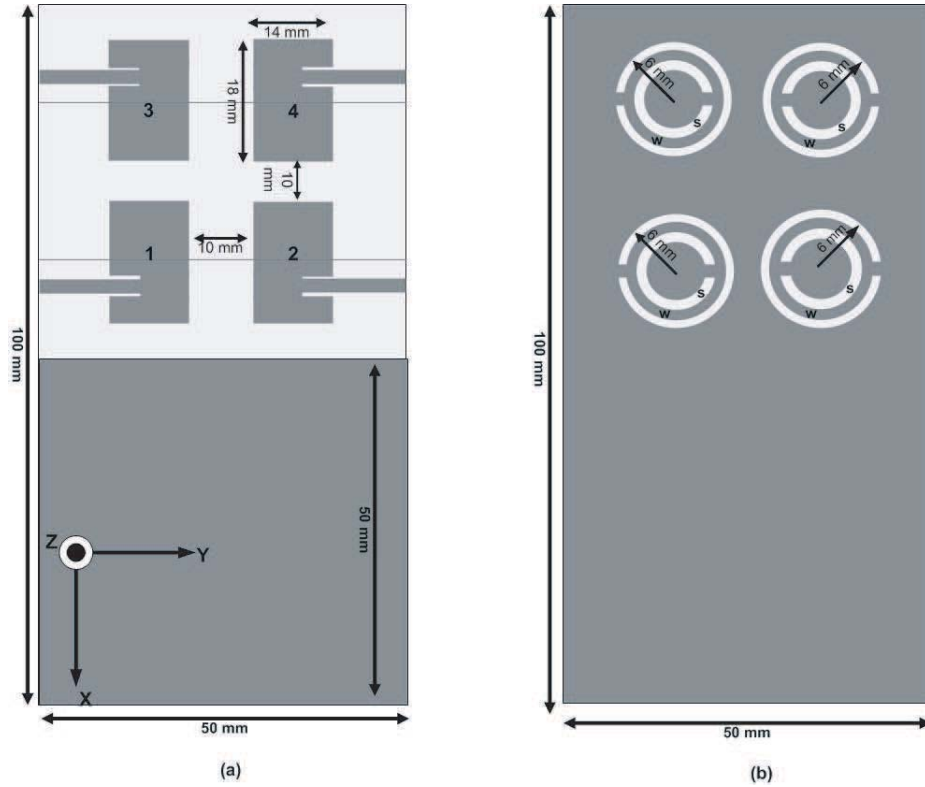


Figure 5.1: Geometry of the 4-element ISM band MIMO antenna system (a) Top view, (b) Bottom view.

A  $2 \times 2$  (4-element) MIMO antenna system was made using the miniaturized MPAs by arranging them in an area of  $50 \times 50 \text{ mm}^2$ . The spacing between the MPA elements was 10 mm. The additional  $50 \times 50 \text{ mm}^2$  space was filled with a ground plane which could be used to mount other electronic devices and ICs for making a complete transceiver design within a standard  $100 \times 50 \times 0.8 \text{ mm}^3$  board size. The top and bottom layers of the proposed design are shown in Fig. 5.1.

### 5.1.2 Simulation & Measurement Results

The 4-element MIMO antenna system was first designed and tuned using HFSS<sup>TM</sup>. It was then fabricated. The scattering parameters of the MIMO an-

tennas were measured using the network analyzer. The two dimensional gain measurements of the MIMO antennas were carried out at an outdoor antenna test facility (at Oakland University, Michigan, USA). The results obtained from the simulations as well as measurements of the MIMO antennas are summarized in the following sub-sections.

### **Reflection Coefficient and Isolation of the MIMO Antenna**

Fig. 5.2 shows the fabricated 4-element MIMO antenna system with CSRR loaded patches. Fig. 5.2(a) shows the top side of the board while Fig. 5.2(b) shows the bottom side. Fig. 5.3 shows the simulated and measured reflection coefficient curves of the various elements of the MIMO antenna. Measurements and simulations were in agreement with a slight shift in the resonance frequencies that was attributed to the fabrication process. The MIMO antenna system covered the frequency band centered around 2.475 GHz with a -10 dB operating bandwidth of at least 20 MHz, and a -6dB operating bandwidth of at least 50 MHz.

Since the diversity performance of MIMO antennas is directly related to the minimum coupling between individual antenna elements, the isolation between the elements of the proposed antenna was measured. The isolation curves between the MIMO antenna elements are shown in Fig. 5.4. In the region of resonance, the worst case isolation was -10 dB which is between antenna elements 1 and 2 (as well as 3 and 4). These were the antenna elements pair whose radiating edges were facing each other.



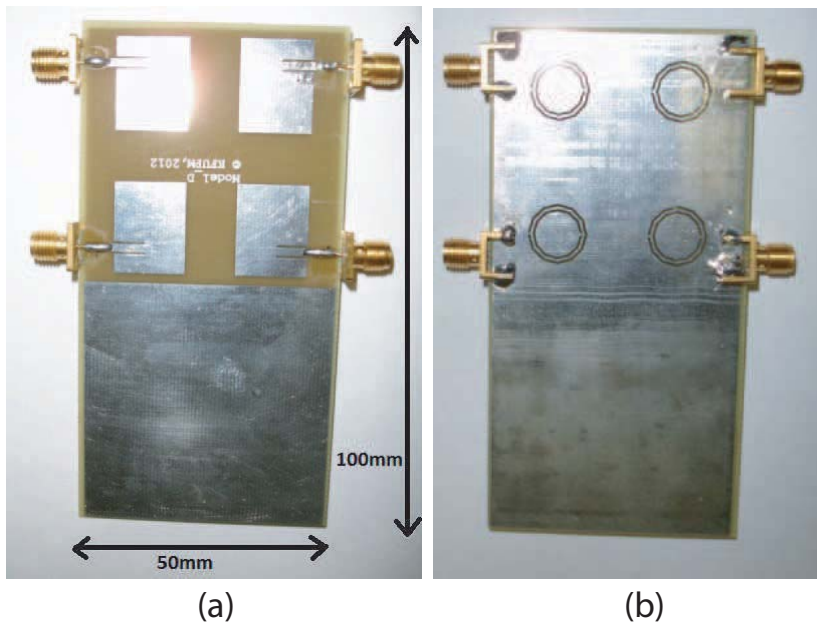


Figure 5.2: Fabricated 4-element ISM Band MIMO antenna system, (a) Top layer, (b) Bottom layer.

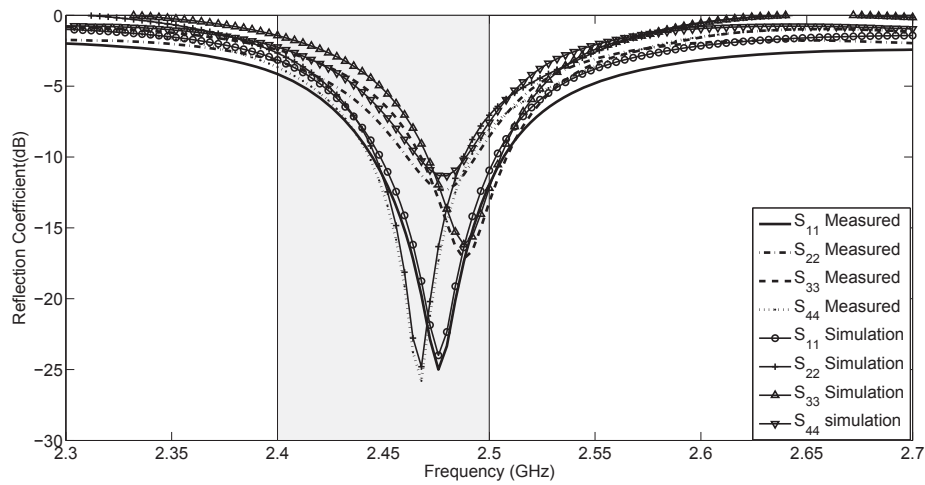


Figure 5.3: Reflection coefficients of the 4-element ISM Band MIMO antenna system (ISM Band)

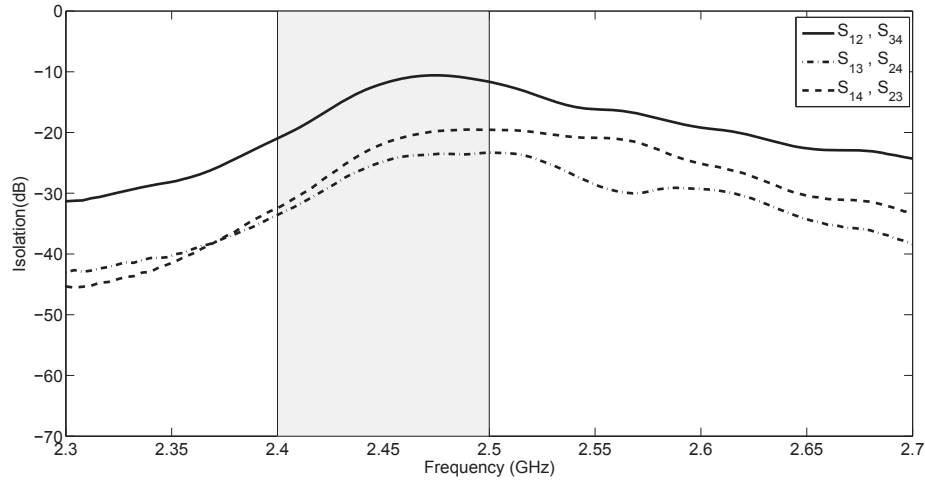


Figure 5.4: Measured isolation between the elements of the ISM Band MIMO antenna system

### Current Distribution

The current distribution for elements 1 and 3 on both the patch as well as the ground plane are shown in Fig. 5.5. These current distributions were obtained from the HFSS simulations. All currents are shown for the 2.48 GHz operating frequency. Fig. 5.5(a) and Fig. 5.5(b) show the patch current distribution when elements 1 and 3 are on, respectively. Notice the high current levels indicating good radiation at the patch edges. In addition, Fig. 5.5(c) and Fig. 5.5(d) show the current levels on the GND plane beneath the patch elements 1 and 3, respectively (flip the board). The CSRR currents are showing high levels beneath the radiating patches at the resonant frequency thus showing that GND plane is also acting as a radiator. The coupling to adjacent elements is also evident in the current levels. Only one portion of the MIMO antenna current distribution is shown (i.e. elements 1 and 3). Since the board is symmetric, similar levels are expected for

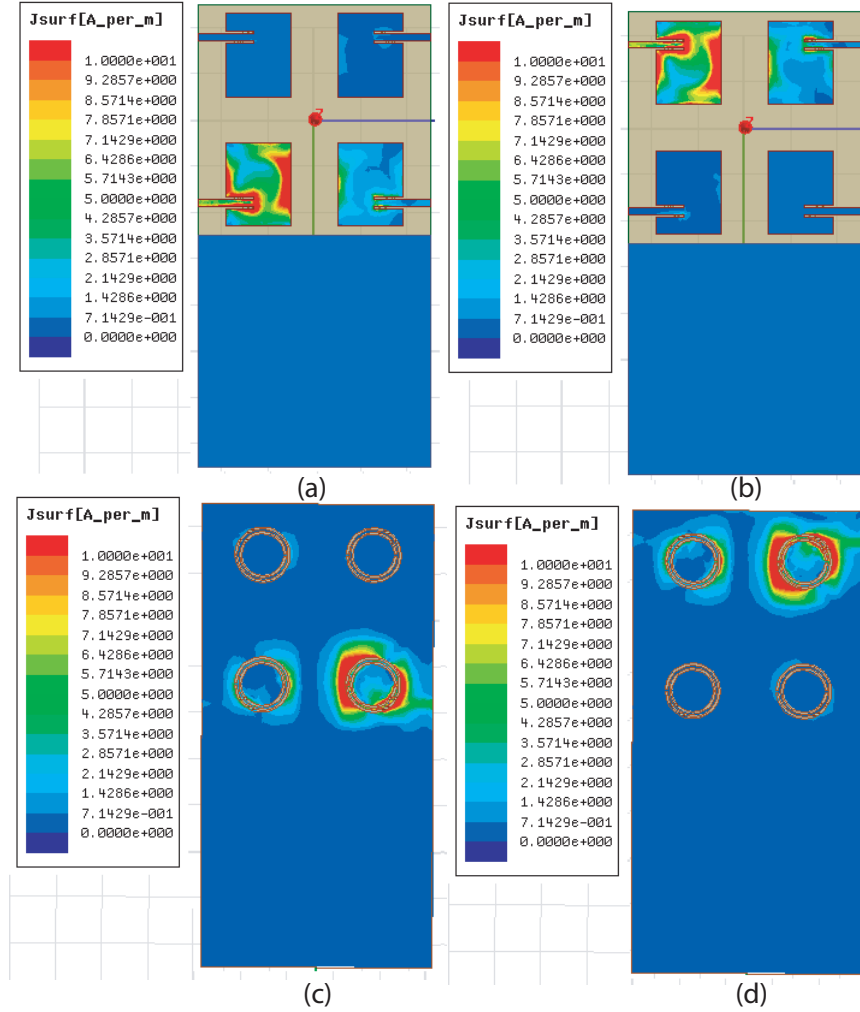


Figure 5.5: Current distribution on the ISM Band MIMO antenna system at 2.48 GHz, (a) Patch 1 is active (top layer), (b) Patch 3 is active (top layer), (c) Patch 1 active (bottom layer) and (d) Patch 3 active (bottom layer).

the other two elements (i.e. 2 and 4).

## TARC and the Correlation Coefficient

The TARC curves of the 4-element MIMO antenna system are shown in Fig. 5.6.

The excitation of port one was kept at  $1e^{j0}$ , while the phases of other ports (i.e. ports 2, 3 and 4) were changed with different phase excitations. Fig. 5.6 shows

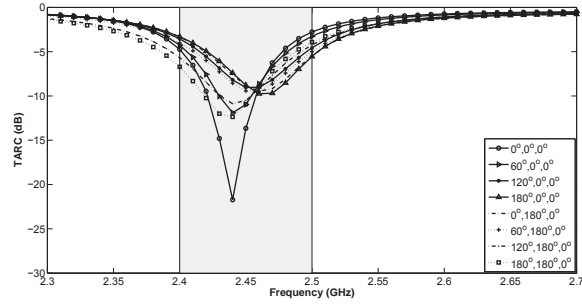
several phase change combinations between the different antennas covering both constructive and destructive interference cases. The curve legend indicates the phases of elements 2, 3 and 4 with respect to element 1. For example, if the legend reads  $(0^\circ, 60^\circ, 180^\circ)$  this means that antenna 2 excitation is in phase with antenna 1, antenna 3 is at  $60^\circ$  phase shift and antenna 4 is completely out of phase with antenna one excitation.

Fig. 5.6(a) shows TARC curves when element 4 was in phase with element 1 while the phases of element 2 and 3 were varied. A -6 dB bandwidth of at least 50 MHz was achieved. This occurred when either the elements 2 and 3 were in phase with element 1 or  $180^\circ$  out of phase with element 1.

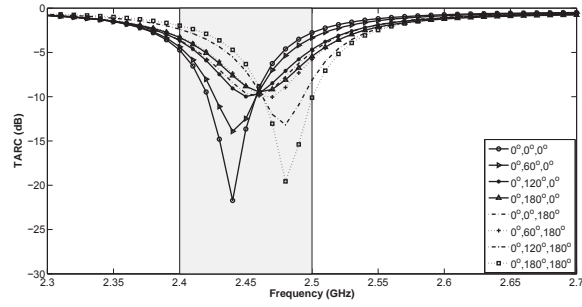
TARC curves shown in Fig. 5.6(b) were obtained when element 2 was kept in phase with element 1 while phases of element 3 and 4 were varied. A minimum of 60 MHz -6 dB bandwidth was achieved when either the antenna elements 3 and 4 were in phase or  $180^\circ$  out of phase with element 1.

Fig. 5.6(c) shows TARC curves when element 3 was kept in phase with element 1 while phases of element 3 and 4 were varied. Here as well, at least 60 MHz of -6 dB bandwidth was achieved.

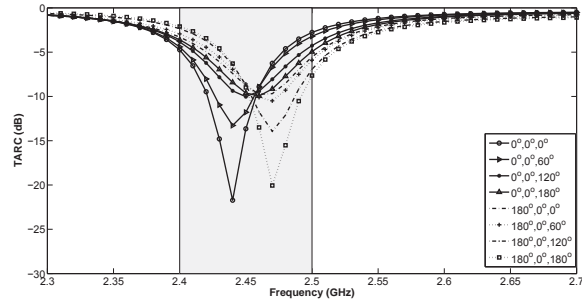
TARC curves of Fig. 5.6(d) were obtained by varying the phases of all three elements with respect to element 1 in order of  $60^\circ$  or  $90^\circ$ . For all combinations, at least 60 MHz of -6 dB bandwidth was achieved. This shows that the MIMO operating bandwidth will be at least 50 MHz for a wide range of antenna excitation combinations.



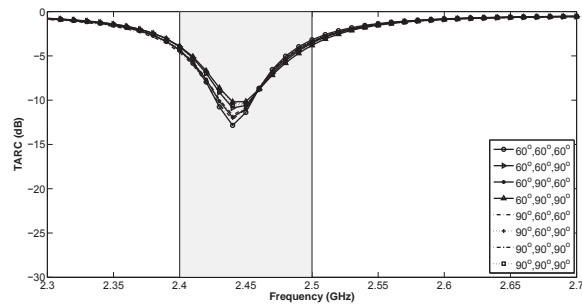
(a)



(b)



(c)



(d)

Figure 5.6: TARC curves of the ISM band MIMO antenna system with different phase combinations between the 4-elements, (a) elements 1 and 4 are in phase, (b) elements 1 and 2 are in phase, (c) elements 1 and 3 are in phase, (d) all elements are out of phase.

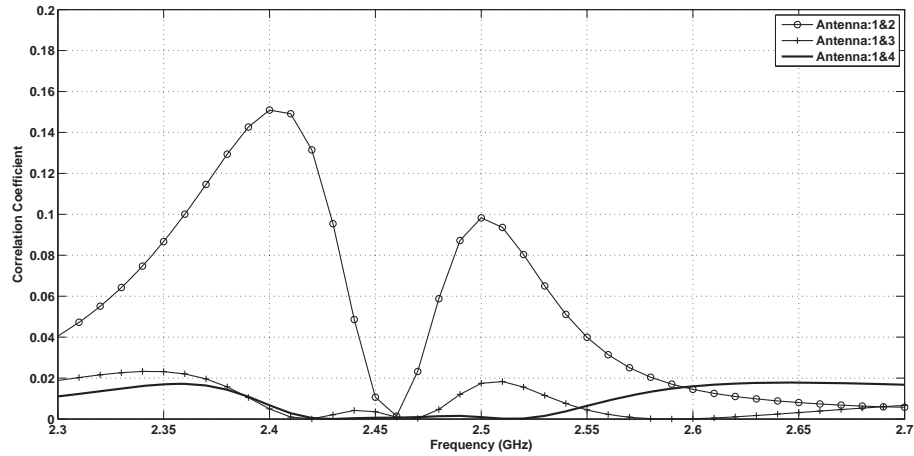


Figure 5.7: Correlation coefficient curves of the ISM band MIMO antenna system.

For a uniformly distributed incident field, the correlation coefficient ( $\rho$ ) between the antenna elements was computed from the measured S-parameters while taking into the account of antenna radiation efficiency as discussed in Chapter 4. Fig. 5.7 shows the correlation coefficient between the antenna elements of the MIMO antenna system. The curves are based on the antenna efficiency of  $\eta = 29\%$ . It is important to note that the maximum value of correlation coefficient was 0.1 in the region of resonance. This value is well below 0.3 which is the maximum value set for 4G standards.

### Far Field Radiation Characteristics

The two dimensional gain patterns of the elements of the MIMO antenna system were measured at an outdoor antenna range facility at Oakland University, Michigan, USA. Fig. 5.8 and Fig. 5.9 show the normalized measured radiation gain patterns of the proposed MIMO antenna system. All measurements were taken

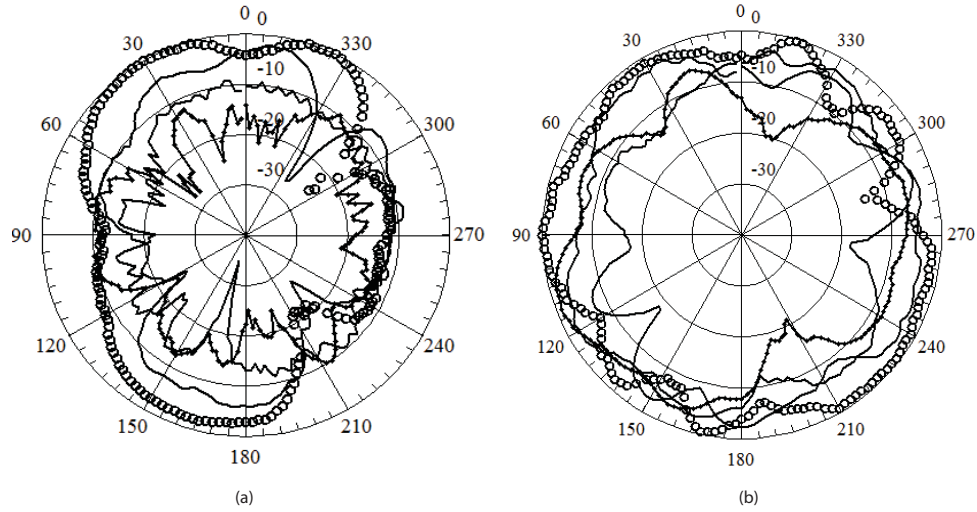


Figure 5.8: Measured gain patterns of the ISM band MIMO antenna system. (a) x-z plane at 2480 MHz, (b) y-z plane at 2480 MHz. Circles is co-pol element 1, solid is co-pol element 2, dots is cross-pol element 1, dashes is cross-pol element 2.

at 2.48 GHz. The maximum measured gain at this frequency was  $-0.8$  dBi. All co-pol and cross-pol patterns for all antenna elements are presented. Fig. 5.8(a) and Fig. 5.8(b) show the normalized gain patterns of antenna elements 1 and 2 for the x-z and the y-z planes, respectively. Similarly, Fig. 5.9(a) and Fig. 5.9(b) show the normalized gain patterns of antenna elements 3 and 4 for the x-z plane and the y-z planes, respectively.

The 3D radiation patterns of the elements of the MIMO antenna system were obtained from HFSS<sup>TM</sup>. The radiation gain pattern of each element was obtained by exciting the element and terminating the other elements with  $50\Omega$  load. The radiation patterns were obtained at an operating frequency of 2.48 GHz. Fig. 5.10 shows the 3D radiation gain patterns of the four antenna elements. A significant back lobe was observed due to the CSRRs. The minimum front to back (F/B)

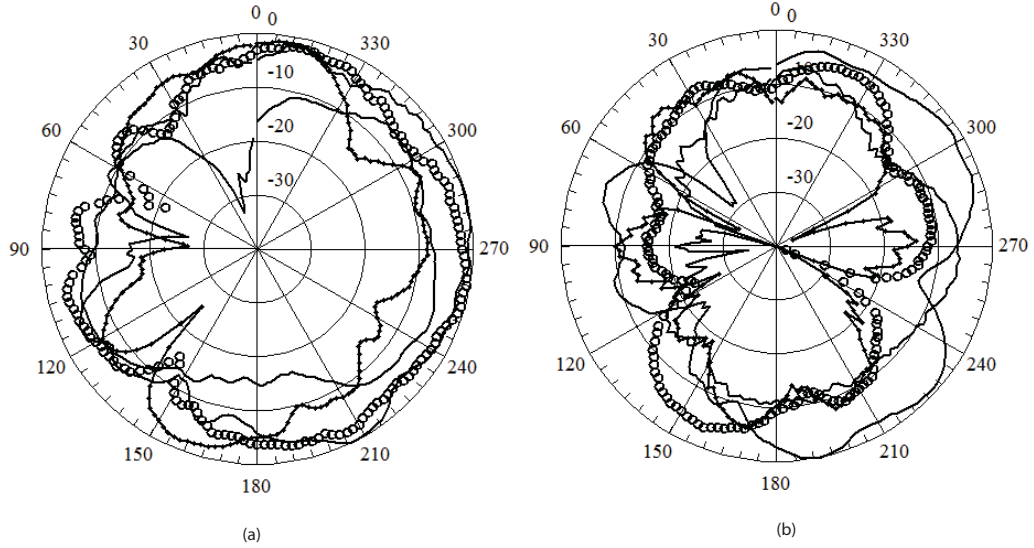


Figure 5.9: Measured gain patterns of the ISM Band MIMO antenna system. (a) x-z plane at 2480 MHz, (b) y-z plane at 2480 MHz. Circles is co-pol element 3, solid is co-pol element 4, dots is cross-pol element 3, dashes is cross-pol element 4.

ratio obtained from the simulations was 2.7 dB.

### Mean Effective Gain

The MEG of each element was computed from their two-dimensional gain patterns using Eq. (4.9) and by assuming the conditions given in [78]. The MEG of the proposed antenna are tabulated in Table 5.1. A cross polarization discrimination ( $\Gamma$ ) of 0 dB corresponded to an outdoor uniform propagation environment while a  $\Gamma$  of 6 dB corresponded to an indoor uniform propagation environment. The antenna showed good MEG performance as the maximum deviation between the various element MEG values was less than 3dB.



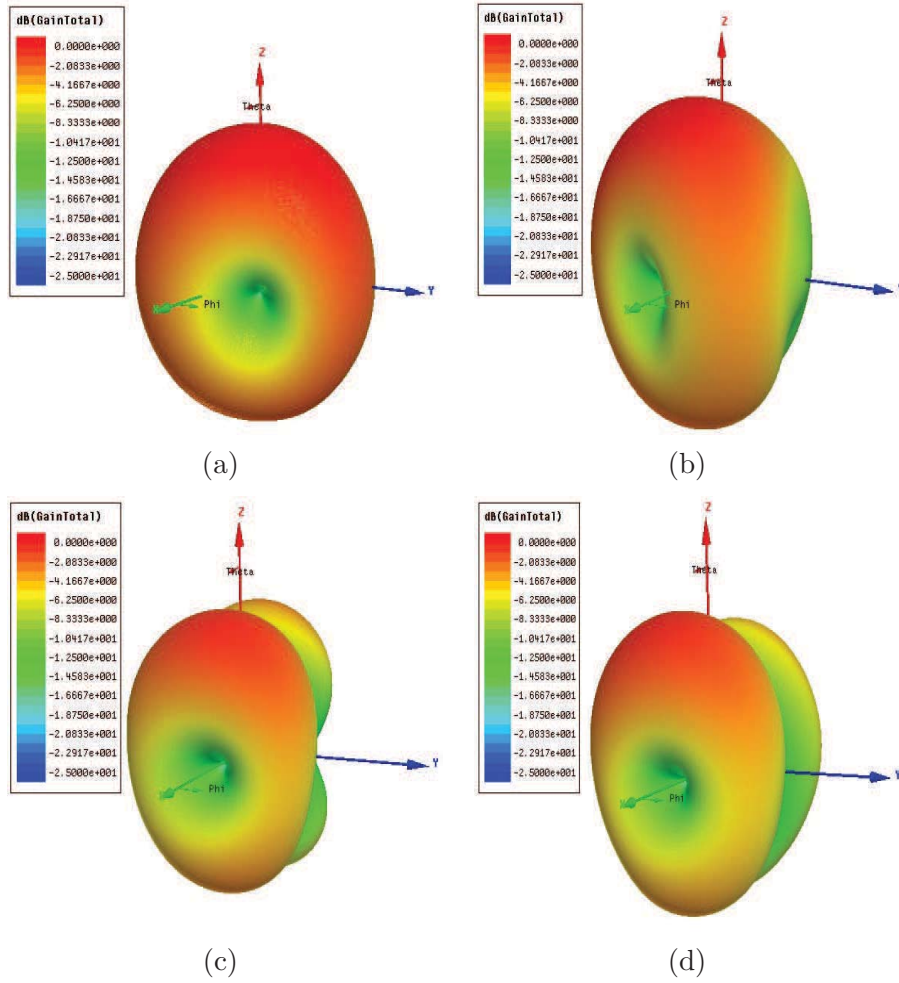


Figure 5.10: 3D radiation patterns of the ISM band MIMO antenna at 2480 MHz. (a) Element 1 (b) Element 2 (c) Element 3 (d) Element 4

Table 5.1: MEG of the Antenna Elements of the ISM Band MIMO Antenna System

Antenna Element	MEG ( $\Gamma = 0$ dB)	MEG ( $\Gamma = 6$ dB)
1	-5.44	-5.43
2	-5.65	-5.64
3	-8.00	-8.00
4	-8.69	-8.69

### 5.1.3 Antenna Behavior Over a Conducting Plane

Since the resonance of the MIMO antenna system was a function of the CSRR dimensions, any change in the CSRR would greatly effect the performance of the antenna. These changes may occur due to the interaction between the CSRR and a conductive plane representing a backplane of an LCD or the electronics behind the antenna system in a real system. The effects of a conductive plane underneath the antenna were investigated through simulations in HFSS<sup>TM</sup>. The antenna model was first placed over a ground plane. It was found that the resonance of the antenna elements were completely lost when the CSRRs were in contact with the ground plane. This was due to the fact that the CSRRs were effectively lost and the MPA elements were operating as if there were no CSRRs. Thus their resonant frequencies were centered at 5.04 GHz.

Later, the MIMO antenna system was placed above a ground plane separated by free space. The separation between the ground plane and antenna bottom side was varied from 1 mm to 5 mm in 1 mm steps. It was found that as the distance between the antenna and ground plane was increased, the reflection coefficient of the individual patch elements improved. At 5 mm height which corresponded to  $0.04\lambda$ , the reflection coefficient of each element of the MIMO antenna system was almost equal to the one without the liquid crystal display (LCD) ground plane. Fig. 5.11 shows the reflection coefficients of antenna element 1 over an LCD ground plane at different distances. The reflection coefficient curves of other antenna elements followed the same trend. From these observations, it is concluded that in

Table 5.2: Antenna Efficiency, Resonant Frequency and Front to Back Ratio in the Presence of a Conducting Plane

Separation Distance	Resonant frequency (GHz)	-6 dB Bandwidth (MHz)	Efficiency $\eta$ (%)	Front to back ratio (dB)
1 mm	2.69	70	19	14.5
2 mm	2.53	70	23	13.9
3 mm	2.47	70	24	4.8
4 mm	2.47	70	24.5	6.7
5 mm	2.46	50	25	4.3

any practical design, the antenna must be placed carefully such that its bottom side maintains a minimum distance of 3-5 mm from any conductive plane. Otherwise, the antenna and the CSRR dimensions need to be optimized to resonate at the desired frequency in the presence of a nearby ground plane.

The resonant frequency of the antenna, bandwidth, its radiation efficiency at the resonant frequency and its F/B ratio for different separation distances between the LCD ground plane and the antenna are tabulated in Table 5.2. These numbers are for all the antenna elements, as they had similar behavior as a function of the distance from the LCD ground plane.

A maximum shift in the resonant frequency of the antenna and lowest efficiency were obtained when the conducting plane was close. Also, the antenna was more directive. As the separation between the conducting plane and antenna increased, the antenna became less directive and the back lobe became more significant representing a ground free case. At a separation distance of 5 mm, there was a significant back lobe and the F/B ratio was 4.3 dB which is 1.6 times better than without an LCD ground plane. The radiation pattern of antenna element 1 in

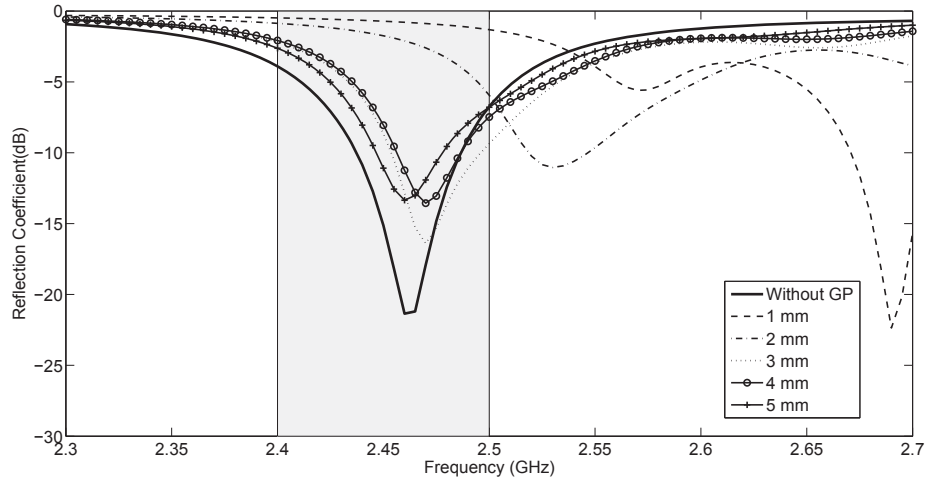


Figure 5.11: Effect of LCD ground plane below the antenna on the reflection coefficient.

the presence of a conducting plane at 5 mm distance is shown in Fig. 5.12. It is evident from the figure that the antenna has significant radiation in the direction of the conducting plane. The same trend was observed for other antenna elements (2 to 4).

The effect of antenna radiation on the conducting plane was observed by finding the surface current density on the conducting plane due to backward radiation. These effects were observed for different separation distances between the antenna and the conducting plane. Each antenna element was excited individually while the others were terminated with matched loads and the surface current density was calculated on the conducting plane. All antenna elements had a similar effect on the conducting plane. Some excited current density on the conducting plane was observed which was below the excited antenna element. This density was 2 A/m when the conducting plane was at a distance of 1 mm from the antenna.

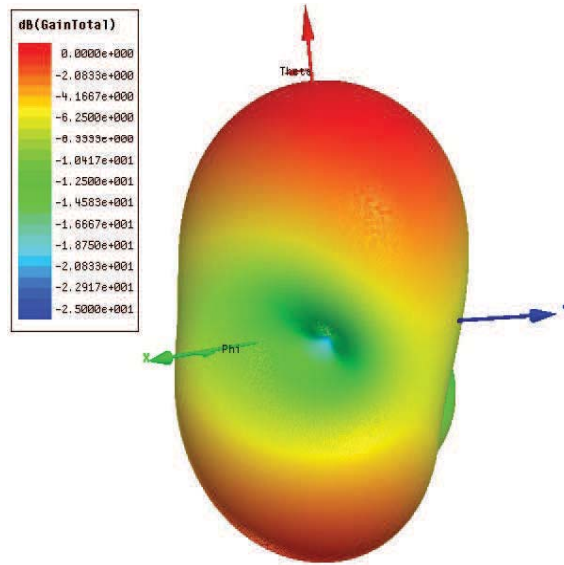


Figure 5.12: Radiation pattern of antenna element 1 in the presence of a conducting plane at 5 mm

The current density decreased significantly as the separation distance between antenna and conducting plane increased. The maximum current density of 0.8 A/m was observed at a separation distance of 5 mm. Fig. 5.13(a) and Fig. 5.13(b) show the current density distribution on the conducting plane due to antenna element 1 for a separation distances of 1 mm and 5 mm, respectively.

#### 5.1.4 Channel Capacity Estimation

An important performance measure of a MIMO antenna system is the measure of its multiplexing gain that it can offer when used in actual environment. To measure this performance of the 4-element ISM band MIMO antenna system, it was used with MIMO system and channel coefficient matrix were computed through measurements in the indoor environment. The matrix was then used with Eq.(4.2) to compute the maximum channel capacity that the MIMO system

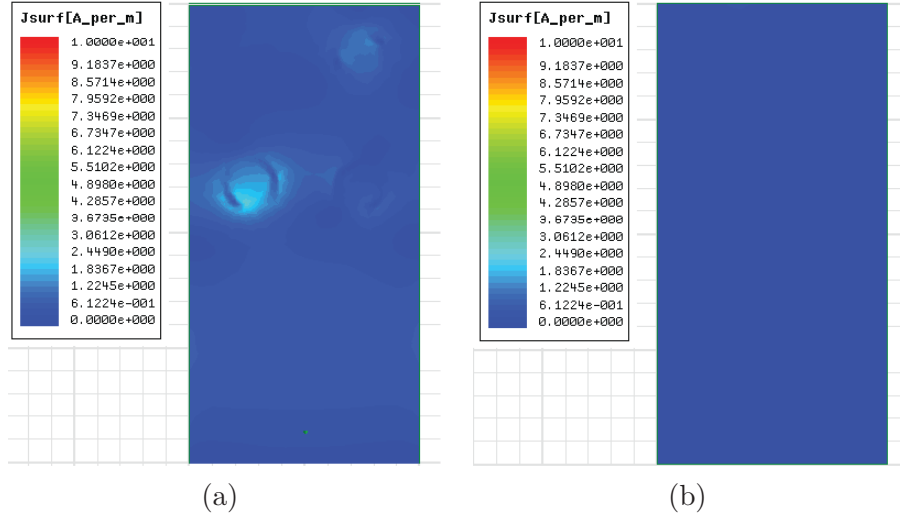


Figure 5.13: Current distribution on the conducting plane when the separation distance is (a) 1 mm , (b) 5 mm

can obtain when using the proposed antenna in the indoor environment. It was also compared with the same system when an array of standard monopoles were used.

### Measurement Setup

A series of measurement campaigns were carried out to compute the channel coefficient matrix for the printed antenna as well as an array of monopoles operating in an indoor environment. A Software Defined Radio (SDR) platform was used for carrying out the channel measurements on the printed antennas. The platform consists of an SDR transmitter and receiver each equipped with a Xilinx Vertix 4 FPGA, 8-channel ADC/DAC, and quad RF modules that operated at the 2.4 GHz/5 GHz unlicensed bands. The SDR platform was capable of implementing a complete 4x4 MIMO communication system. A single carrier BPSK burst modem

communication system was implemented on the SDR platform.

On the transmitter side, bursts were transmitted at the rate of 97.7 kBursts/s. In a 4x4 MIMO communication system context, a transmitted burst consisted of a start bit followed by 4 channel estimation pulses of equal magnitude with each pulse being transmitted from one of the transmitters in a time-division multiplexed form, and the data was transmitted afterwards. During the channel estimation pulses, each transmitter remained silent at the time at which other transmitters were transmitting their pulses. On the receiver side, the start bit of each burst of data was used for frame and bit synchronization. The start bit allows each receiver to adjust the timing for detecting the channel estimation pulses as well as the data bits. Each receiver at the proper time following the reception of the start bit the magnitude and phase associated with each of the 4 transmitted channel estimation pulses resulting in producing a complex-valued channel matrix. For each channel being measured, the channel matrix was averaged over around 10,000 bursts to get a more accurate channel matrix estimation. The measurement setup consisting of the MIMO antenna system mounted on the SDR platform is shown in Fig. 5.14.

### **Measurement Scenario**

The measurements were carried out in an indoor environment. The indoor environment was comprised of a corridor which was 10 feet (3 meters) wide and 10 feet (3 meters) high. There were concrete walls on each side while the ceiling was made up of conducting sheet. The measurements were taken for LOS as well as



Figure 5.14: Measurement setup at the receiver end

NLOS case. Fig. 5.15(a) shows the measurement scenario for the LOS case and Fig. 5.15(b) shows the measurement scenario for the NLOS case. In the LOS case, the two radios were placed at an average distance of 20 feet from each other. Since the environment was time varying, a number of realizations of ‘H’ were obtained by slightly varying the position of transmitter and receiver. The channel matrices obtained were then normalized using the procedure given in [136].

The NLOS measurement were taken by moving the receiver to a corner of the corridor. The average distance of transmitter during the measurements was 20 feet (6 meter) from the corner while the distance of receiver from the corner was 10 feet (3 meter) as shown in Fig. 5.15(b).

## Measurement Results

Initially, monopole antennas were mounted on the receiver and the transmitter end. The distance between the adjacent monopoles was  $\lambda/2$ . The measurements were taken for the LOS and NLOS case to compute channel coefficient matrix. Then the printed antenna was mounted on the receiver and transmitter end and



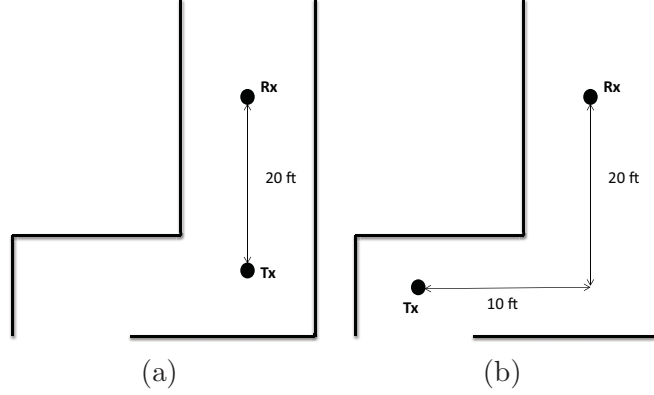


Figure 5.15: Layout of measurement scenario (a) LOS measurement , (b) NLOS measurement

similar procedure was followed. The channel coefficient matrix obtained for the printed antenna for the LOS case is given below :

$$\begin{bmatrix} 0.2223\angle 3.27 & 0.3697\angle 4.4 & 0.2423\angle 3.17 & 0.2771\angle 3.61 \\ 0.3795\angle 4.06 & 0.4485\angle 0.25 & 0.5481\angle 4.19 & 0.2676\angle 5.55 \\ 0.3160\angle 5.3 & 0.6124\angle 0.64 & 0.3306\angle 5.39 & 0.4227\angle 5.96 \\ 0.4177\angle 5.67 & 0.2820\angle 1.99 & 0.6085\angle 5.81 & 0.1576\angle 0.92 \end{bmatrix} \quad (5.1)$$

For the NLOS case, the channel matrix obtained is

$$\begin{bmatrix} 0.07\angle 2.47 & 0.36\angle 0.62 & 0.18\angle 4.41 & 0.43\angle 5.94 \\ 0.19\angle 0.32 & 0.52\angle 6.13 & 0.25\angle 3.58 & 0.64\angle 4.86 \\ 0.26\angle 2.23 & 0.45\angle 1.35 & 0.61\angle 5.34 & 0.30\angle 0.22 \\ 0.37\angle 2.73 & 0.80\angle 1.29 & 0.44\angle 5.41 & 0.98\angle 0.11 \end{bmatrix} \quad (5.2)$$

From these measured channel matrices for the LOS and NLOS cases in indoor environment, the channel capacity of the MIMO system when using the 4-element

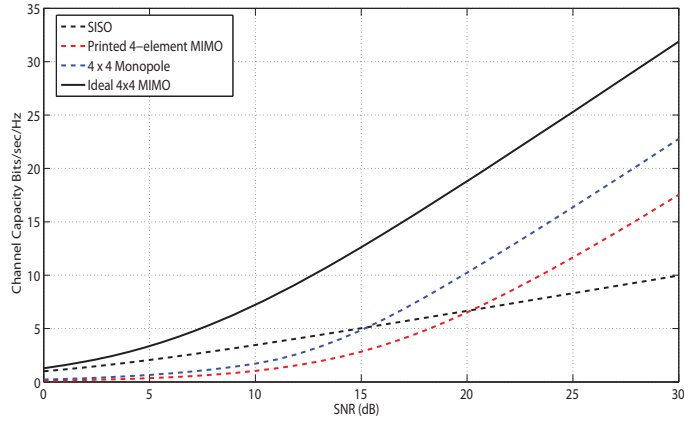


Figure 5.16: Average channel capacity in LOS indoor environment

MIMO antenna system as well as when using the array of monopoles was calculated using Eq. 4.2. Fig. 5.16 shows the measured channel capacity curves of the two antenna in the LOS environment. As evident from the capacity curves in Fig. 5.16, the channel capacity of the 4-element MIMO antenna system was less than the capacity of a  $4 \times 4$  monopole antenna array while the capacity of both the systems was less than the ideal capacity of a  $4 \times 4$  MIMO antenna system. This was mainly due to the high correlation between the channels which degrades the performance of a MIMO system. The capacity of the printed antenna was lower than the monopole antenna array because of the fact that the antenna elements were very closely placed and the isolation between antenna elements was only 10 dB. Similar observations were obtained in the NLOS case for which the capacity curves of the two antenna systems are shown in Fig. 5.17.

Fig. 5.18 shows the cumulative distribution function of the channel capacity of the printed antenna in LOS as well as NLOS environments calculated at an

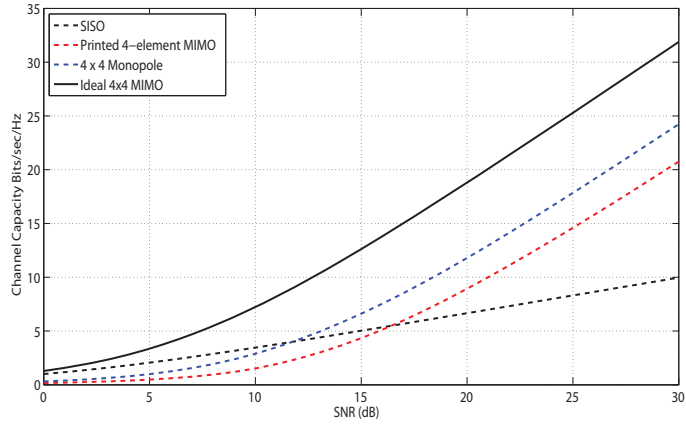


Figure 5.17: Average channel capacity in NLOS indoor environment

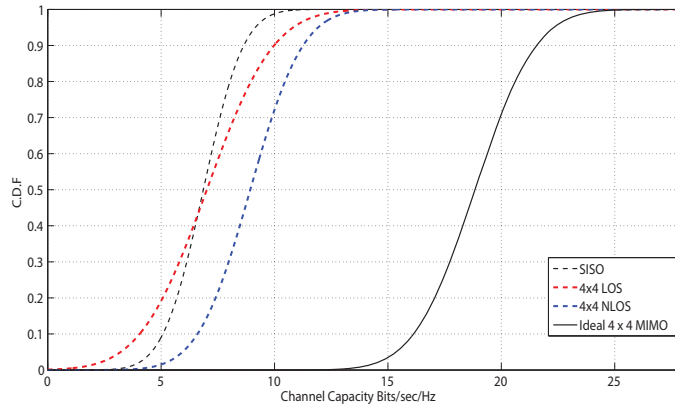


Figure 5.18: CDF of the channel capacity of the MIMO antenna system in Indoor environment

SNR of 20 dB. The curves show that although the performance obtained was less than the ideal capacity, the printed MIMO antenna system performance was still better than a SISO system in such environments.

The average capacity curves of the 4-element MIMO antenna system in the LOS and NLOS environment were compared. The antenna showed a better performance in the NLOS case since the channel induced correlation in such a case

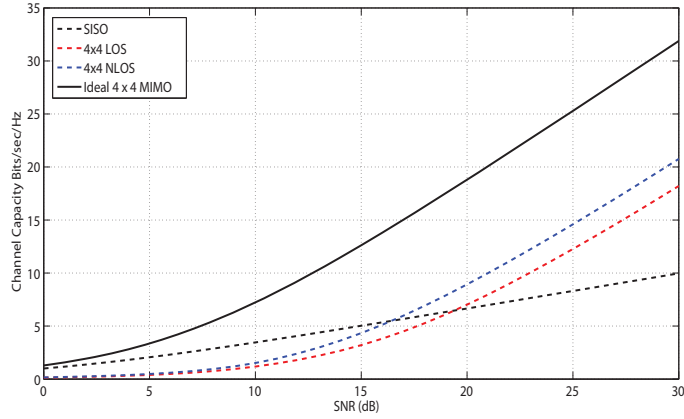


Figure 5.19: Comparison of the average channel capacity of the printed MIMO antenna system in LOS and NLOS scenario

was less than the LOS case. Fig. 5.19 shows the average channel capacity curves of the printed antenna in the LOS and NLOS environment. It can be seen that the average channel capacity of the antenna at 20 dB SNR is 8.9 bits/sec/Hz and 7.1 bits/sec/Hz in the NLOS and LOS indoor environment, respectively. These figures were higher than a SISO system operating at the same SNR.

## 5.2 4-Element and 8-Element MIMO Antenna Systems Operating in the 5 GHz Band

The 5 GHz is a new band which has been assigned for WiFi in the IEEE 802.11ac standard for high data rates [3]. This standard specifies 2-element, 4-element and 8-element MIMO antennas. The maximum bandwidth in this standard has been enhanced to 80 MHz and 160 MHz. Thus, compared to the conventional standard for WiFi in the 2.45 GHz band, this new standard offers highly enhanced

performance. Apart from the use for WiFi, the 5 GHz band contains the ISM bands too which are likely to be utilized for up-coming short range communication systems. Some of these systems will use the MIMO architecture for high data rate communication. Therefore, MIMO antennas designs covering this band are also required.

Using the proposed CSRR-loaded miniaturized MPAs as the elements, a compact  $2 \times 2$  (4-element) and  $4 \times 2$  (8-element) MIMO antenna system were designed and analyzed. The antenna operated in the 5 GHz band and comply with the standards of IEEE 802.11ac. The form factor of the design was chosen such that it can be easily integrated in hand-held devices. The antenna was designed, fabricated and analyzed. The design and analysis of the antennas are presented in the following sub-sections.

### **5.2.1 MIMO Antenna Design**

A MPA of dimensions  $11 \times 8$  mm<sup>2</sup> was first designed on an FR-4 substrate with dielectric constant of 4.4 and thickness of 0.8 mm. This dimension of the MPA was chosen so that when a 4-element and 8-element MIMO antenna system was to be designed with the MPAs as its elements, the total area of the MIMO antenna system remained within the form factor of a typical hand-held device with reasonable spacing between antenna elements. The MPA was fed by a microstrip line with inset feed to match antenna with  $50\Omega$ . The MPA was miniaturized and tuned at 5 GHz using the proposed technique as outlined in Chapter 3.

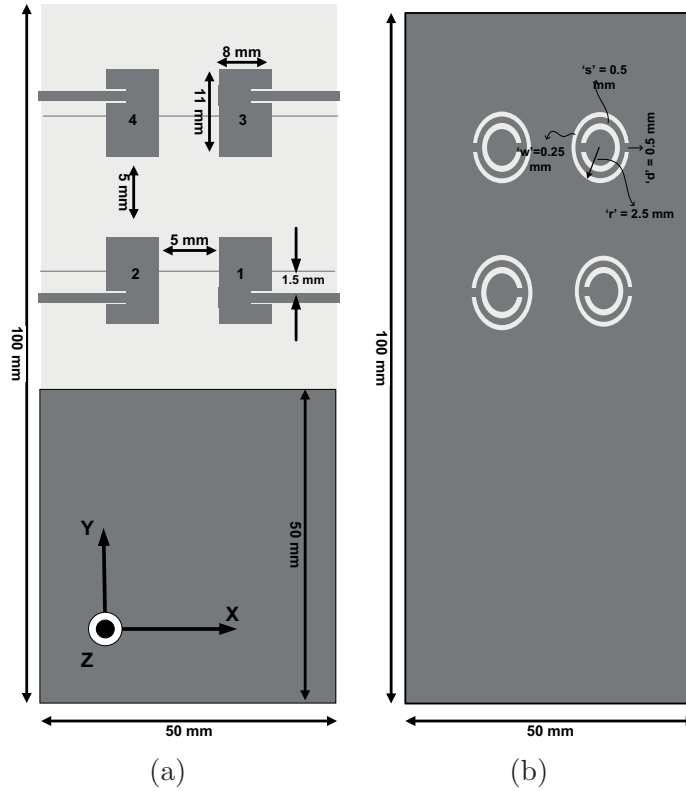


Figure 5.20: Geometry of the 4-element 5 GHz band MIMO antenna system, (a) Top view, (b) Bottom view.

Once the design of single MPA was finalized, it was used to make MIMO antenna system by replicating the same design with spacing. For the  $2 \times 2$  (4-element) MIMO antenna system, four patch elements were placed together with a spacing of 5 mm from each other. The total space occupied by the four antenna elements was  $50 \times 50 \text{ mm}^2$ . An additional space of  $50 \times 50 \text{ mm}^2$  was left as GND plane which could be used by IC's and other electronic equipment used in a practical transceiver design. The diagram of top and bottom side of 4-element MIMO antenna system is shown in Fig. 5.20.

For the  $4 \times 2$  (8-element) MIMO antenna system, eight patch elements were placed together with a spacing of 5 mm from each other. The total space occupied

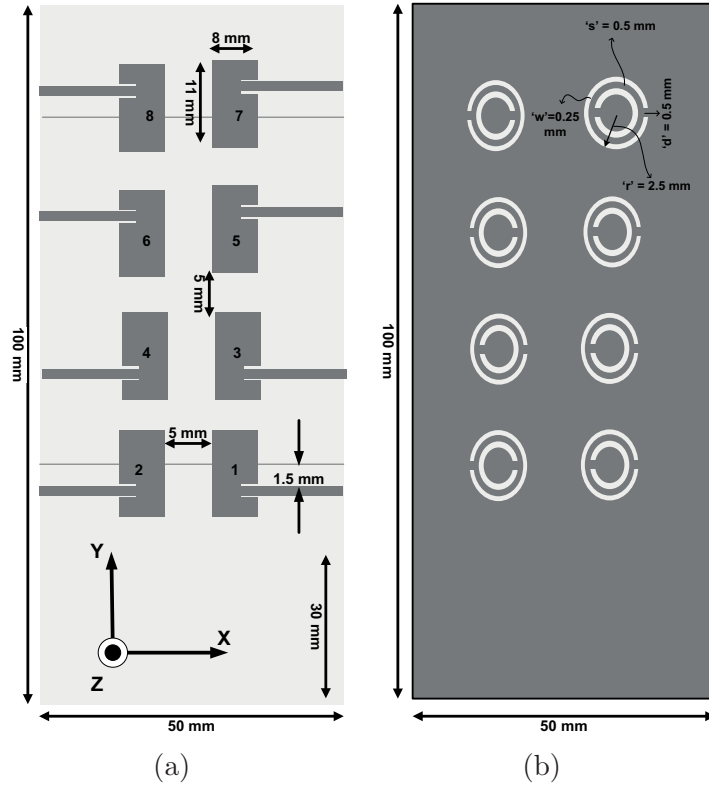


Figure 5.21: Geometry of the 8-element 5 GHz band MIMO antenna system, (a) Top view, (b) Bottom view.

by the four antenna elements was  $50 \times 70 \text{ mm}^2$ . an additional space of  $50 \times 30 \text{ mm}^2$  for other IC's and electronic equipment was left as GND plane. Thus the total size of the antenna was  $50 \times 100 \text{ mm}^2$ . The diagram of top and bottom side of 8-element MIMO antenna system is shown in Fig. 5.21.

### 5.2.2 Simulation & Measurement Results

The 4-element and 8-element MIMO antenna systems working in the 5 GHz bands were first designed and tuned using HFSS<sup>TM</sup>. They were then fabricated. The scattering parameters of the MIMO antennas were measured using the network analyzer. The two dimensional gain measurements of the MIMO antennas were

carried out at an outdoor antenna test facility (at Oakland University, Michigan, USA). The results obtained from the simulations as well as measurements of the MIMO antennas and their analysis is given in the following sub-sections.

### **Reflection Coefficient and Isolation**

The reflection coefficients of the MIMO antenna systems were first obtained by simulation in HFSS<sup>TM</sup>. All antenna elements were resonating roughly at 5.01 GHz with a minimum -6dB (VSWR<3) bandwidth of 160 MHz. The reflection coefficients obtained through the measurements of the fabricated MIMO antenna system were slightly different. The resonant frequency of the antenna elements of 4-element MIMO antenna system was around 5.08 GHz while it varied between 5.04 GHz to 5.08 GHz for the antenna elements of 8-element MIMO antenna system. These differences are attributed to the difference in the material properties of the substrate used in fabrication from the one defined in the simulations. The reflection coefficients of the 4-element MIMO antenna system are shown in Fig. 5.22. A minimum -6dB (VSWR<3) bandwidth of 95 MHz was obtained through measured reflection coefficients.

The measured reflection coefficients of the 8-element MIMO antenna system are shown in Fig. 5.23. A minimum -6dB bandwidth of 80 MHz was observed in these measurements.

The isolations between the antenna elements of the 4-element antenna are shown in Fig. 5.24. These curves shows the isolation of antenna element 1 with other antenna elements. Due to symmetry in the design, the isolation between



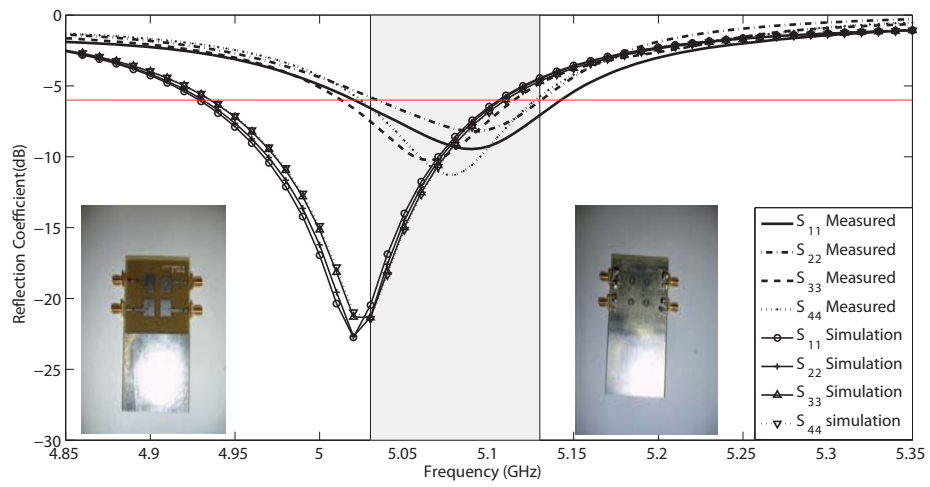


Figure 5.22: Reflection coefficient of the 4-element 5 GHz band MIMO antenna system

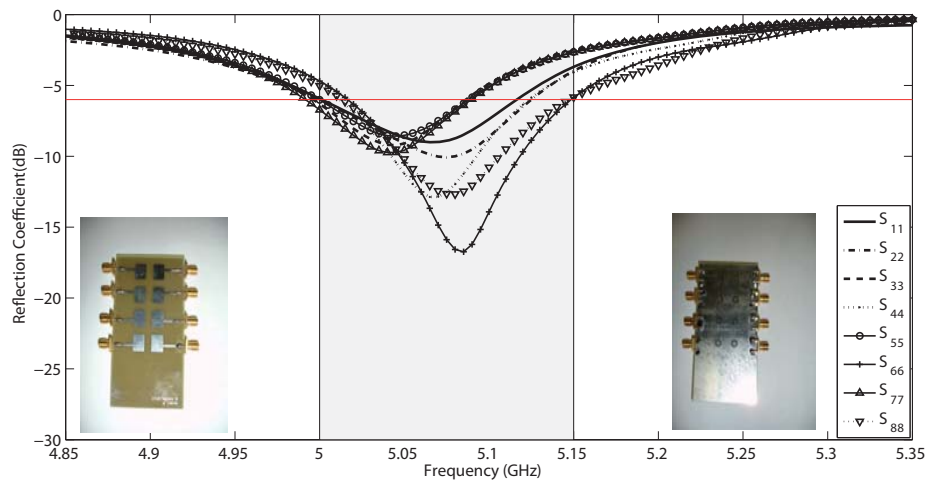


Figure 5.23: Measured reflection coefficient of the 8-element 5 GHz band MIMO antenna system

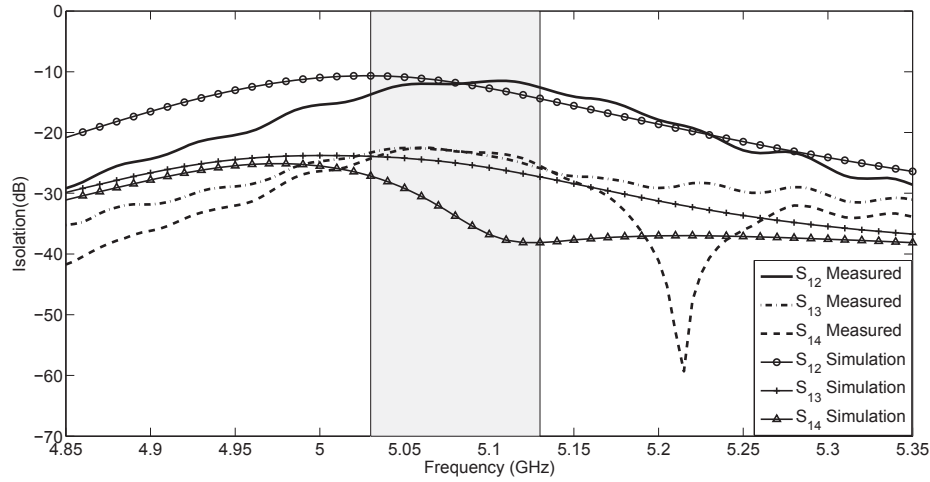


Figure 5.24: Isolation between the antenna elements of the 4-element 5 GHz band MIMO antenna system

other sets of antenna elements can be found from the same curves. A minimum isolation of 10.66 dB is obtained which is between the antenna elements whose radiating edges are facing each other. For all other combination of antenna elements, the isolation is much higher than 10.66 dB.

The isolation curves for 8-element MIMO antenna system are shown in Fig. 5.25. Here too, only the isolation between antenna element 1 with other antenna elements is shown. Due to symmetry in design, isolation for all other combination of antenna elements resembles one of the curve. A minimum isolation of 10.53 dB was observed between antenna elements whose radiating edges were facing each other.

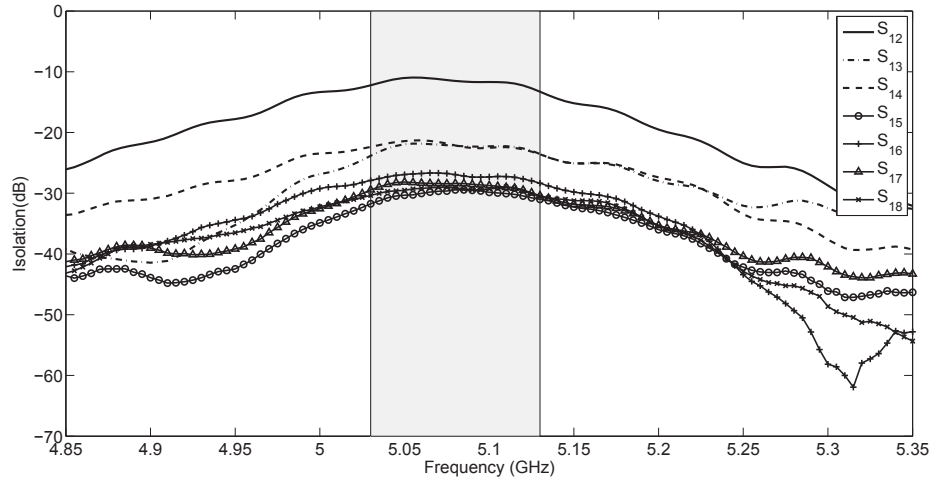


Figure 5.25: Isolation between the antenna elements of the 8-element 5 GHz band MIMO antenna system

### Current Distribution

The surface current distributions on the antenna were obtained through simulations. For the 4-element MIMO antenna system, these distributions were obtained at an operating frequency of 5.08 GHz. Fig. 5.26 shows the current distribution on the top and bottom side of the 4-element MIMO antenna when element 1 was excited while all other ports were terminated with  $50\Omega$ . From the current distribution it was observed that the main radiating element is patch while some radiation was also along the edges of the CSRR underneath the patch. The coupling between antenna elements 1 and 2 was visible since the isolation between these two antenna was low. The coupling between antenna element 1,3 and 1,4 was insignificant.

Fig. 5.27 shows the surface current distribution of 4-element antenna when element 4 was excited while other ports were terminated with  $50\Omega$ . A high current

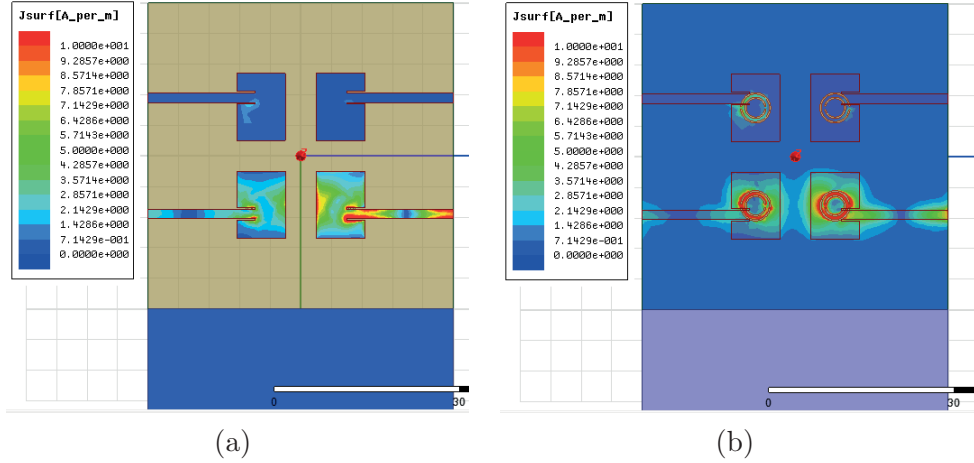


Figure 5.26: Current distribution on the 4-element MIMO antenna system at 5.08 GHz when element 1 is active, (a) Top side, (b) Bottom side

distribution along the radiating edge of patch showed that main radiating element was patch. Significant currents were also visible along the edges of the CSRR underneath the patch. The coupling with antenna element 3 was observed while coupling with antenna elements 1 and 2 was insignificant.

The surface current distributions for the 8-element MIMO antenna system were obtained at an operating frequency of 5.04 GHz. Fig. 5.28 shows the current distribution on the top and bottom of the antenna when element 1 was active while other ports were terminated with  $50\Omega$ . Fig. 5.29 shows the current distribution on the top and bottom of the antenna when element 3 was active while other ports were terminated with  $50\Omega$ . Due to symmetry in the design, similar current distributions were obtained when other antenna elements were active. These current distributions showed a high current density along the radiating edge of the active patch, significant currents along the edges of the CSRR and a coupling between active element with the element facing the radiating edge of the active

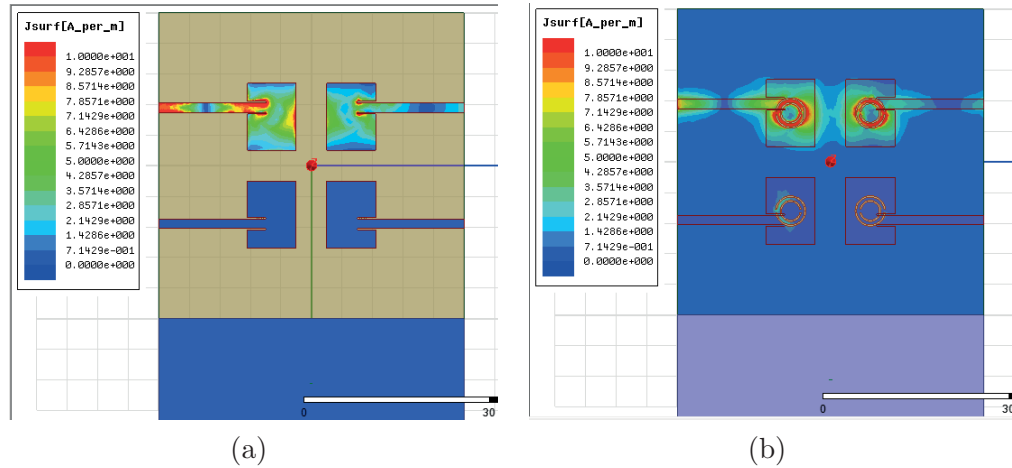


Figure 5.27: Current distribution on the 4-element MIMO antenna system at 5.08 GHz when element 4 is active, (a) Top side, (b) Bottom side

element.

### TARC ,Correlation Coefficient

The TARC curves was obtained by keeping the amplitude of all ports at unity and varying their phases. Fig. 5.30 shows the TARC curves for the 4-element MIMO antenna system. Fig. 5.30(a) shows the TARC curves when element 4 was in phase with element 1 while the phases of element 2 and 3 were varied. A -6 dB bandwidth of at least 80 MHz was observed. This occurred when either the elements 2 and 3 were in phase with element 1 or  $180^\circ$  out of phase with element 1. TARC curves shown in Fig. 5.30(b) were obtained when element 2 was kept in phase with element 1 while phases of element 3 and 4 were varied. Fig. 5.30(c) shows TARC curves when element 3 was kept in phase with element 1 while phases of element 3 and 4 were varied. TARC curves of Fig. 5.30(d) were obtained by varying the phases of all three elements with respect to element 1 in

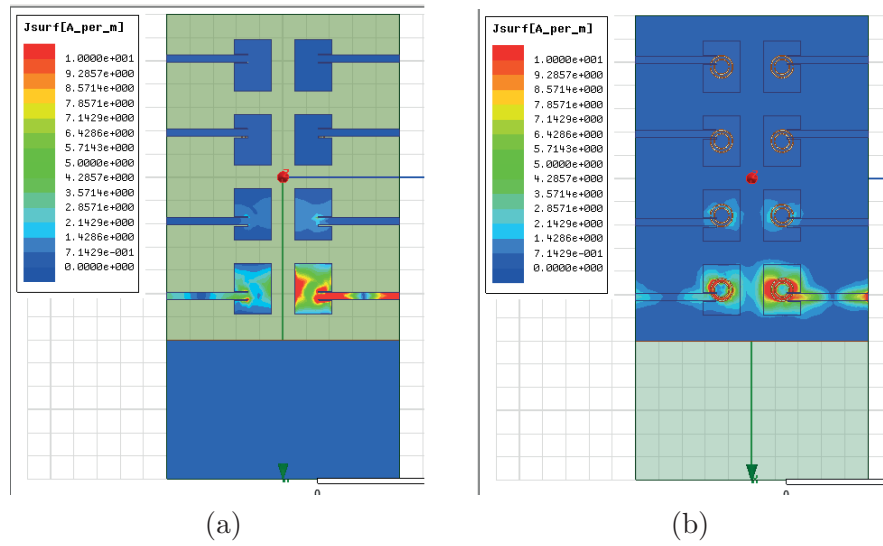


Figure 5.28: Current distribution on the 8-element MIMO antenna system at 5.04 GHz when element 1 is active, (a) Top side, (b) Bottom side

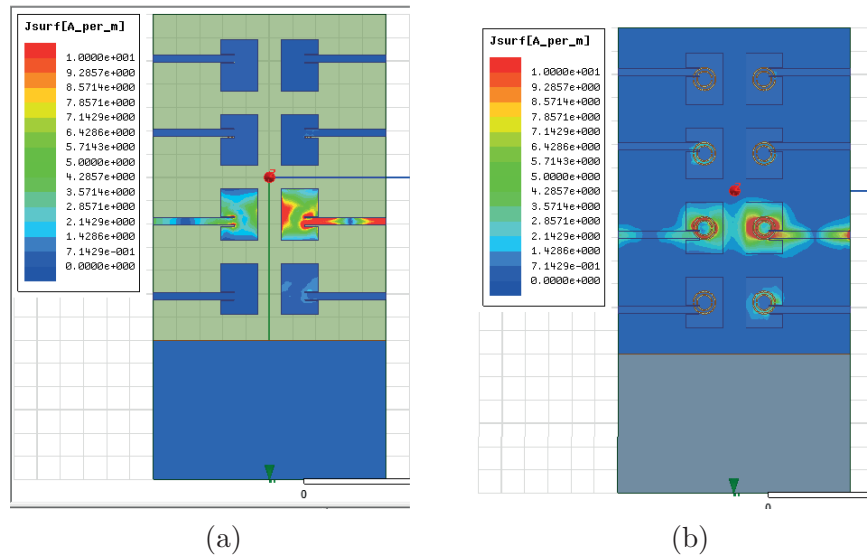


Figure 5.29: Current distribution on the 8-element MIMO antenna system at 5.04 GHz when element 3 is active, (a) Top side, (b) Bottom side

order of  $60^\circ$  or  $90^\circ$ . For all combinations, at least 80 MHz of -6 dB bandwidth was achieved. This showed that the MIMO operating bandwidth was at least 80 MHz for a wide range of antenna excitation combinations.

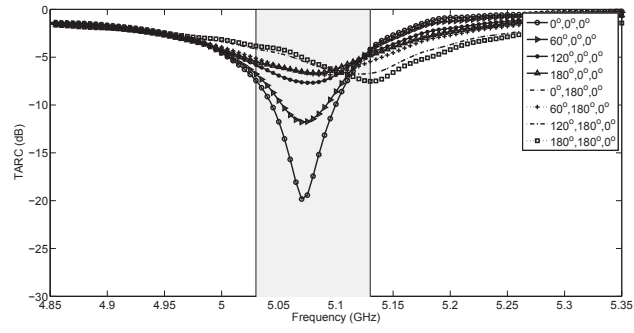
For the 8-element MIMO antenna, the TARC curves for various combination were evaluated. A minimum of 80 MHz bandwidth was obtained in each combination of the phases of the excited ports. Fig. 5.31 shows the TARC curves of 8-element antenna system when element 1 was kept as  $1e^{j0}$  while the phases of all other ports were either  $0^\circ$ ,  $60^\circ$ ,  $90^\circ$ ,  $120^\circ$  or  $180^\circ$ .

For the 4-element MIMO antenna system, the envelope correlation coefficient obtained between antenna elements is shown in Fig. 5.32. A maximum correlation coefficient of 0.28 was obtained between antenna elements whose radiating edges were facing each other. A high coupling between these antenna elements was observed earlier in the isolation and current distribution figures.

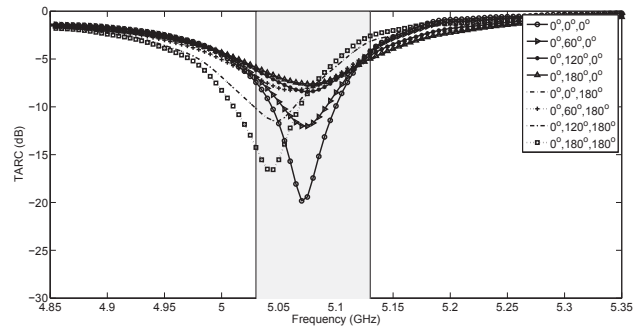
Fig. 5.33 shows the envelope correlation coefficient obtained between the antenna elements of 8-element MIMO antenna system. Here too, a maximum correlation coefficient of 0.3 was observed between antenna elements whose radiating edges were facing each other.

### **Far Field Radiation Characteristics**

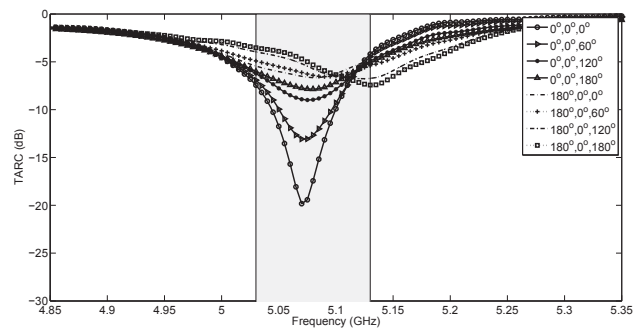
The two dimensional gain patterns of both the antennas were measured. These measurements were taken at 5.08 GHz for 4-element MIMO antenna system and at 5.04 GHz for 8-element MIMO antenna system. Fig. 5.34 shows the normalized gain patterns of all the four elements of 4-element MIMO antenna system. The



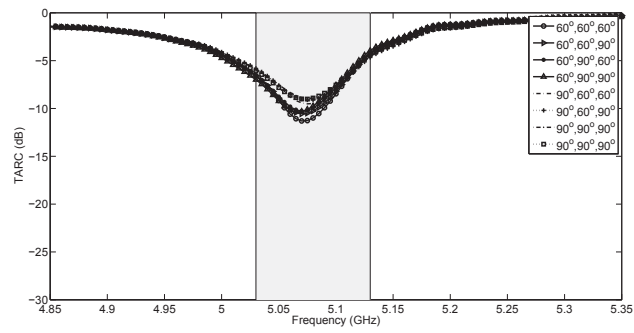
(a)



(b)



(c)



(d)

Figure 5.30: TARC curves for the 4-element 5 GHz band MIMO antenna system



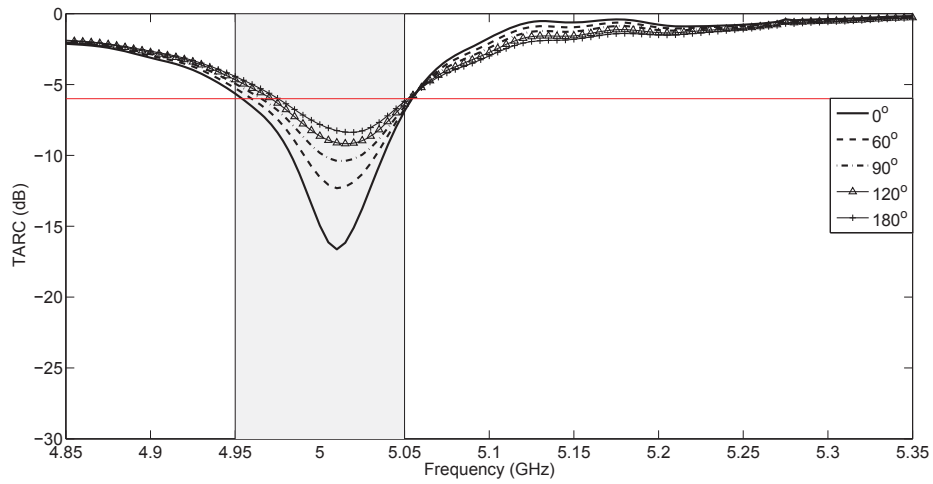


Figure 5.31: TARC curves for the 8-element 5 GHz band MIMO antenna system

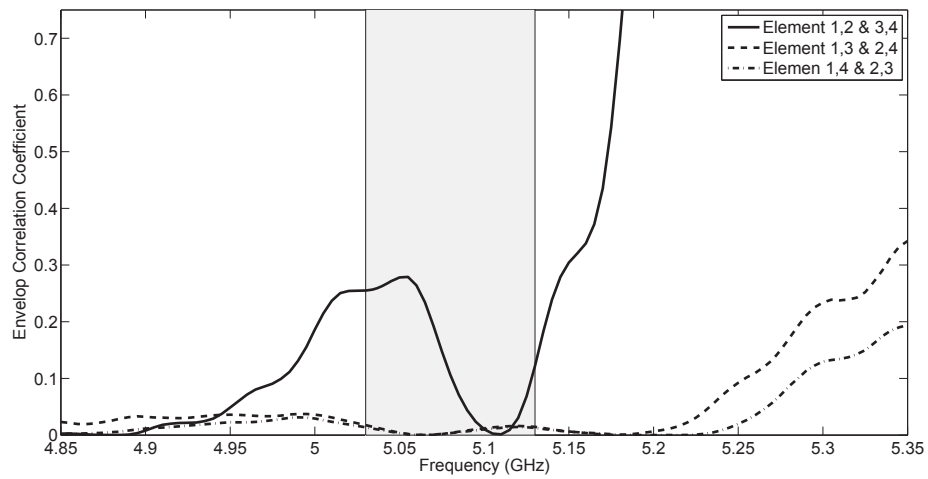


Figure 5.32: Correlation coefficient curves of the 4-element 5 GHz band MIMO antenna system

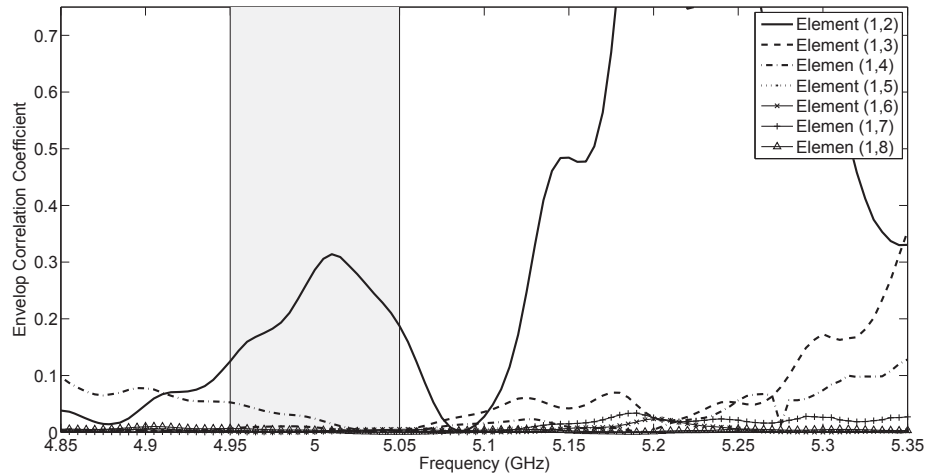


Figure 5.33: Correlation coefficient curves of the 8-element 5 GHz band MIMO antenna system

maximum measured gain was -0.8 dBi. Fig. 5.34(a) shows the gain patterns of antenna elements in elevation plane while Fig. 5.34(b) shows the gain patterns of antenna elements in the azimuth plane.

Fig. 5.35 shows the normalized gain patterns of the first four elements of the 8-element MIMO antenna system in the azimuth and elevation plane. For the other four elements i.e. Element 5 to 8, the normalized gain patterns for the azimuth and elevation plane are shown in Fig. 5.36. It was observed that the patterns were similar to that of a conventional MPA with higher back lobes which were due to the CSRR. The maximum gain measured at 5.04 GHz was -0.9 dBi.

### Mean Effective Gain

The MEG values for the MIMO antenna systems with  $\Gamma$  of 0 dB and 6 dB were evaluated using the measured 2D radiation patterns. Table 5.3 shows the MEG

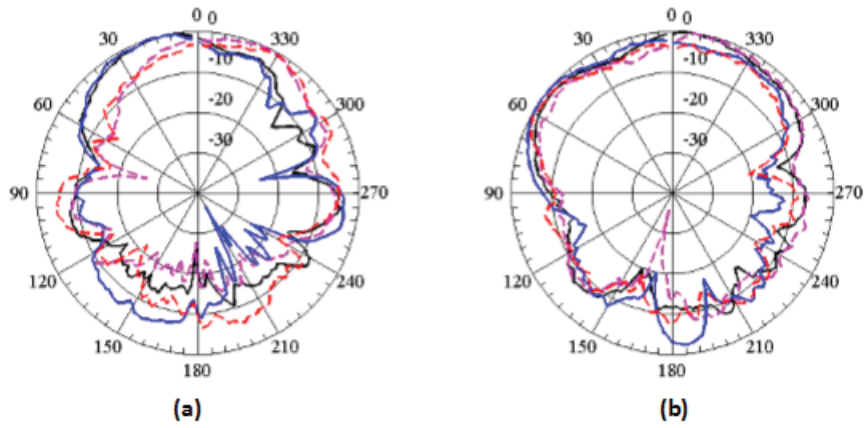


Figure 5.34: Normalized Gain patterns of the 4-element MIMO antenna system measured at 5.08 GHz. (a) x-z plane (b) y-z plane [Black = Element 1, Pink = Element 2, Blue = Element 3, Red = Element 4]

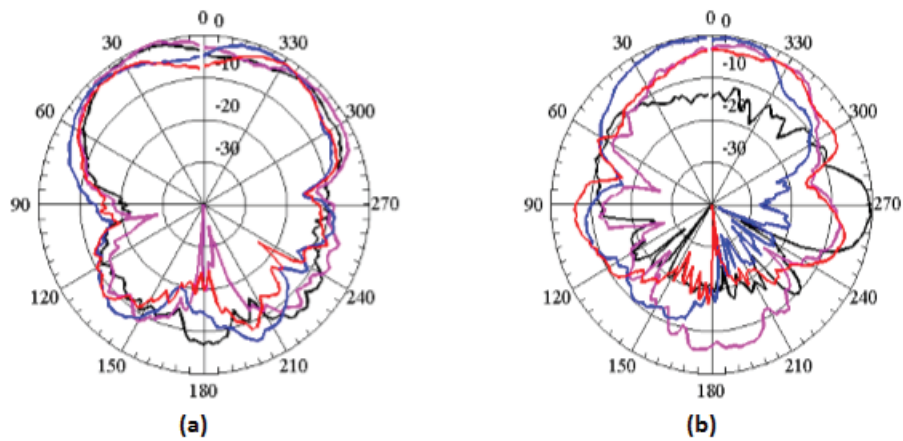


Figure 5.35: Normalized Gain patterns of the Element 1 to 4 of 8-element MIMO antenna system measured at 5.04 GHz. (a) x-z plane (b) y-z plane [Black = Element 1, Pink = Element 2, Blue = Element 3, Red = Element 4]

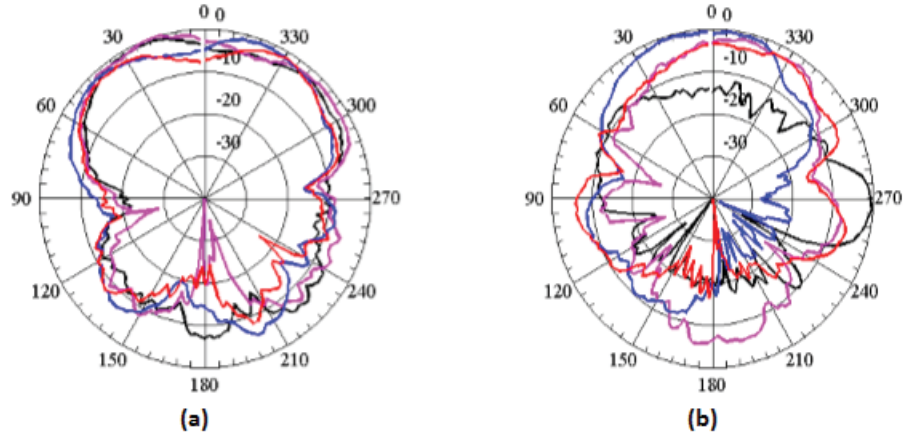


Figure 5.36: Normalized Gain patterns of the Element 5 to 8 of 8-element MIMO antenna system measured at 5.04 GHz. (a) x-z plane (b) y-z plane [Black = Element 5, Pink = Element 6, Blue = Element 7, Red = Element 8]

Table 5.3: MEG of the 4-Element MIMO Antenna Systems

Antenna_Element	$MEG(\Gamma = 0dB)$	$MEG(\Gamma = 6dB)$
1	-6.51 dB	-5.24 dB
2	-6.5 dB	-5.25 dB
3	-6.82 dB	-5.85 dB
4	-6.92 dB	-5.9 dB

values for 4-element MIMO antenna system and Table 5.4 shows the MEG values for 8-element MIMO antenna system. In both designs, a 30% antenna efficiency was considered for the calculations of MEG. In both the designs, the ratio of MEG between the antenna elements differs by less than 1 dB which is well below the maximum 3 dB limit.

### 5.2.3 Channel Capacity Estimation

Since the measurement setup to find the channel capacity was only available for the ISM band, the channel capacity of the 5 GHz band 4-element and 8-element

Table 5.4: MEG for the 8-Element MIMO Antenna Systems

Antenna_Element	$MEG(\Gamma = 0dB)$	$MEG(\Gamma = 6dB)$
1	-6.2 dB	-5.17 dB
2	-6.41 dB	-5.34 dB
3	-6.62 dB	-5.58 dB
4	-6.7 dB	-5.77 dB
5	-6.8 dB	-5.56 dB
6	-6.5 dB	-5.22 dB
7	-7.13 dB	-6.41 dB
8	-7.08 dB	-6.40 dB

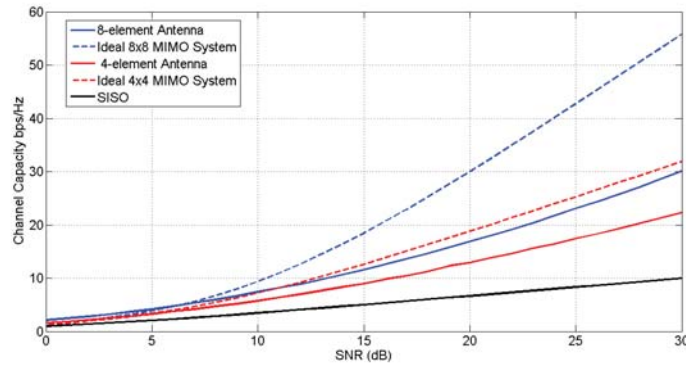


Figure 5.37: Average channel capacity of the 5 GHz band MIMO Antenna Systems

MIMO antenna systems was estimated using the theoretical models for a multi-path urban environment operating at 5 GHz. The 2D field patterns of the antenna elements in the x-z plane were used in the calculations. The H matrix was computed using Eq.(4.10) as outlined in the Chapter 4. Fig. 5.37 shows the average channel capacity of the MIMO system using the proposed antennas. Both antennas showed a good multiplexing gain for the MIMO system. At an SNR of 20 dB, the average capacity offered by the 4×4 system using the 4-element antennas was 13 bits/sec/Hz while for the 8×8 system, it was 17 bits/sec/Hz. The CDF for the antennas calculated at 20 dB SNR is shown in Fig. 5.38.

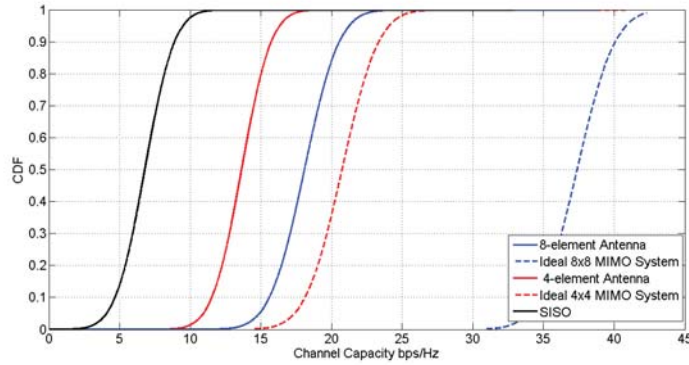


Figure 5.38: CDF of the channel capacity of the 5 GHz band MIMO antenna systems

Fig. 5.38 shows the cumulative distribution function of the channel capacity of the printed antenna in LOS as well as NLOS environments calculated at an SNR of 20 dB. The curves show that although the performance obtained was less than the ideal capacity, the printed MIMO antenna system performance was still better than a SISO system in such environments.

### 5.3 2-Element Multi-band MIMO Antenna System

In the 4G-LTE standards, several bands are designated for the cellular communication. As these standards require the use of MIMO systems, the most challenging MIMO antenna designs are in the lower bands such as 700 MHz band. Since the size of antenna is large in this bands, making a MIMO antenna compatible with hand-held devices require highly miniaturized antenna elements. Also, most of the devices operate on multiple bands providing the various communication services

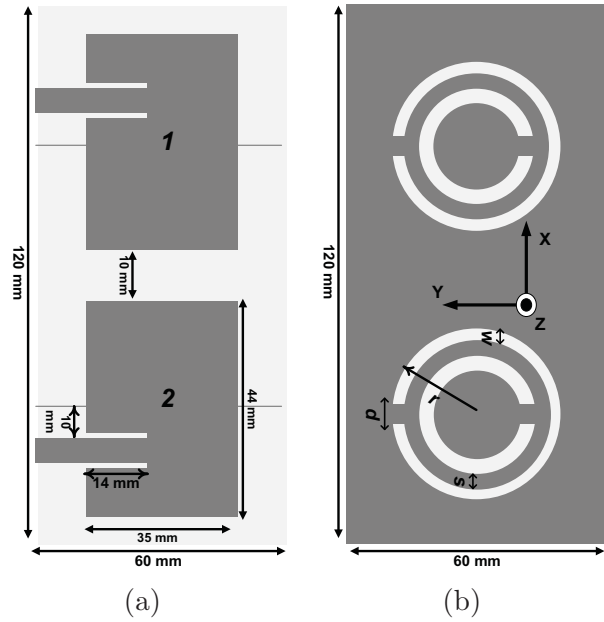


Figure 5.39: Geometry of the 2-element LTE band MIMO Antenna System (a) Top side , (b) Bottom side

simultaneously. Therefore, multi-band MIMO antenna systems are preferred for such applications. A compact  $2 \times 1$  (2-element) MIMO antenna system was therefore made for the lower LTE band. The antenna was made up of miniaturized MPAs which were designed using the proposed technique of etching the CSRR underneath the patch and tuning it to get the required resonance. The antenna was also analyzed for multi-band operation and its operation in higher bands was also examined. This antenna can be used in small tablets, wireless routers and tablet PCs.

### 5.3.1 MIMO Antenna Design

Fig. 5.39 shows the geometry of the MIMO antenna system which consists of the miniaturized MPAs. The antenna was designed on an FR4 substrate having a

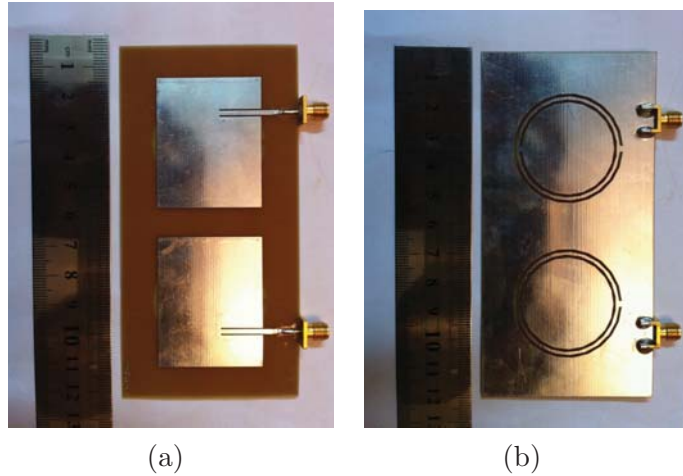


Figure 5.40: Fabricated 2-element LTE band MIMO Antenna System (a) Top side , (b) Bottom side

dielectric constant of 4.4 and thickness of 0.8 mm. Two identical patch antennas with a 10 mm separation were used. The dimensions of each patch were  $44 \times 35 \text{ mm}^2$ . Each patch was excited by a  $50\Omega$  microstrip feedline. The patch resonated at 2.04 GHz without CSRR loading. The CSRR was etched out underneath each MPA and its dimensions were varied according to the proposed methodology discussed in Chapter 3 to tune the MPA to have their lowest resonance at 750 MHz. An 85% reduction in the size of a single patch was achieved using the proposed technique compared to an single regular patch operating at 750MHz.

### 5.3.2 Simulation & Measurement Results

The antenna was first designed and tuned in HFSS. It was then fabricated and its S-parameters were measured using Agilent vector network analyzer (N9918A). The far-field radiation patterns and gain measurements of the antenna were carried out



using the Satimo Starlab anechoic chamber at KAUST, Saudi Arabia. Fig. 5.40 shows the fabricated antenna structure. The results obtained from simulations and measurements and their analysis is given in the following sub-sections.

### **Reflection Coefficient and Isolation**

The S-parameters of the MIMO antenna system obtained from simulations and measurements are shown in Fig. 5.41. The antenna resonated at 750 MHz with a -6dB bandwidth of 40 MHz. A further analysis showed that the antenna also resonated at 1.17 GHz, 1.7 GHz and 2.35 GHz. The -6dB bandwidths covered in these bands were, 1.16-1.21 GHz, 1.68-1.73 GHz and 2.33-2.39 GHz, respectively. These relatively narrow bandwidths are considered useful for some of the currently available wireless standards such as LTE 700 MHz band 13, GPS L5 band and LTE TDD bands. The minimum measured isolation between the antenna elements of the MIMO antenna system were -10 dB, -13.28 dB, -16.23 dB and -20 dB in the 750 MHz, 1.17 GHz, 1.7 GHz and 2.35 GHz bands, respectively.

### **Current Distribution**

The current distributions over the top and bottom surfaces of the MIMO antenna system were obtained to get a better understanding of the antenna behavior. Antenna element 1 was excited and antenna element 2 was terminated with a  $50\Omega$  load. These current distributions were obtained at the frequencies of 750 MHz, 1170 MHz, 1700 MHz and 2350 MHz. Fig. 5.42 shows these current distribution on the antenna surfaces. It is obvious that the patch is the main radiator and it

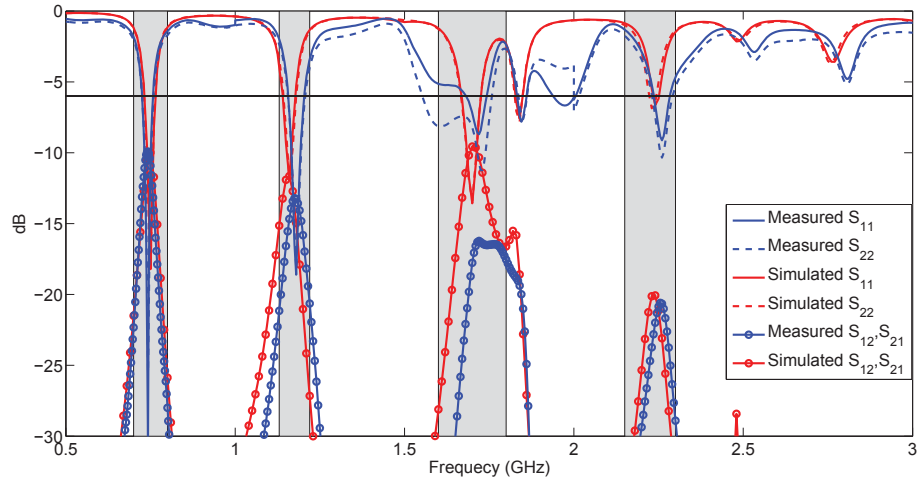


Figure 5.41: S-parameters of the 2-element LTE band MIMO antenna system radiates well at all of the four frequencies with different modes. Due to symmetry in antenna design, similar current distributions were obtained when antenna element 2 was excited.

### TARC, Correlation Coefficient & MEG

The TARC for the 2-element MIMO antenna system was calculated. Fig. 5.43 shows the TARC curves of the antenna for different phase differences ( $0^\circ - 180^\circ$  in  $30^\circ$  steps). The curves show that the antenna maintains its resonance in all four bands for different phase combinations with only a slight decrease in bandwidth.

MEG was calculated from the 2D radiation pattern of each antenna element in the y-z plane. In the calculation of MEG,  $\Gamma = 0$  dB was considered because it represents a mobile urban environment. Correlation coefficient was calculated from the measured S-parameters while taking into the account of antenna's radiation efficiency. The values of  $\rho$  and MEG along with the radiation efficiency

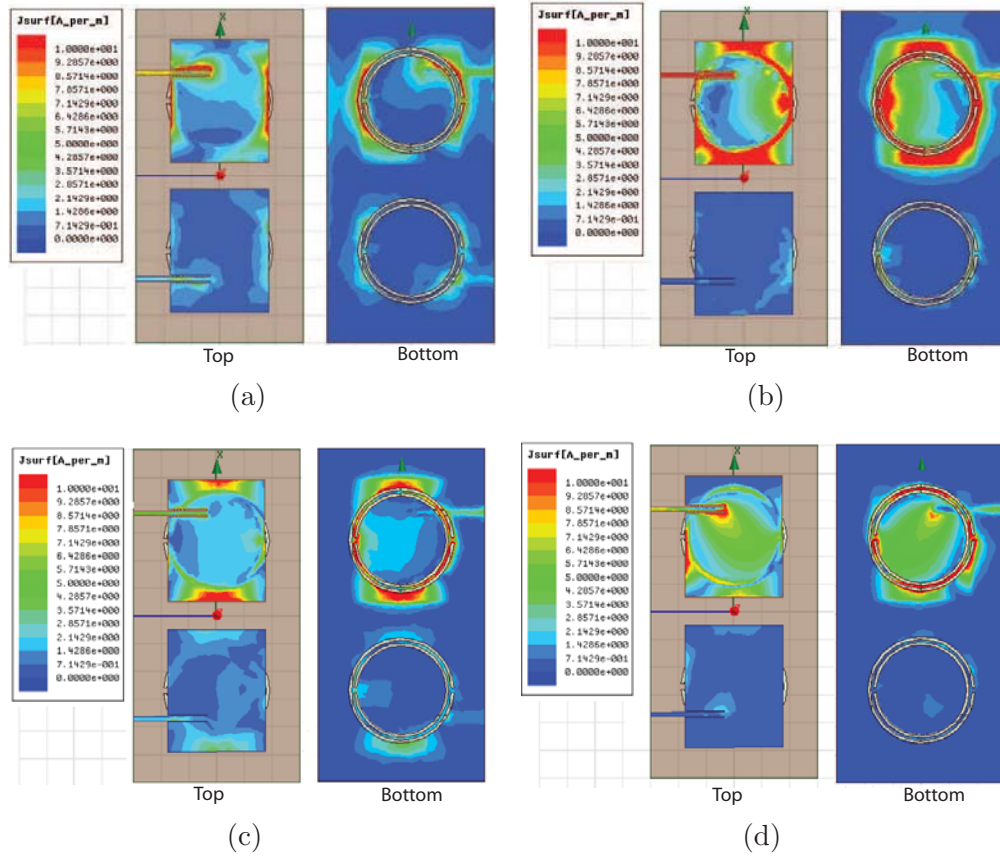


Figure 5.42: Current distribution on the 2-element LTE band MIMO antenna system when element 1 is active, (a) at 750 MHz, (b) at 1170 MHz, (c) at 1700 MHz, (d) at 2350 MHz

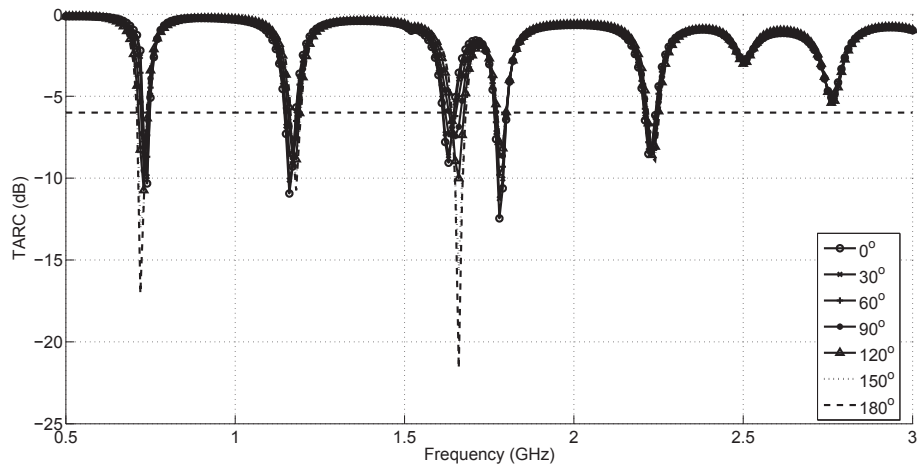


Figure 5.43: TARC curves of the 2-element LTE band MIMO antenna system

Table 5.5: MEG, Radiation Efficiency and Correlation Coefficient of the Multi-band MIMO Antenna System

Band	MEG Element 1 (dB)	MEG Element 2 (dB)	Radiation Efficiency $\eta_1$ (%)	Radiation Efficiency $\eta_2$ (%)	Correlation Coefficient $\rho_{12}$
750 MHz	-5.88	-5.67	28	27.62	0.05
1170 MHz	-7.05	-6.68	12.40	14.30	0.05
1700 MHz	-5.28	-5.35	21	21	0.05
2350 MHz	-13.13	-11.27	19	19	0.01

of the antenna elements are tabulated in Table 5.5. The low radiation efficiency of the antenna elements in all bands is due to the use of the CSRR and due to small electrical size of the antenna in the lower band. The antenna diversity performance in all the four bands was within the acceptable limits of MIMO antenna standards.

## 2D Radiation Patterns

The gain patterns of the antenna were measured at 750 MHz, 1170 MHz, 1700 MHz and 2350 MHz. Fig. 5.44 shows the normalized gain patterns of each antenna element. Figs. 5.44(a) and Fig. 5.44(b) show the normalized gain patterns of the antenna elements measured at 750 MHz in x-z plane and y-z plane, respectively. The maximum gain of the antenna at this frequency was 3.36 dBi. The patterns of the antenna elements at 1170 MHz and 1700 MHz for the two planes are shown in Figs. 5.44(c), Fig. 5.44(d) and Figs. 5.44(e), Fig. 5.44(f), respectively. The

maximum measured gain of antenna at 1170 MHz and 1700 MHz was -1.13 dBi and -5.17 dBi, respectively. The maximum gain of the antenna at 2350 MHz was -3.11 dBi. Fig. 5.44(g) and Fig. 5.44(h) show the normalized gain patterns of the antenna elements at 2350 MHz in the two planes.

## 5.4 Isolation Enhancement in the MIMO Antenna System

The gains of MIMO system over SISO system depends on the number of uncorrelated channel between the receiver and the transmitter. Therefore, MIMO systems are successful in only those environments where such condition is met. Apart from the propagation environment, the correlation among channels is also introduced due to the coupling between antenna elements of the MIMO system. The simplest method to improve isolation between antenna elements is to increase the spacing between them. However, this increases the size of the design and beyond a certain limit, it makes the design incompatible for use in practical devices. Therefore, much of the work on MIMO antenna system design solely focus on designing isolation improvement mechanisms for closely spaced antenna elements. This includes the use of slots in the ground plane [137], microstrip line based decoupling structures [138] and neutralization line between antenna elements [139].

For our proposed MIMO antenna systems using the miniaturized patches as the antenna elements, the isolation was achieved by the element placement and

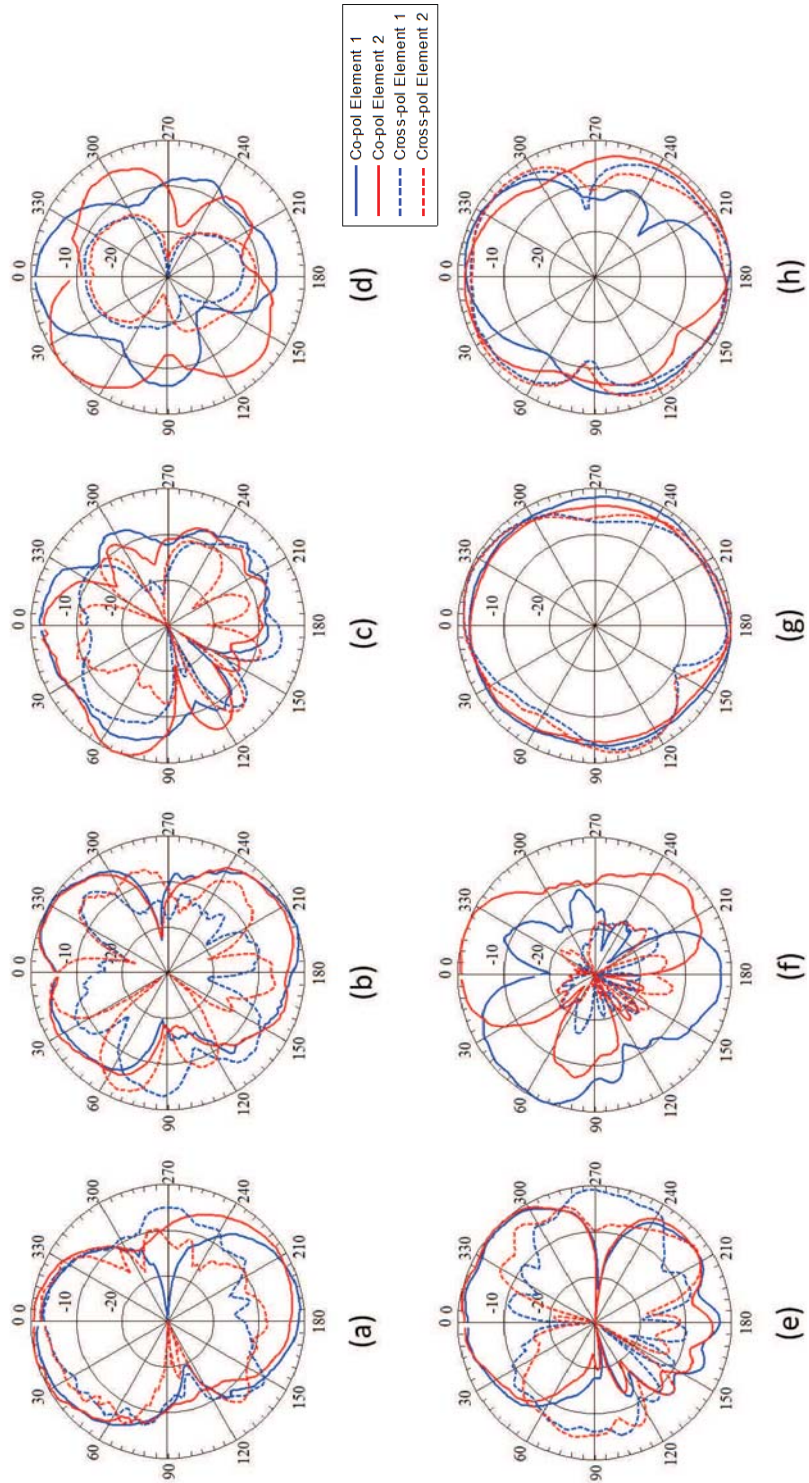


Figure 5.44: Measured gain pattern of the proposed MIMO antenna system (a) 750 MHz x-z plane, (b) 750 MHz y-z plane, (c) 1170 MHz x-z plane, (d) 1170 MHz y-z plane, (e) 1700 MHz x-z plane, (f) 1700 MHz y-z plane, (g) 2350 MHz x-z plane, (h) 2350 MHz y-z plane

spacing between them. A reasonable and acceptable isolation was achieved in each case. However, to further improve the isolation between the antenna elements of the proposed MIMO antenna systems, a new metamaterial-inspired method was developed. In this method, a metamaterial (MTM) structure, split-ring resonator (SRR) was used for isolation improvement by placing the SRR between the antenna elements. An SRR is a MTM structure which was first proposed in [140]. It behaves as an LC resonator and act as a magnetic dipole when excited by an axial magnetic field [59]. The resonant frequency of the SRR depends on its dimensions. Its equivalent circuit was derived in [59]. A simple empirical formulation for predicting the resonant frequency of the SRR or getting the dimensions of the SRR for a particular resonant frequency was given in [60].

In the proposed technique, the SRR with a resonant frequency equal to the operating frequency of antenna was placed between the antenna elements pair which had high coupling as compared to other pairs. The dimensions of the SRR corresponding to the resonant frequency were calculated from the empirical equations given in [60]. This resulted in a minimum of 4 dB increase in the isolation between the antenna elements. The method was applied to the 4-element antenna designed for the 2.45 GHz ISM band and thoroughly analyzed. The details of this design and analysis is provided in the next sections. To prove the generality of the method, it was also applied to the 4-element antenna operating in the 5 GHz band, results of which are discussed in the subsequent sections.

### 5.4.1 Isolation Improvement for the ISM Band MIMO Antenna system

When properly designed and placed between antenna elements, the SRR can interact with the magnetic fields and increase the isolation between antenna elements. For the 4-element MIMO antenna system, the minimum isolation was measured between antenna elements 1 & 2 and 3 & 4. Therefore, an SRR was placed between element 1 & 2 as well as between element 3 & 4 as shown in Fig 5.45. The resonant frequency of the SRR was the same as that of antenna elements. The dimensions of the SRR for this particular resonant frequency were obtained from [60]. The SRR had a resonant frequency of 2.45 GHz on an FR4 substrate of dielectric constant 4 and thickness 0.8 mm when its radius ' $r_2$ ' was 5.8 mm, width of each ring ' $w_2$ ' was 0.6 mm, spacing between the two rings ' $s_2$ ' was 1.4 mm and width of slit in each ring ' $d_2$ ' each was 1 mm.

The antenna was first simulated in HFSS and then fabricated. The S-parameters of the fabricated antenna were measured. A close agreement was found between the simulation and measurement results. Fig. 5.46 shows the measured S-parameters of the antenna. The antenna maintained its minimum bandwidth of 50 MHz while the minimum isolation in the operating band was increased to 18 dB without affecting the reflection coefficients significantly. By comparison with the measured S-parameters of antenna without isolation structure, a minimum increase of 7 dB in isolation was achieved using the SRR based isolation structure.



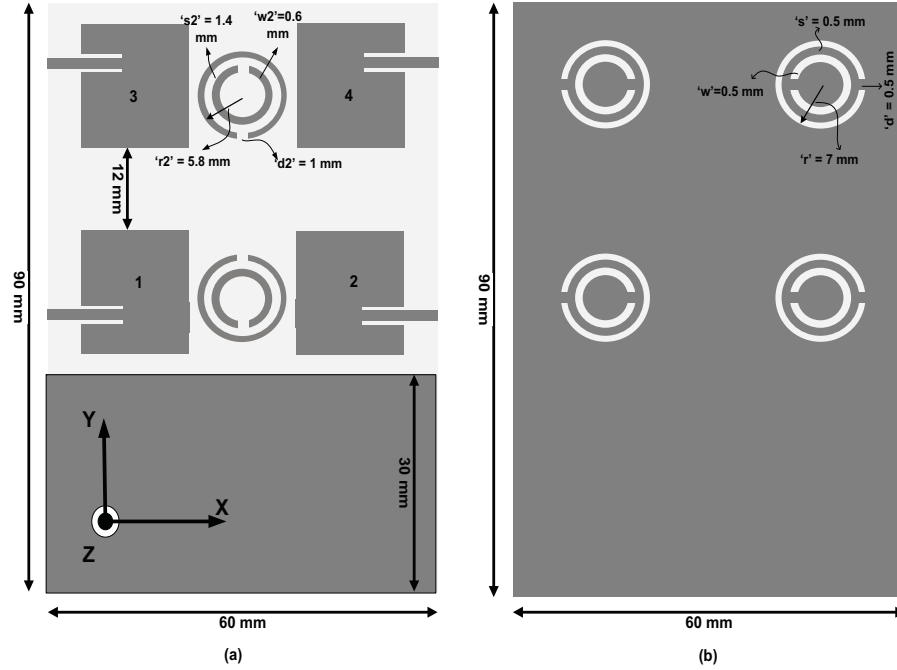


Figure 5.45: Geometry of the 4-element ISM band MIMO antenna system with SRR based isolation, (a) Top side, (b) Bottom side

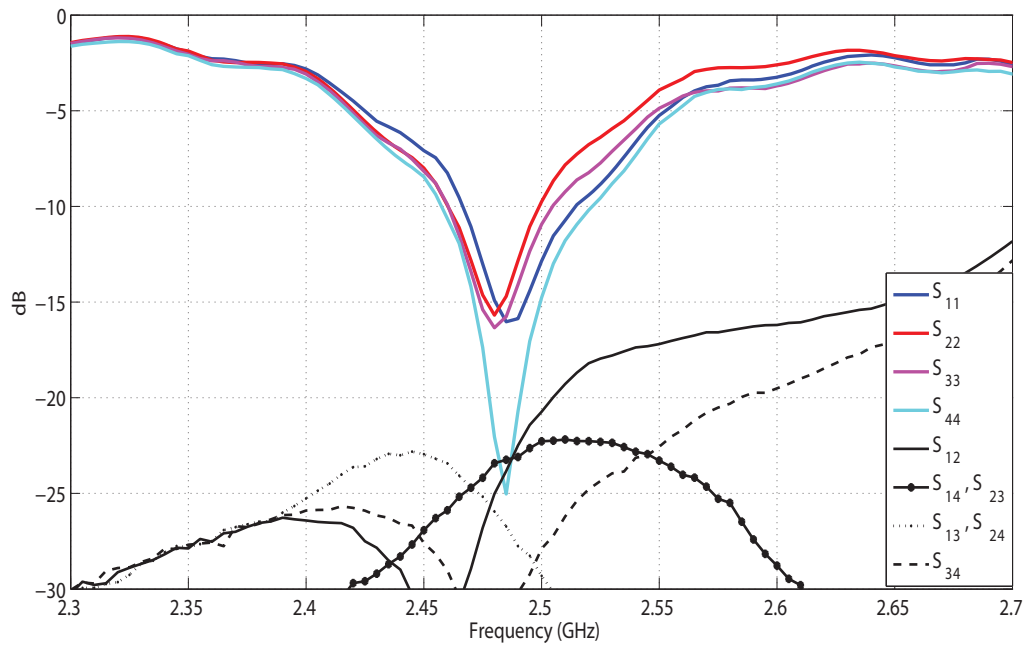


Figure 5.46: Measured S-parameters of the 4-element ISM band MIMO antenna system with SRR based isolation

The isolation mechanism was further analyzed by obtaining the surface current density on the antenna surface and comparing it with the one obtained without the isolation structure. Fig. 5.47 shows the current density on the top and bottom sides of the antenna with and without the SRR based isolation structure. These surface current densities were obtained by exciting antenna element 1 and terminating all other elements with  $50\Omega$ . As seen from Fig. 5.47(a) & (b), high coupling between antenna element 1 and 2 is observed. With the use of the SRR, the radiated energy from the top as well as the bottom of antenna element 1 directed towards antenna element 2 was coupled into the SRR as shown in Fig. 5.47(c) & (d). This resulted in better isolation between the two elements. Due to symmetry in the design, the same affect was found between antenna elements 3 & 4.

Apart from isolation, the SRR based antenna was thoroughly analyzed and compared with the antenna without the isolation structure. For this purpose, different parameters were obtained from simulations. These parameters included the radiation efficiency, maximum gain and gain pattern of each antenna element. These parameters were obtained by exciting the particular antenna element and terminating other elements with  $50\Omega$  load.

From the obtained antenna efficiencies, it was found that the isolation structure did not affect the radiation efficiencies of the antenna elements and they remained almost the same. The antenna gain also remained the same for each antenna element by the introduction of the SRR. For antenna elements 3 and 4, the maximum gain was -0.1 dBi without the isolation structure. The gain of these

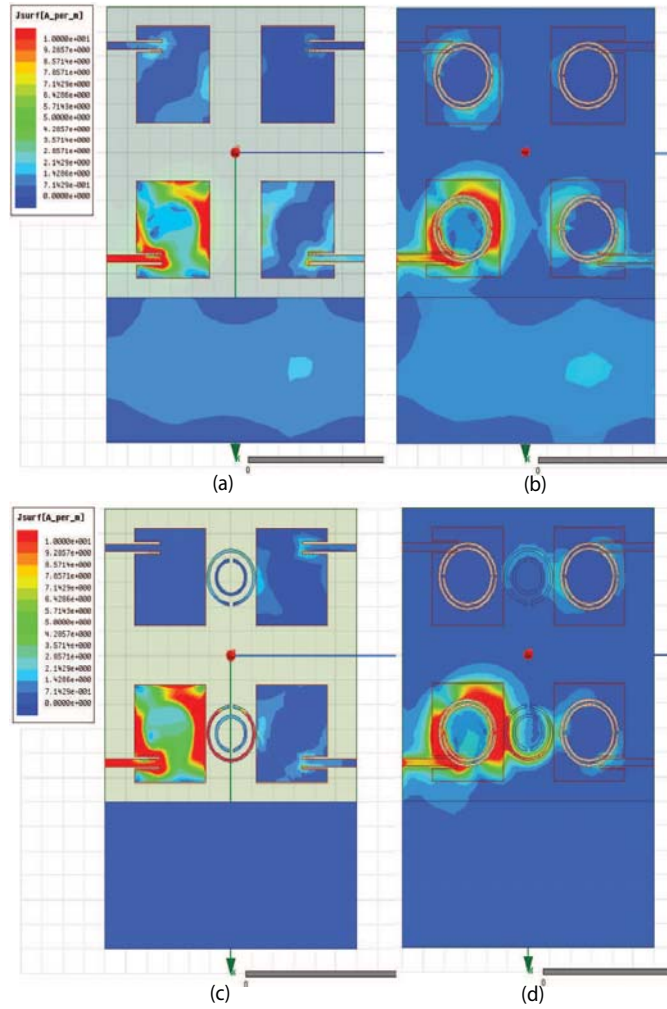


Figure 5.47: Surface current density on the 4-element MIMO antenna system when antenna element 1 is active,(a) Top side (without isolation structure), (b) Bottom side (without isolation structure), (c) Top side (with SRR based isolation structure),(d) Bottom side (with SRR based isolation structure)

Table 5.6: Gain and Efficiency of the MIMO Antenna System with and without the SRR Based Isolation Structure

	<b>Gain without SRR</b>	<b>Gain with SRR</b>	<b>Efficiency without SRR</b>	<b>Efficiency with SRR</b>
<b>Element 1</b>	-1.0 dBi	-0.55 dBi	32.5%	31.5%
<b>Element 2</b>	-0.9 dBi	-0.55 dBi	32.5%	31.5%
<b>Element 3</b>	-0.1 dBi	-0.5 dBi	28%	28%
<b>Element 4</b>	-0.1 dBi	-0.5 dBi	28%	28%

two antennas decreased a little due to the isolation structure. Thus with the SRR between antenna elements 3 and 4, there maximum gain was -0.5 dBi. In the case of antenna element 1 and 2, the isolation structure improved the maximum gains of antenna elements slightly. Without the isolation structure, the gain was -0.9 dBi which increased to -0.55 dBi with the use of the SRR (the presence of the close ground plane played a role here as well). The radiation efficiencies and peak gain of the antenna elements of the two MIMO antenna systems are tabulated in Table 5.6.

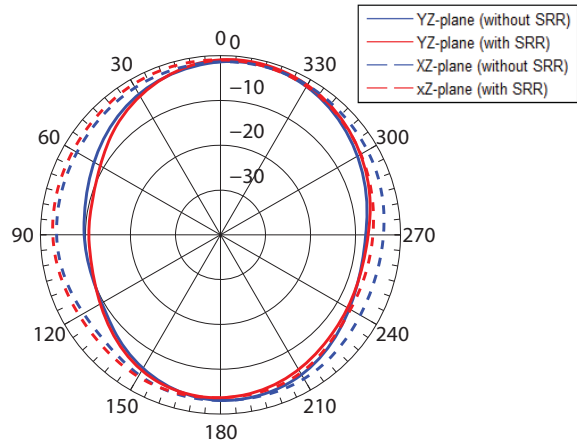
The correlation coefficients between the antenna elements of the SRR-isolated antenna were computed from its measured S-parameters. From the correlation coefficient curves, it was found that the increase in isolation also improved the correlation coefficient. The maximum correlation coefficient for the SRR-isolated MIMO antenna system was 0.058 in the operating band. The SRR based isolation structure slightly changed the surface current densities on the patches and there-

fore their radiation patterns were affected. However, this effect was negligible. Fig. 5.48 shows the radiation patterns of antenna elements when used without the isolation structure as well as with the SRR based isolation structure.

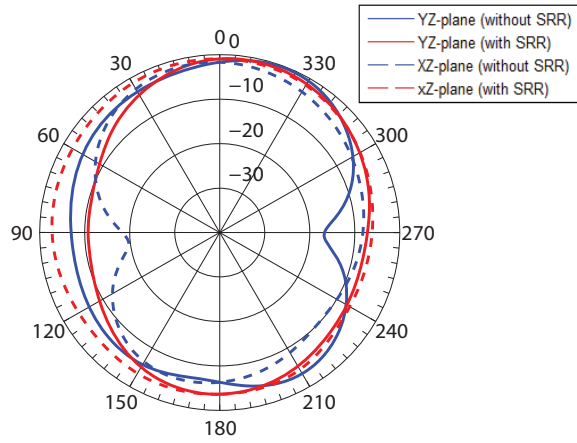
Fig. 5.48(a) shows the gain pattern of antenna element 1 in the x-z and y-z planes with and without the use of isolation structure. Clearly, the radiation patterns are only slightly affected due to the SRR. Same results are seen in Fig 5.48(b) where the radiation patterns of antenna element 4 in the x-z and y-z planes are hardly affected by the isolation structure. The radiation patterns for antenna element 2 and 3 were same as that of antenna element 1 and 4, respectively.

#### 5.4.2 SRR Based Isolation Improvement for Other Bands

To validate the generality of this method for the CSRR loaded patch antenna based MIMO antennas, the SRR based isolation method was also applied to a 4-element MIMO antenna system operating in the 5 GHz band. Two SRR were placed between antenna element pairs 1& 2 and 3& 4. The dimensions of the SRR with resonant frequency of 5 GHz were calculated using the empirical formulas given in [60]. The SRR resonated at 5 GHz when its radius ( $r_2$ ) was 2.4 mm, width of each ring ( $w_2$ ) was 0.3 mm, spacing between the two rings ( $s_2$ ) was 0.7 mm and width of slit in each ring ( $d_2$ ) each was 0.5 mm. From the simulations, it was found that the SRR resulted in an increase of more than 4 dB isolation between the antenna elements. Fig. 5.49 shows the S-parameters of the antenna with SRR based isolation structure. The increase in isolation is clearly visible when



(a)



(b)

Figure 5.48: Radiation patterns with and without the SRR based isolation structure, (a) Antenna element 1, (b) Antenna element 4

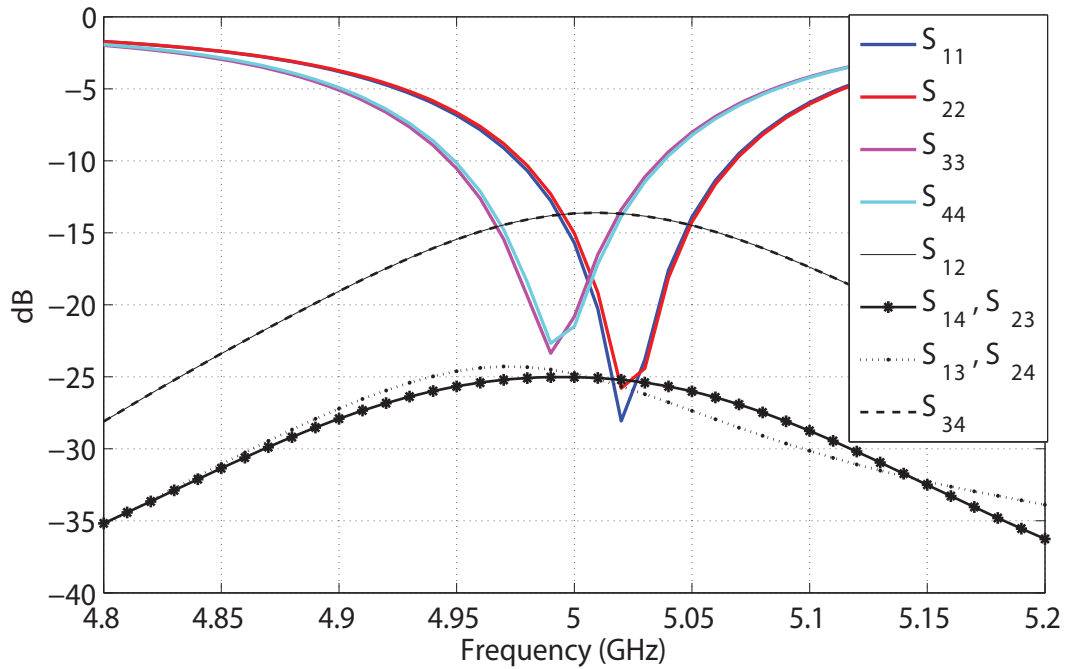


Figure 5.49: Simulated S-parameters of the 4-element MIMO antenna system operating in the 5 GHz band with SRR based isolation

compared to the isolation curves given in Fig. 5.22.

From these results, it was concluded that the SRR based isolation technique was simple and easy to implement and provided increase in isolation without affecting other antenna parameters. However, like any other technique, this too has its drawback. This isolation technique is limited to single-band operations and cannot be applied to improve isolation for all bands in a multi-band antenna. Secondly, the size of the SRR depends on the frequency of operation. At lower frequencies, the size of the SRR may become too large and render the implementation useless. Therefore, careful consideration is required to use this method.

## 5.5 Comparison & Conclusions

A comparison of the proposed MIMO antenna system with some of the other well sited designs in literature is shown in Table 5.7. The proposed antennas are planar and compact and make use of the MPA which is rarely used as an element of the MIMO antenna system. In the 5 GHz band, an 8-element compact and planar MIMO antenna system was proposed which comply with the new standards. Such an 8-element MIMO antenna systems are new in the literature. Due to their ease of design, compact size and planar structure, the proposed antennas show a huge potential for the practical use.



Table 5.7: A Summary & Comparison of the Proposed MIMO Antenna Systems with Other MIMO Antenna Systems in Literature

Ref.	Band of Operation	Elements Type	No. of Elements	Size	Minimum Iso-lation	Structure
[85]	2.4 GHz, 5.4 GHz, 5.8 GHz (Multi-Band)	Printed Monopoles	2	90×35×0.8 mm <sup>3</sup>	10 dB	Planar
[123]	2.3 GHz (Single Band)	PIFA	2	38×28×1.6 mm <sup>3</sup>	20 dB	Planar
[81]	2 GHz (Single Band)	Printed Monopoles	4	95×60×0.8 mm <sup>3</sup>	11.5 dB	Planar
[109]	2.65 GHz (Single Band)	MPA	3	90×120×1 mm <sup>3</sup>	28 dB	Planar
[99]	2.45 GHz (Single Band)	PIFA	4	120×120×18 mm <sup>3</sup>	-	Non-Planar
[126]	5 GHz (Single Band)	Printed Yagi-Uda	3	55×48×1.28 mm <sup>3</sup>	-	Planar
[94]	5.2 GHz (Single Band)	Dipoles	4	270×210×10 mm <sup>3</sup>	20 dB	Non-Planar
[127]	750 MHz (Single Band)	PIFA	2	110×55×4 mm <sup>3</sup>	12 dB	Non-Planar
[102]	700 MHz (Single Band)	PIFA	2	40×90×5 mm <sup>3</sup>	13 dB	Non-Planar
[101]	700 MHz (Single Band)	PIFA	2	95×60×9 mm <sup>3</sup>	20 dB	Non-Planar
<b>Proposed 1</b>	<b>2.45 GHz (Single Band)</b>	<b>MPA</b>	<b>4</b>	<b>100×50×0.8 mm<sup>3</sup></b>	<b>-10 dB</b>	<b>Planar</b>
<b>Proposed 2</b>	<b>5 GHz (Single Band)</b>	<b>MPA</b>	<b>8</b>	<b>100×50×0.8 mm<sup>3</sup></b>	<b>-11 dB</b>	<b>Planar</b>
<b>Proposed 3</b>	<b>750 MHz, 1.17 GHz, 1.7 GHz, 2.35 GHz (Multi-Band)</b>	<b>MPA</b>	<b>2</b>	<b>120×60×0.8 mm<sup>3</sup></b>	<b>-10 dB</b>	<b>Planar</b>

## CHAPTER 6

# CONCLUSIONS & FUTURE WORK

### 6.1 Conclusions

MIMO systems have received considerable attention among the researchers since they can offer higher data rates with better spectral efficiency. The performance of a MIMO system greatly depends on the design and radiation characteristics of its antenna. Therefore, the design and evaluation of MIMO antenna system has been a topic of interest for the past few years. Many innovative designs of antenna for MIMO system have appeared during this time.

The main objective of this research work was also to design and evaluate several compact and low-profile MIMO antenna systems for wireless devices. The main issues in the design of MIMO antenna system were discussed and it was highlighted that the research community working on this topic mainly focus on two

main issues. The first one arised from the size of wireless devices which required low-profile and small antenna. This demanded the antenna designer to find a way to miniaturize the antenna elements beyond its conventional dimensions of half-wavelength, so that it was possible to add multiple elements in limited space for the MIMO antenna design. The second issue arised from the performance consideration of MIMO system which required to have low correlation among its channels. Therefore, from antenna designer's point of view, it was to achieve high port isolation and low correlation coefficient among the antenna elements of the MIMO antenna system.

This work mainly focused on the first issue and tried to make compact MIMO antenna systems by first miniaturizing the antenna elements. MPA was studied for use as an element of the MIMO antenna systems that were to be designed for the lower LTE band, the 2.45 GHz ISM band the 5 GHz WiFi band. In all of these bands, the conventional size of the MPA was too big to be used as an element of the MIMO antenna system. An MTM-inspired miniaturization technique was proposed for the MPA. The technique was based on the CSRR-loading of the MPA. It was evaluated thoroughly and a systematic design methodology was developed for the miniaturization of MPA. The technique proved useful in the design of miniaturized MPA in several bands with good radiation characteristics. The designed MPA remained planar while achieving an 85% reduction in the path area for the design made for the 750 MHz LTE Band. The proposed miniaturization method also stood out from other MPA miniaturization techniques since

most of them lacked a design methodology for various bands.

Using the proposed miniaturized MPA as elements, MIMO antenna systems were designed for the 750 MHz LTE-band, 2.45 GHz ISM-band and 5 GHz WiFi-band. All antennas were made in a limited space and they conformed to the dimensions of wireless devices where they could be used. The proposed antenna were analyzed for various MIMO parameters where they showed satisfactory performances. The designed MIMO antenna systems were also evaluated in real environment by implementing a MIMO system using SDR and using the proposed antennas at its front end. The multiplexing gain of the system was analyzed and the effect of the antenna design on the multiplexing gain was shown.

An MTM-inspired isolation enhancement technique was also designed which was incorporated with the proposed MIMO antenna systems. The single band isolation enhancement was achieved by the placement of the SRR between the antenna elements which resulted in lowering the coupling between the antenna elements.

## **6.2 Future Work**

The use of 4G services is increasing globally and in the year to come, more and more devices will be implementing the MIMO systems. Therefore, the design of MIMO antenna system will remain a topic of interest for few years to come. Although several issues regarding the miniaturization of antenna for MIMO system were addressed in this work, there are a lot of things that should be considered

as future work.

The miniaturization technique should be improved further in terms of the radiation efficiency of the antenna. Although, most of the reported MTM-inspired miniaturization techniques have low yielded low efficiency antennas, the proposed technique should be analyzed further and better designs of miniaturized MPA should be sought.

The design proposed in this work were mainly focused on single band operation. Since, most of the wireless devices operate for several standards simultaneously (*e.g. Cellular service + GPS + WiFi*), therefore, it is important to look into the multi-band characteristics of MIMO antenna system. Although, in one of its operation, the proposed design showed multi-band behavior, it should be further analyzed that how the higher order modes of the antenna can be controlled and how efficiently will they radiate. For this purpose, the theory of characteristic modes might be of great use, since it can provide the location of resonance of higher order modes of the antenna, their corresponding radiation patterns and an idea on how to excite those modes.

The placement of the proposed antenna elements to make a MIMO antenna system can be analyzed further to decrease the correlation coefficient between antenna elements. This can also be achieved with the use of theory of characteristic modes. Since the theory gives the idea of the radiation pattern of each mode, it can be used to place the elements in such a way so as to minimize the correlation coefficient.

# REFERENCES

- [1] “Forecast: Devices by operating system and user type, worldwide, 2010-2017,” July 2013. [Online]. Available: <http://www.gartner.com/>
- [2] I. F. Akyildiz, D. M. Gutierrez-Estevez, and E. C. Reyes, “The evolution to 4g cellular systems: Lte-advanced,” *Physical Communication*, vol. 3, no. 4, pp. 217 – 244, 2010.
- [3] H. Y. E. Alsabbagh and K. Gallagher, “802.11ac Design Considerations for Mobile Devices,” *Microwave Journal*, pp. 80–88, 2013.
- [4] J. L. Volakis, C.-C. Chen, and K. Fujimoto, *Small Antennas : Miniaturization Techniques & Applications*. McGraw-Hill, 2010.
- [5] K. Lee and K. Tong, “Microstrip Patch Antennas - Basic Characteristics and Some Recent Advances,” *Proceedings of the IEEE*, vol. 100, no. 7, pp. 2169–2180, 2012.
- [6] H. A. Wheeler, “Fundamental Limitations of Small Antenna,” *Proceedings of the IRE*, no. 12, pp. 1479–1484, 1947.

- [7] C. G. Kakoyiannis, “Robust, Electrically Small, Circular Inverted-F Antenna for Energy-Efficient Wireless Microsensors,” *IET Microwaves, Antennas & Propagation*, vol. 8, no. 13, pp. 1047–1056, 1947.
- [8] R. Garg, P. Bhartia, I. Bhal, and A. Ittipiboon, *Microstrip Antenna Design Handbook*. Artech House, 2001.
- [9] K. F. Lee and K. M. Luk, *Microstrip Patch Antennas*. Imperial College Press, 2011.
- [10] C. A. Balanis, *Antenna Theory : Analysis and Design*, 2nd ed. John Wiley & Sons, 2004.
- [11] D. H. Schaubert and K. S. Yngvesson, “Experimental Study of a Microstrip Array on High Permittivity Substrate,” *IEEE Transactions on Antennas and Propagation*, vol. AP-34, no. 1, pp. 92–97, 1986.
- [12] B. Lee and F. J. Harackiewicz, “Miniature Microstrip Antenna With a Partially Filled High-Permittivity Substrate,” *IEEE Transactions on Antennas and Propagation*, vol. 50, no. 8, pp. 1160–1162, 2002.
- [13] J. Kula, D. Psychoudakis, W. Liao, C. Chen, J. Volakis, and J. Halloran, “Patch-antenna miniaturization using recently available ceramic substrates,” *IEEE Antennas and Propagation Magazine*, vol. 48, no. 6, pp. 13–20, Dec. 2006.
- [14] A. Hoorfar and A. Perrotta, “An Experimental Study of Microstrip Antennas on Very High Permittivity Ceramic Substrates and Very Small Ground

- Planes,” *IEEE Transactions on Antennas and Propagation*, vol. 49, no. 4, pp. 838–840, 2001.
- [15] P. M. T. Ikonen, K. N. Rozanov, A. V. Osipov, P. Alitalo, and S. A. Tretyakov, “Magnetodielectric Substrates in Antenna Miniaturization : Potential and Limitations,” *IEEE Transactions on Antennas and Propagation*, vol. 54, no. 11, pp. 3391–3399, 2006.
- [16] F. Farzami and K. Forooraghi, “Miniaturization of a Microstrip Antenna Using a Compact and Thin Magneto-Dielectric Substrate,” *IEEE Antennas and Wireless Propagation Letters*, vol. 10, pp. 1540–1542, 2012.
- [17] D. Psychoudakis, Y.-H. Koh, J. Volakis, and J. Halloran, “Design Method for Aperture-Coupled Microstrip Patch Antennas on Textured Dielectric Substrates,” *IEEE Transactions on Antennas and Propagation*, vol. 52, no. 10, pp. 2763–2765, Oct. 2004.
- [18] J. S. Colburn and Y. R. Samii, “Patch Antennas on Externally Perforated,” *IEEE Transactions on Antennas and Propagation*, vol. 47, no. 12, pp. 1785–1794, 1999.
- [19] R. Li, G. Dejean, M. M. Tentzeris, and J. Laskar, “Development and Analysis of a Folded Shorted-Patch Antenna With Reduced Size,” *IEEE Transactions on Antennas and Propagation*, vol. 52, no. 2, pp. 555–562, 2004.



- [20] C. Y. Chiu, C. H. Chan, and K. M. Luk, "Study of a Small Wide-band Patch Antenna with Double Shorting Walls," *IEEE Antennas and Wireless Propagation Letters*, vol. 3, no. 1, pp. 230–231, Dec. 2004.
- [21] A. Holub and M. Polivka, "A Novel Microstrip Patch Antenna Miniaturization Technique: A Meanderly Folded Shorted-Patch Antenna," *2008 14th Conference on Microwave Techniques*, pp. 1–4, Apr. 2008.
- [22] K. Luk, R. Chair, and K. Lee, "Small rectangular patch antenna," *Electronics Letters*, vol. 34, no. 25, p. 2366, 1998.
- [23] S. M. Moon, H. K. Ryu, J. M. Woo, and H. Ling, "Miniaturisation of  $\lambda/4$  microstrip antenna using perturbation effect and plate loading for low-VHF-band applications," *Electronics Letters*, vol. 47, no. 3, p. 162, 2011.
- [24] R. Porath, "Theory of miniaturized shorting-post microstrip antennas," *IEEE Transactions on Antennas and Propagation*, vol. 48, no. 1, pp. 41–47, 2000.
- [25] A. Mishra, P. Singh, N. P. Yadav, and J. Ansari, "Compact Shorted Microstrip Patch Antenna for Dual Band Operation," *Progress In Electromagnetic Research C*, vol. 9, pp. 171–182, 2009.
- [26] S. Wang, H. W. Lai, K. K. So, and K. B. Ng, "Wideband Shorted Patch Antenna With a Modified Half U-Slot," *IEEE Antennas and Wireless Propagation Letters*, vol. 11, pp. 689–692, 2012.

- [27] R. Waterhouse, S. Targonski, and D. Kokotoff, "Design and performance of small printed antennas," *IEEE Transactions on Antennas and Propagation*, vol. 46, no. 11, pp. 1629–1633, 1998.
- [28] N. Herscovici, M. F. Osorio, and C. Peixeiro, "Miniaturization of Rectangular Microstrip Patches Using Genetic Algorithms," *IEEE Antennas and Wireless Propagation Letters*, vol. 1, pp. 94–97, 2002.
- [29] H. Oraizi and S. Hedayati, "Miniaturization of Microstrip Antennas by the Novel Application of the Giuseppe Peano," *IEEE Transactions on Antennas and Propagation*, vol. 60, no. 8, pp. 3559–3567, 2012.
- [30] J. P. Gianvittorio and Y. Rahmat-samii, "Fractal Antennas : A Novel Antenna Miniaturization Technique , and Applications," *IEEE Antennas and Propagation Magazine*, vol. 44, no. 1, pp. 20–36, 2002.
- [31] S. I. Latif, L. Shafai, and C. Shafai, "An Engineered Conductor for Gain and Efficiency Improvement of Miniaturized Microstrip Antennas," *IEEE Antennas and Propagation Magazine*, vol. 55, no. 2, pp. 77–90, 2013.
- [32] J. Anguera, L. Boada, C. Puente, C. Borja, and A. Abstract, "Stacked H-Shaped Microstrip Patch Antenna," *IEEE Transactions on Antennas and Propagation*, vol. 52, no. 4, pp. 983–993, 2004.
- [33] S. A. Bokhari, J.-F. Zurcher, J. R. Mosig, and F. E. Gardiol, "A Small Microstrip Patch Antenna with a Convenient Tuning Option," *IEEE Transactions on Antennas and Propagation*, vol. 44, no. 11, pp. 1521–1528, 1996.

- [34] S. Chatterjee, K. Ghosh, J. Paul, S. K. Chowdhury, D. Chanda, and P. P. Sarkar, "Compact Microstrip Antenna for Mobile Communication," *Microwave and Optical Technology Letters*, vol. 55, no. 5, pp. 954–957, 2013.
- [35] W.-S. Chen, C.-K. Wu, and K.-l. Wong, "Square-Ring Microstrip Antenna with a Cross Strip for Compact Circular Polarization Operation," *IEEE Transactions on Antennas and Propagation*, vol. 47, no. 10, pp. 1566–1568, 1999.
- [36] A. K. Shackelford, K.-f. Lee, and K. M. Luk, "Design of Small-Size Wide-Bandwidth Microstrip-Patch Antennas," *IEEE Antennas and Propagation Magazine*, vol. 45, no. 1, pp. 75–83, 2003.
- [37] H. Iwasaki, "A Circularly Polarized Small-Size Microstrip Antenna with a Cross Slot," *IEEE Transactions on Antennas and Propagation*, vol. 44, no. 10, pp. 1399–1401, 1996.
- [38] J. A. Tirado-Mendez, H. Jardon-Aguilar, and F. Iturbide-Sanchez, "Application of the Defected Microstrip Structure as a Tuning Technique for Rectangular Printed Antennas," *Microwave and Optical Technology Letters*, vol. 48, no. 2, pp. 16–19, 2006.
- [39] S. Dey and R. Mittra, "Compact microstrip patch antenna," *Microwave and Optical Technology Letters*, vol. 13, no. 1, pp. 12–14, 1997.

- [40] X.-X. Zhang and F. Yang, "Study of a slit cut on a microstrip antenna and its applications," *Microwave and Optical Technology Letters*, vol. 18, no. 4, pp. 297–300, Jul. 1998.
- [41] S. Noghianian and L. Shafai, "Microstrip patch miniaturization by slots loading," *2005 IEEE Antennas and Propagation Society International Symposium*, vol. 1B, pp. 215–218, 2005.
- [42] J. Huang, "The Finite Ground Plane Effect on the Microstrip Antenna Radiation Patterns," *IEEE Transactions on Antennas and Propagation*, vol. AP-31, no. 4, pp. 649–653, 1983.
- [43] A. Bhattacharyya, "Effects of finite ground plane on the radiation characteristics of a circular patch antenna," *IEEE Transactions on Antennas and Propagation*, vol. 38, no. 2, pp. 152–159, 1990.
- [44] E. Lier and K. R. Jakobsen, "Rectangular Microstrip Patch Antennas with Infinite and Finite Ground Plane Dimensions," *IEEE Transactions on Antennas and Propagation*, vol. AP-31, no. 6, pp. 978–984, 1983.
- [45] S. Sarkar, A. D. Majumdar, S. Mondal, S. Biswas, D. Sarkar, and P. P. Sarkar, "Miniaturization of Rectangular Microstrip Patch Antenna using Optimized Single-Slotted Ground Plane," *Microwave and Optical Technology Letters*, vol. 53, no. 1, pp. 111–115, 2011.

- [46] M. Sarkar and S. K. Chowdhury, "A new compact microstrip patch antenna," *Microwave and Optical Technology Letters*, vol. 47, no. 4, pp. 379–381, Nov. 2005.
- [47] H. V. Prabhakar, U. K. Kummuri, R. M. Yadahalli, and V. Munnappa, "Effect of various meandering slots in rectangular microstrip antenna ground plane for compact broadband operation," *Electronics Letters*, vol. 43, no. 16, pp. 16–17, 2007.
- [48] S.-y. Lin and K.-c. Huang, "A Compact Microstrip Antenna for GPS and SCS Application," *IEEE Transactions on Antennas and Propagation*, vol. 53, no. 3, pp. 1227–1229, 2005.
- [49] J.-s. Kuo and K.-l. Wong, "A Compact Microstrip Antenna with Meandering Slots in the Ground Plane," *Microwave and Optical Technology Letters*, vol. 29, no. 2, pp. 95–97, 2001.
- [50] D. Wang, H. Wong, and C. H. Chan, "Small Patch Antennas Incorporated With a Substrate Integrated Irregular Ground," *IEEE Transactions on Antennas and Propagation*, vol. 60, no. 7, pp. 3096–3103, 2012.
- [51] D. Guha and Y. M. Antar, *Microstrip and Printed Antennas : New Trends, Techniques and Applications*. Wiley, 2011.
- [52] J. X. Liu, W. Y. Yin, and S. L. He, "A New Defected Ground Structure and its Application for Miniaturized Switchable Antenna," *Progress In Electromagnetic Research, PIER*, vol. 107, no. May, pp. 115–128, 2010.

- [53] S. F. Mahmoud, "A New Miniaturized Annular Ring Patch Resonator Partially Loaded by a Metamaterial Ring With Negative Permeability and Permittivity," *IEEE Antenna and Wireless Propagation Letters*, no. 3, pp. 19–22, 2004.
- [54] A. Alu, F. Bilotti, N. Engheta, and L. Vegni, "Subwavelength, Compact, Resonant Patch Antennas Loaded With Metamaterials," *IEEE Transactions on Antennas and Propagation*, vol. 55, no. 1, pp. 13–25, 2007.
- [55] P. Mookiah and K. Dandekar, "Metamaterial-Substrate Antenna Array for MIMO Communication System," *IEEE Transactions on Antennas and Propagation*, vol. 57, no. 10, pp. 3283–3292, Oct. 2009.
- [56] R. O. Ouedraogo, E. J. Rothwell, A. R. Diaz, K. Fuchi, and A. Temme, "Miniaturization of Patch Antennas Using a Metamaterial-Inspired Technique," *IEEE Transactions on Antennas and Propagation*, vol. 60, no. 5, pp. 2175–2182, 2012.
- [57] S. Jahani, J. Rashed-Mohassel, and M. Shahabadi, "Miniaturization of Circular Patch Antennas Using MNG Metamaterials," *IEEE Antenna & Wireless Propagation Letters*, vol. 9, pp. 1194–1196, 2013.
- [58] K. Z. Rajab, R. Mittra, and M. T. Lanagan, "Size reduction of microstrip patch antennas with left-handed transmission line loading," *IET microwaves antennas & propagation*, vol. 1, no. 1, pp. 39–44, 2007.

- [59] J. Baena, J. Bonache, F. Martin, R. Sillero, F. Falcone, T. Lopetegui, M. Laso, J. Garcia-Garcia, I. Gil, M. Portillo, and M. Sorolla, "Equivalent-circuit models for split-ring resonators and complementary split-ring resonators coupled to planar transmission lines," *IEEE Transactions on Microwave Theory and Techniques*, vol. 53, no. 4, pp. 1451–1461, Apr. 2005.
- [60] A. Pradeep, S. Mridula, and P. Mohanan, "Design of edge-coupled dual split-ring resonator," *IEEE Antennas and Propagation Magazine*, vol. 53, no. 4, pp. 45–54, 2011.
- [61] M. Cabedo, "Systematic design of antennas using the theory of characteristic modes," Ph.D. dissertation, Universidad Politecnica de Valencia Spain, 2007.
- [62] R. J. Garbacz and R. H. Turpin, "A generalized expansion for radiated and scattered fields," *IEEE Transactions on Antennas and Propagation*, vol. AP-19, no. 3, pp. 348–358, 1971.
- [63] R. F. Harrington and J. R. Mautz, "Theory of characteristic modes for conducting bodies," *IEEE Transactions on Antennas and Propagation*, vol. AP-19, no. 5, pp. 622–628, 1971.
- [64] R. Harrington and J. Mautz, "Computation of characteristic modes for conducting bodies," *IEEE Transactions on Antennas and Propagation*, vol. AP-19, no. 5, pp. 629–639, 1971.

- [65] A. Lozano, F. R. Farrokhi, R. A. Valenzuela, B. Laboratories, and L. Technologies, "Lifting the Limits on High-speed Wireless Data Access Using Antenna Arrays," *IEEE Communications Magazine*, no. September, pp. 156–162, 2001.
- [66] D. Gesbert, M. Shafi, P. Smith, and A. Naguib, "From theory to practice: an overview of MIMO space-time coded wireless systems," *IEEE Journal on Selected Areas in Communications*, vol. 21, no. 3, pp. 281–302, 2003.
- [67] A. Goldsmith, S. A. Jafar, and N. Jindal, "Capacity Limits of MIMO Channels," *IEEE Journal on Selected Areas in Communications*, vol. 21, no. 5, pp. 684–702, 2003.
- [68] L. Zheng and D. Tse, "Diversity and multiplexing: a Fundamental Tradeoff in Multiple-Antenna Channels," *IEEE Transactions on Information Theory*, vol. 49, no. 5, pp. 1073–1096, 2003.
- [69] A. Paulraj, D. Gore, R. Nabar, and H. Bolcskei, "An Overview of MIMO Communications : A Key to Gigabit Wireless," *Proceedings of the IEEE*, vol. 92, no. 2, pp. 198–218, Feb. 2004.
- [70] K. Rosengren and P. Kildal, "Radiation efficiency , correlation , diversity gain and capacity of a six-monopole antenna array for a MIMO system : theory , simulation and measurement in reverberation chamber," *IEE Proc. Microw. Antennas Propag.*, vol. 152, no. 1, pp. 7–16, 2005.



- [71] M. P. Karaboikis, V. C. Papamichael, G. F. Tsachtsiris, C. F. Soras, and V. T. Makios, "Integrating Compact Printed Antennas Onto Small Diversity / MIMO Terminals," *IEEE Transactions on Antennas and Propagation*, vol. 56, no. 7, pp. 2067–2078, 2008.
- [72] Y. Gao, C. C. Chiau, X. Chen, and C. G. Parini, "Modified PIFA and its array for MIMO terminals," *IEE Proc. Microw. Antennas Propag.*, vol. 152, no. 4, pp. 255–259, 2005.
- [73] M. Manteghi, Y. Rahmat-samii, and L. Angeles, "Broadband characterization of the Total Active Reflection Coefficient of Multiport Antennas," pp. 20–23, 2003.
- [74] T. Taga, "Analysis for the Mean Effective Gain of the Mobile Antennas in Land Mobile Radio," *IEEE Transactions on Vehicular Technology*, vol. 39, no. 2, pp. 117–131, 1990.
- [75] J. Romeu, "Exact Representation of antenna system diversity performance from input parameter description," *Electronics Letters*, vol. 39, no. 52, pp. 705–707, 2003.
- [76] Z. Li, Z. Du, M. Takahashi, and K. Saito, "Reducing Mutual Coupling of MIMO Antennas With Parasitic Elements for Mobile Terminals," *IEEE Transactions on Antennas and Propagation*, vol. 60, no. 2, pp. 473–481, 2012.

- [77] M. Muramoto, N. Ishii, and K. Itoh, "Radiation efficiency measurement of a small antenna using the wheeler method," *Electronics and Communications in Japan (Part I: Communications)*, vol. 79, no. 6, pp. 93–100, 1996.
- [78] S. C. K. Ko and R. D. Murch, "Compact Integrated Diversity Antenna for Wireless Communications," *IEEE Transactions on Antennas and Propagation*, vol. 49, no. 6, pp. 954–960, 2001.
- [79] P. Kildal, "Adaptive Antennas and Correlation and Capacity of MIMO Systems and Mutual Coupling, Radiation Efficiency, and Diversity Gain of Their Antennas: Simulations and Measurements in a Reverberation Chamber," *IEEE Communications Magazine*, no. December, pp. 104–112, 2004.
- [80] K. Chung and J. H. Yoon, "Integrated MIMO antenna with high isolation characteristic," *Electronics Letters*, vol. 43, no. 4, pp. 3–4, 2007.
- [81] Y. Ding, Z. Du, K. Gong, and Z. Feng, "A Four-Element Antenna System for Mobile Phones," *IEEE Antennas and Wireless Propagation Letters*, vol. 6, pp. 655–658, 2007.
- [82] S.-c. Chen, Y.-s. Wang, and S.-j. Chung, "A Decoupling Technique for Increasing the Port Isolation Between Two Strongly Coupled Antennas," *IEEE Transactions on Antennas and Propagation*, vol. 56, no. 12, pp. 3650–3658, Dec. 2008.

- [83] Q. Luo, J. Pereira, and H. Salgado, "Reconfigurable dual-band C-shaped monopole antenna array with high isolation," *Electronics Letters*, vol. 46, no. 13, p. 888, 2010.
- [84] S. Park and C. Jung, "Compact MIMO antenna with high isolation performance," *Electronics Letters*, vol. 46, no. 6, p. 390, 2010.
- [85] A. Neзад, M. Sajid, and H. R. Hassani, "A Novel Triband E-Shaped Printed Monopole Antenna for MIMO Application," *IEEE Antennas and Wireless Propagation Letters*, vol. 9, pp. 576–579, 2010.
- [86] C.-C. Hsu, K.-H. Lin, and H.-L. Su, "Implementation of Broadband Isolator Using Metamaterial-Inspired Resonators and a T-Shaped Branch for MIMO Antennas," *IEEE Transactions on Antennas and Propagation*, vol. 59, no. 10, pp. 3936–3939, Oct. 2011.
- [87] S. Cui, Y. Liu, W. Jiang, and S. Gong, "Compact dual-band monopole antennas with high port isolation," *Electronics Letters*, vol. 47, no. 10, p. 579, 2011.
- [88] Y. Li, Z. Zhang, J. Zheng, and Z. Feng, "Dual-polarised monopole-slot co-located MIMO antenna for small-volume terminals," *Electronics Letters*, vol. 47, no. 23, p. 1259, 2011.
- [89] X. Ling and R. Li, "A Novel Dual-Band MIMO Antenna Array With Low Mutual Coupling for Portable Wireless Devices," *IEEE Antennas and Wireless Propagation Letters*, vol. 10, pp. 1039–1042, 2011.

- [90] J.-f. Li, Q.-x. Chu, S. Member, and T.-g. Huang, "A Compact Wideband MIMO Antenna With Two Novel Bent Slits," *IEEE Transactions on Antennas and Propagation*, vol. 60, no. 2, pp. 482–489, 2012.
- [91] M. S. Sharawi, S. S. Iqbal, and Y. S. Faouri, "An 800 MHz 2 x 1 Compact MIMO Antenna System for LTE Handsets," *IEEE Transactions on Antennas and Propagation*, vol. 59, no. 8, pp. 3128–3131, 2011.
- [92] H. Liu, S. Gao, and T. H. Loh, "Compact MIMO Antenna With Frequency Reconfigurability and Adaptive Radiation Patterns," *IEEE Antennas and Wireless Propagation Letters*, vol. 12, pp. 269–272, 2013.
- [93] L. Liu, S. W. Cheung, and T. I. Yuk, "Compact MIMO Antenna for Portable Devices in UWB Applications," *IEEE Transactions on Antennas and Propagation*, vol. 61, no. 8, pp. 4257–4264, Aug. 2013.
- [94] S. B. Yeap, X. Chen, J. A. Dupuy, C. C. Chiau, and C. G. Parini, "Integrated diversity antenna for laptop and PDA terminal in a MIMO system," *IEE Proc. Microw. Antennas Propag.*, vol. 152, no. 6, pp. 495–504, 2005.
- [95] Y. T. Im, J. H. Lee, R. A. Bhatti, and S. Park, "A spiral-dipole antenna for mimo systems," *IEEE Antennas and Wireless Propagation Letters*, vol. 7, pp. 803–806, 2008.
- [96] M. Sonkki, E. Antonino-daviu, M. F. Cabedo, M. Ferrando-bataller, and E. T. Salonen, "Improved Planar Wideband Antenna Element and Its Us-

- age in a Mobile MIMO System,” *IEEE Antennas and Wireless Propagation Letters*, vol. 11, pp. 826–829, 2012.
- [97] A. N. Kulkarni and S. K. Sharma, “Frequency Reconfigurable Microstrip Loop Antenna Covering LTE Bands With MIMO Implementation and Wideband Microstrip Slot Antenna all for Portable Wireless DTV Media Player,” *IEEE Transactions on Antennas and Propagation*, vol. 61, no. 2, pp. 964–968, 2013.
- [98] R. Karimian, H. Oraizi, S. Fakhte, and M. Farahani, “Novel F-Shaped Quad-Band Printed Slot Antenna for WLAN and WiMAX MIMO Systems,” *IEEE Antennas and Wireless Propagation Letters*, vol. 12, pp. 405–408, 2013.
- [99] A. Jain, P. Verma, and V. Singh, “Performance analysis of PIFA based  $4 \times 4$  MIMO antenna,” *Electronics Letters*, vol. 48, no. 9, p. 474, 2012.
- [100] S. Ghosh, T.-N. Tran, and T. Le-Ngoc, “Miniaturized Four-Element Diversity PIFA,” *IEEE Antennas and Wireless Propagation Letters*, vol. 12, pp. 396–400, 2013.
- [101] K. Payandehjoo and R. Abhari, “Compact Multi-Band PIFAs on a Semi-Populated Mobile Handset with Tunable Isolation,” *IEEE Transactions on Antennas and Propagation*, pp. 4–9, 2013.
- [102] B. Kim, Y. Park, H. Wi, M.-j. Park, Y. Choi, J. Lee, W. Jung, D. Kim, and B. Lee, “Isolation Enhancement of USB Dongle MIMO Antenna in LTE

- 700 Band Applications,” *IEEE Antennas and Wireless Propagation Letters*, vol. 11, pp. 961–964, 2012.
- [103] J. Park, J. Choi, J.-Y. Park, and Y.-S. Kim, “Study of a T-Shaped Slot With a Capacitor for High Isolation Between MIMO Antennas,” *IEEE Antennas and Wireless Propagation Letters*, vol. 11, pp. 1541–1544, 2012.
- [104] S. Zhang, B. K. Lau, Y. Tan, Z. Ying, and S. He, “Mutual Coupling Reduction of Two PIFAs With a T-Shape Slot Impedance Transformer for MIMO Mobile Terminals,” *IEEE Transactions on Antennas and Propagation*, vol. 60, no. 3, pp. 1521–1531, Mar. 2012.
- [105] R. A. Bhatti, J.-H. Choi, and S.-O. Park, “Quad-Band MIMO Antenna Array for Portable Wireless Communications Terminals,” *IEEE Antennas and Wireless Propagation Letters*, vol. 8, pp. 129–132, 2009.
- [106] P. Chen, W. Hong, Z. Kuai, J. Xu, H. Wang, J. Chen, H. Tang, J. Zhou, and K. Wu, “A Multibeam Antenna Based on Substrate Integrated Waveguide Technology for MIMO Wireless Communications,” *IEEE Transactions on Antennas and Propagation*, vol. 57, no. 6, pp. 1813–1821, Jun. 2009.
- [107] A. Mak, C. Rowell, and R. Murch, “Isolation enhancement between two closely packed antennas,” *IEEE Transactions on Antennas and Propagation*, vol. 56, no. 11, pp. 3411–3419, Nov. 2008.
- [108] Y. Gao, X. Chen, Z. Ying, and C. Parini, “Design and Performance Investigation of a Dual Element PIFA Array at 2.5 GHz for MIMO Terminal,”

- IEEE Transactions on Antennas and Propagation*, vol. 55, no. 12, pp. 3433–3441, 2007.
- [109] H. Zhang, Z. Wang, J. Yu, and J. Huang, “A compact mimo antenna for wireless communication,” *IEEE Antennas and Propagation Magazine*, vol. 50, no. 6, pp. 104–107, Dec. 2008.
- [110] L. Wang, M. Q. Yuan, and Q. H. Liu, “A Dual-Band Printed Electrically Small Antenna Covered by Two Capacitive Split-Ring Resonators,” *IEEE Antennas and Wireless Propagation Letters*, vol. 10, pp. 824–826, 2011.
- [111] S. Zhang, B. K. Lau, A. Sunesson, and S. He, “Closely-packed uwb mimo/diversity antenna with different patterns and polarizations for usb dongle applications,” *IEEE Transactions on Antennas and Propagation*, vol. 60, no. 9, pp. 4372–4380, Sep. 2012.
- [112] C. Yang, J. Kim, H. Kim, J. Wee, B. Kim, and C. Jung, “Quad-Band Antenna With High Isolation MIMO and Broadband SCS for Broadcasting and Telecommunication Services,” *IEEE Antennas and Wireless Propagation Letters*, vol. 9, pp. 584–587, 2010.
- [113] K.-C. Lin, C.-H. Wu, C.-H. Lai, and T.-G. Ma, “Novel Dual-Band Decoupling Network for Two-Element Closely Spaced Array Using Synthesized Microstrip Lines,” *IEEE Transactions on Antennas and Propagation*, vol. 60, no. 11, pp. 5118–5128, Nov. 2012.

- [114] D. A. Ketzaki and T. V. Yioultis, “Metamaterial-Based Design of Planar Compact MIMO Monopoles,” *IEEE Transactions on Antennas and Propagation*, vol. 61, no. 5, pp. 2758–2766, May 2013.
- [115] Z. Li, Z. Du, M. Takahashi, K. Saito, and K. Ito, “Reducing Mutual Coupling of MIMO Antennas With Parasitic Elements for Mobile Terminals,” *IEEE Transactions on Antennas and Propagation*, vol. 60, no. 2, pp. 473–481, Feb. 2012.
- [116] Z.-J. Jin, J.-H. Lim, and T.-Y. Yun, “Frequency reconfigurable multiple-input multiple-output antenna with high isolation,” *IET Microwaves, Antennas & Propagation*, vol. 6, no. 10, p. 1095, 2012.
- [117] S.-W. Su, C.-T. Lee, and F.-S. Chang, “Printed MIMO-Antenna System Using Neutralization-Line Technique for Wireless USB-Dongle Applications,” *IEEE Transactions on Antennas and Propagation*, vol. 60, no. 2, pp. 456–463, Feb. 2012.
- [118] H. Li, J. Xiong, and S. He, “Extremely compact dual-band PIFAs for MIMO application,” *Electronics Letters*, vol. 45, no. 17, p. 869, 2009.
- [119] A. Diallo, C. Luxey, P. L. Thuc, and R. Staraj, “Dual-Band WLAN Diversity Antenna System With High Port-to-Port Isolation,” *IEEE Antennas and Wireless Propagation Letters*, vol. 11, pp. 244–247, 2012.
- [120] J. Xiong and S. He, “A Compact Planar MIMO Antenna System of Four Elements With Similar Radiation Characteristics and Isolation Structure,”



- IEEE Antennas and Wireless Propagation Letters*, vol. 8, pp. 1107–1110, 2009.
- [121] J. OuYang, F. Yang, and Z. M. Wang, “Reducing Mutual Coupling of Closely Spaced Microstrip MIMO Antennas for WLAN Application,” *IEEE Antennas and Wireless Propagation Letters*, vol. 10, pp. 310–313, 2011.
- [122] C.-y. Chiu, J.-b. Yan, and R. D. Murch, “24-port and 36-port antenna cubes suitable for mimo wireless communications,” *IEEE Transactions on Antennas and Propagation*, vol. 56, no. 4, pp. 1170–1176, Apr. 2008.
- [123] S. Baek and S. Lim, “Compact planar MIMO antenna array with polarisation diversity on single layer,” *Electronics Letters*, vol. 46, no. 13, p. 880, 2010.
- [124] S. Zhang, P. Zetterberg, and S. He, “Printed MIMO antenna system of four closely-spaced elements with large bandwidth and high isolation,” *Electronics Letters*, vol. 46, no. 15, p. 1052, 2010.
- [125] S.-W. Su, “High-Gain Dual-Loop Antennas for MIMO Access,” *IEEE Transactions on Antennas and Propagation*, vol. 58, no. 7, pp. 2412–2419, 2010.
- [126] A.-D. Capobianco, F. M. Pigozzo, A. Assalini, M. Midrio, and S. Boscolo, “A Compact MIMO Array of Planar End-Fire Antennas for WLAN Applications,” *IEEE Transactions on Antennas and Propagation*, vol. 59, no. 9, pp. 3897–3900, 2011.

- [127] J. Lee, Y. K. Hong, S. Bae, G. S. Abo, W. M. Seong, and K. G. H., "Miniature Long-Term Evolution (LTE) MIMO Ferrite Antenna," *IEEE Antennas and Wireless Propagation Letters*, vol. 10, pp. 603–606, 2011.
- [128] S. Dumanli, C. J. Railton, and D. L. Paul, "A Slot Antenna Array With Low Mutual Coupling for Use on Small Mobile Terminals," *IEEE Transactions on Antennas and Propagation*, vol. 59, no. 5, pp. 1512–1520, May 2011.
- [129] Y. Cheon, J. Lee, and J. Lee, "Quad-Band Monopole Antenna Including LTE 700 MHz With Magneto-Dielectric Material," *IEEE Antennas and Wireless Propagation Letters*, vol. 11, pp. 137–140, 2012.
- [130] P.-y. Qin, Y. J. Guo, and A. R. Weily, "A Pattern Reconfigurable U-Slot Antenna and Its Applications in MIMO Systems," *IEEE Transactions on Antennas and Propagation*, vol. 60, no. 2, pp. 516–528, 2012.
- [131] M. S. Sharawi, A. B. Numan, M. U. Khan, and D. N. Aloï, "A Dual-Element Dual-Band MIMO Antenna System With Enhanced Isolation for Mobile Terminals," *IEEE Antennas and Wireless Propagation Letters*, vol. 11, pp. 1006–1009, 2012.
- [132] M. Sharawi, M. Jan, and D. Aloï, "Four-shaped 2 x 2 multi-standard compact multiple-inputmultiple-output antenna system for long-term evolution mobile handsets," *IET Microwaves, Antennas & Propagation*, vol. 6, no. 6, p. 685, 2012.

- [133] X. Zhou, X. Quan, and R. Li, "A Dual-Broadband MIMO Antenna System for GSM/UMTS/LTE and WLAN Handsets," *IEEE Antennas and Wireless Propagation Letters*, vol. 11, pp. 551–554, 2012.
- [134] H. Li, J. Xiong, Z. Ying, and S. He, "Compact and low profile co-located MIMO antenna structure with polarisation diversity and high port isolation," *Electronics Letters*, vol. 46, no. 2, p. 108, 2010.
- [135] C.-y. Chiu, J.-b. Yan, and R. D. Murch, "Compact Three-Port Orthogonally Polarized MIMO Antennas," *IEEE Antennas and Wireless Propagation Letters*, vol. 6, pp. 619–622, 2007.
- [136] M. A. Jensen and J. W. Wallace, "A Review of Antennas and Propagation for MIMO Wireless Communications," *IEEE Transactions on Antennas and Propagation*, vol. 52, no. 11, pp. 2810–2824, 2004.
- [137] N. B. Slits, J. Li, Q. Chu, and T. Huang, "A Compact Wideband MIMO Antenna With Two Novel Bent Slits," *IEEE Transactions on Antennas and Propagation*, vol. 60, no. 2, pp. 482–489, 2012.
- [138] K. Lin, C. Wu, C. Lai, and T. G. Ma, "Novel Dual-Band Decoupling Network for Two-Element Closely Spaced Array Using Synthesized Microstrip Lines," *IEEE Transactions on Antennas and Propagation*, vol. 60, no. 11, pp. 5118–5128, 2012.
- [139] S. W. Su, C. T. Lee, and F. S. Chang, "Printed MIMO-Antenna System Using Neutralization-Line Technique for Wireless USB-Dongle Applications,"

*IEEE Transactions on Antennas and Propagation*, vol. 60, no. 2, pp. 456–463, 2012.

- [140] J. B. Pendry, A. J. Holden, D. J. Robbins, and W. J. Stewart, “Magnetism from Conductors and Enhanced Nonlinear Phenomena,” *IEEE Transactions on Microwave Theory and Techniques*, vol. 47, no. 8, pp. 2075–2084, 1999.

# Vitae

- Name: Muhammad Umar Khan
- Nationality: Pakistani
- Date of Birth: 7th August, 1984
- Email: *umar608@gmail.com*
- Permenant Address: House No. 103-A, Street No. 5, Phase II, Bahria Town, Rawalpindi, Pakistan.
- PhD (Electrical Engineering) KFUPM, Saudi Arabia Jan. 2015
- MS (Electronic Engineering) GIKI, Pakistan Jun. 2008
- BE (Electrical Engineering) NUST, Pakistan Jun. 2006

# LIST OF PUBLICATIONS

- **Journal Publications**

1. M. U. Khan, M. S. Sharawi and R. Mittra “Microstrip Patch Antenna Miniaturization Techniques : A Review”, accepted in IET Microwave, Antennas & Propagation, Dec. 2014.
2. M. U. Khan and M. S. Sharawi, “A dual band microstrip annular slot based MIMO antenna system”, Microwave & Optical Technology Letters, Vol. 57, No. 2, pp. 360-364, Feb. 2015.
3. M. U. Khan and M. S. Sharawi, “A 2 x 1 multi-band MIMO antenna system consisting of miniaturized patch elements”, Microwave & Optical Technology Letters, Vol. 56, No. 6, pp. 1371-1375, Jun. 2014.
4. M. S. Sharawi, M. U. Khan, A. B. Numan and D. N. Aloï, “A CSRR loaded MIMO antenna system for ISM band operation”, IEEE Transactions on Antenna and Propagation, vol. 61, no. 8, pp. 4265-4274, Aug. 2013.
5. M. S. Sharawi, A. B. Numan, M. U. Khan and D. N. Aloï, “A dual-element dual-band MIMO antenna system with enhanced Isolation for Mobile Terminals”, IEEE Antennas and Wireless Propagation Letters, vol. 11, pp. 1006-1009, 2012.

- **International Conferences**

1. M. U. Khan , and M. S. Sharawi, “Analysis of Miniaturized MPA Design Using Theory of Characteristic Modes”, submitted to 2015 IEEE International Symposium on Antenna and Propagation, Vancouver, Canada, July 2015.
2. M. U. Khan , and M. S. Sharawi, “Annular Slot Based Printed MIMO Antenna System Design”, 2014 IEEE International Symposium on Antenna and Propagation, Memphis, TN, USA, July 6-12, 2014.
3. M. U. Khan , W. A. Al-Saud and M. S. Sharawi, “Isolation Enhancement Effect on the Measured Channel Capacity of a Printed MIMO Antenna System”, The 8th European Conference on Antennas and Propagation, The Hague, The Netherlands, April 6-11, 2014.
4. M. U. Khan , and M. S. Sharawi, “Isolation Improvement Using an MTM Inspired Structure with a Patch Based MIMO Antenna System”, The 8th European Conference on Antennas and Propagation, The Hague, The Netherlands, April 6-11, 2014.
5. M. U. Khan , W. A. Al-Saud and M. S. Sharawi, “Channel Capacity Measurement of a 4-Element Printed MIMO Antenna System”, The 8th German Microwave Conference, Aachen, March 10-12, 2014.
6. M. U. Khan , and M. S. Sharawi, “Channel capacity analysis of a novel printed MIMO antenna system in wireless mobile environment”, 2013 IEEE

International Symposium on Antenna and Propagation, Florida, USA, July 7-13, 2013

7. M. U. Khan , M. S. Sharawi, and D. A. Aloi, “A multi-band 2 x 1 MIMO antenna system consisting of CSRR loaded patch elements”, 2013 IEEE International Symposium on Antenna and Propagation, Florida, USA, July 7-13, 2013.
8. M. U. Khan, M. S. Sharawi, A. Steffes, and D. N. Aloi, “A 4-element MIMO antenna system loaded with CSRRs and patch antenna elements”, 7th European Conference on Antenna and Propagation (EuCAP 2013), Gothenburg, Sweden , April 8-12, 2013.
9. M. U. Khan and M. S. Sharawi, “A compact 8-element MIMO antenna system for 802.11ac WLAN applications”, International Workshop on Antenna Technology (IWAT 13), Karlsruhe, Germany, March 4-6, 2013.

- **Patent**

1. “CSRR Loaded Multiple-Input-Multiple-Output (MIMO) Antenna System,” Mohammad S. Sharawi, Muhammad U. Khan and Ahmed B. Numan (KFUPM, KSA), Filed on Sep. 2012 to USPO, Patent Pending.